

University of Alberta

Catalytic Conversion of Pyrolysis Gases

by

Ladan Shamaei

A thesis submitted to the Faculty of Graduate Studies and Research
in partial fulfillment of the requirements for the degree of

Master of Science
in
Chemical Engineering

Department of Chemical and Materials Engineering

©Ladan Shamaei
Spring 2013
Edmonton, Alberta

Permission is hereby granted to the University of Alberta Libraries to reproduce single copies of this thesis and to lend or sell such copies for private, scholarly or scientific research purposes only. Where the thesis is converted to, or otherwise made available in digital form, the University of Alberta will advise potential users of the thesis of these terms.

The author reserves all other publication and other rights in association with the copyright in the thesis and, except as herein before provided, neither the thesis nor any substantial portion thereof may be printed or otherwise reproduced in any material form whatsoever without the author's prior written permission.

Dedication

To my brother who immensely supported me to be where I am today

To my parents for all their sacrifices

Abstract

In every thermal upgrading process, short-chain hydrocarbons contain a part of the gas byproducts. These compounds are hydrogen-rich materials, which are considered as low value wastes. In this study, the efforts were made to catalytically convert these off-gases to liquid fuels. Synthetic gases were used as model reactant gases. Four types of zeolite including ZSM-5, Mordenite, Ferrierite, and Zeolite Y were tested. Among these catalysts, ZSM-5 was the most active one for alkene conversion. At adiabatic condition, it had the capability of producing aromatic compounds. Performance of four types of nickel incorporated catalysts including ZSM-5, two kinds of silica-alumina (with 20 wt.% and 40 wt.% SiO₂), and silica were also investigated for this purpose. Among these catalysts, reduced form Ni (on silica) exhibited significant dehydrogenating activity for butane. ZSM-5 had the capability of making cyclic compounds, while silica-aluminas mainly had nickel aluminate in their framework.

Acknowledgments

We are grateful for the funding and support provided by the Canadian Government through the Helmholtz-Alberta Initiative (HAI) and Natural Resources Canada (NRCan) under their EcoEnergy Technology Initiative Grant (Eco-ETI) program.

I would like to thank my supervisor, Dr. Arno De Clerk for the great guidance and support I received throughout the development of the work. His encouragements, accompanying, enthusiastic supervision and patience meant a lot to me during the research time.

I am also grateful to the research group members for providing kind helps in a friendly environment. Special thanks to Yuhua Xia and Shaofeng Yang for sharing the lab experiences and helpful suggestions. My sincere thanks also go to my great friends Jing Shen, Hessam Ziae, and Blake Olson for their valuable contributions to the success of the work.

Finally, I would like to thank my family for the perpetual faith and love during my research life in Canada, and all my friends who were always next to me as close as my family.

Table of content

1. INTRODUCTION TO PYROLYSIS GAS CONVERSION	1
1.1. BACKGROUND	1
1.2. OBJECTIVE/PURPOSE	3
2. LITERATURE REVIEW ON OLIGOMERISATION.....	5
2.1. INTRODUCTION.....	5
2.2. BASICS OF OLIGOMERISATION REACTIONS.....	6
2.3. MECHANISM AND KINETICS OF OLEFIN OLIGOMERISATION	7
2.4. CATALYSTS APPLIED FOR OLIGOMERISATION.....	8
2.4.1. <i>Solid phosphoric acid catalysts</i>	8
2.4.2. <i>Heteropolyacid (HPA) catalysts</i>	10
2.4.3. <i>Zeolites</i>	10
2.4.4. <i>Amorphous silica-alumina (ASA) catalysts</i>	15
2.4.5. <i>Silico-aluminophosphate (SAPO) catalysts</i>	16
2.4.6. <i>Sulfated zirconia catalysts</i>	17
2.4.7. <i>Acidic resin catalysts</i>	17
2.4.8. <i>Heterogeneous nickel catalysts</i>	18
2.4.9. <i>Homogeneous nickel catalysts</i>	19
2.4.10. <i>Metals other than nickel</i>	21
2.4.11. <i>Metallocene</i>	22
2.5. OLIGOMERISATION OVER H-ZSM-5	22
2.5.1. <i>General information</i>	22
2.5.2. <i>Structure</i>	24
2.5.3. <i>Metal-loaded ZSM-5</i>	26
2.5.4. <i>Poisons</i>	31
3. BATCH REACTOR STUDIES.....	36
3.1. INTRODUCTION.....	36
3.2. EXPERIMENTAL	37
3.2.1. <i>Materials</i>	37
3.2.2. <i>Equipment</i>	38
3.2.3. <i>Analyses</i>	40

3.2.4. <i>Calculations</i>	42
3.3. RESULTS AND DISCUSSION	43
3.3.1. <i>Catalyst characterization</i>	43
3.3.2. <i>Measuring the cracking temperature of long-chain olefins over H-ZSM-5</i>	47
3.3.3. <i>Reaction of ethene over zeolite catalysts</i>	51
3.4. CONCLUSION	53
4. FLOW REACTOR STUDIES WITH H-ZSM-5.....	56
4.1. INTRODUCTION.....	56
4.2. EXPERIMENTAL	57
4.2.1. <i>Materials</i>	57
4.2.2. <i>Equipment</i>	58
4.2.3. <i>Analyses</i>	60
4.2.4. <i>Calculations</i>	60
4.3. RESULTS AND DISCUSSION	61
4.3.1. <i>Background - Conceptual design for applied study</i>	61
4.3.2. <i>Catalytic investigations</i>	62
4.4. CONCLUSION	70
5. FLOW REACTOR STUDIES WITH SUPPORTED NICKEL CATALYSTS	72
5.1. INTRODUCTION.....	72
5.2. EXPERIMENTAL	73
5.2.1. <i>Materials</i>	73
5.2.2. <i>Equipment and procedure</i>	74
5.2.3. <i>Analyses</i>	75
5.2.4. <i>Calculations</i>	76
5.3. RESULTS AND DISCUSSION	77
5.3.1. <i>Catalyst Characterization</i>	77
5.3.2. <i>Catalyst screening in the presence of light hydrocarbons</i>	85
5.4. CONCLUSION	96
6. CONCLUSIONS AND SIGNIFICANCE	100
6.1. INTRODUCTION.....	100
6.2. MAIN CONCLUSIONS	101

6.3. SIGNIFICANCE OF THIS WORK	103
6.4. FUTURE WORK.....	103
6.5. PRESENTATIONS AND PUBLICATIONS	104
A. APPENDIX I.....	106
B. APPENDIX II	111
C. APPENDIX III.....	117

List of tables

<i>Table 1-1. Price comparison of white products, bitumen and fuel gas.</i>	1
<i>Table 2-1. Equilibrium distribution of the products obtained from the reaction of different alkenes over H-ZSM-5 at 270 - 275 °C and alkene partial pressure of 5-15 kPa (WHSV 0.5 - 0.9 h⁻¹) [7]</i>	11
<i>Table 2-2. Product yielded from C₃-C₆ feed (82% alkenes, 15% alkanes, 1.5% aromatics and 1.8% oxygenates) over H-ZSM-5 [7]</i>	12
<i>Table 2-3. Propene oligomerisation over SAPO-11 (AEL)-based catalysts [7]</i>	16
<i>Table 3-1. Properties of the zeolites provided by supplier</i>	38
<i>Table 3-2. Acid site strength and density of each zeolite (at 25 °C)</i>	44
<i>Table 3-3. Cracking temperature of C₆ - C₁₄ alkenes measured from the reaction of 0.5 g alkene in the presence of 0.5 g H-ZSM-5, and atmospheric pressure</i>	50
<i>Table 3-4. Carbon number distribution from the reaction of different alkenes over H-ZSM-5 (atmospheric pressure, 0.5 g H-ZSM-5, 0.5 g reactant, and temperature of 450 °C)</i>	51
<i>Table 3-5. Pressure drops observed during the reaction of ethene over different zeolites (at 300 °C, 100 psi, and 0.5 g catalyst)</i>	52
<i>Table 3-6. TG results of spent H-ZSM-5 after reacting with ethene</i>	52
<i>Table 4-1. Conversion of pyrolysis gas mixtures to liquids over H-ZSM-5 with inlet at 190-200 °C and 0.6 MPa</i>	63
<i>Table 4-2. Amount of aliphatics and aromatics in the liquid products from the conversion of different mixture of gases over H-ZSM-5</i>	66
<i>Table 4-3. Carbon number distribution of the products from the conversion of different gas mixtures</i>	66
<i>Table 4-4. Summary of the 1H-NMR analysis for the products obtained from the reaction of mixture of propene and butane over H-ZSM-5</i>	69
<i>Table 5-1. General properties of silica-aluminas provided by supplier</i>	74
<i>Table 5-2. Peak temperatures and amount of hydrogen consumed for the reduction of each catalyst</i>	81
<i>Table 5-3. Concentration and distribution of acid sites for different catalysts</i>	83
<i>Table 5-4. Flow rate and conversion rate for the reaction of propene over 0.5Ni/ZSM-5 (at furnace temperature of 300 °C and atmospheric pressure)</i>	86
<i>Table 5-5. Carbon number distribution of the products obtained from the reaction of propene over 0.5Ni/ZSM-5 (at furnace temperature of 300 °C and atmospheric pressure)</i>	86
<i>Table 5-6. Conversion rate of the reaction of propene over 5Ni/ZSM-5 (at furnace temperature of 300 °C and atmospheric pressure)</i>	87

<i>Table 5-7. Carbon number distribution of hydrocarbon compounds in the product of the reaction of propene over 5Ni/ZSM-5 (at furnace temperature of 300 °C and atmospheric pressure)</i>	87
<i>Table 5-8. Amount of alkyl-cyclopentene compounds in the liquid product captured from the reaction of propene over 5Ni/ZSM-5</i>	88
<i>Table 5-9. Conversion and distribution (vol. %) of the products from the reaction of propene over reduced 5Ni/Siral-40 (flow rate of 60 L_{C3}·g_{cat}⁻¹·h⁻¹)</i>	89
<i>Table 5-10. Distribution (vol. %) of the products of the reaction of propene over 5NiO/Siral-40 (flow rate of 60 L_{C3}·g_{cat}⁻¹·h⁻¹)</i>	90
<i>Table 5-11. TG results of spent 5NiO/Siral-40 after the reaction with propene</i>	91
<i>Table 5-12. Conversion and carbon number distribution (vol.%) of butane over 5Ni/SiO₂ at different temperatures and atmospheric pressure (flow rate of 30 L_{C4}·h⁻¹·g_{cat}⁻¹)</i>	93
<i>Table 5-13. TG results of spent 5Ni/SiO₂ after the reaction with butane</i>	94
<i>Table 5-14. Conversion and product distribution (vol.%) of the reaction of ethene over 5Ni/SiO₂ at different temperatures and atmospheric pressure (flow rate of 120 L_{C2}·h⁻¹·g_{cat}⁻¹)</i>	95
<i>Table 5-15. Product distribution of the reaction of propene over 5Ni/SiO₂ at different temperatures and atmospheric pressure (flow rate of 41 L_{C3}·h⁻¹·g_{cat}⁻¹)</i>	95
<i>Table 5-16. TG results of spent 5Ni/SiO₂ after the reaction with ethene and propene</i>	96
<i>Table A-1. Pressure changes as temperature increases for the reaction of 1-hexene (left) and 1-heptene (right) over H-ZSM-5</i>	106
<i>Table A-2. Pressure changes as temperature increases for the reaction of 1-octene (left) and 1-nonene (right) over H-ZSM-5</i>	107
<i>Table A-3. Pressure changes as the temperature increases for the reaction of 1-decene (left) and 1-undecene (right) over H-ZSM-5</i>	108
<i>Table A-4. Pressure versus temperature for the reaction of 1-dodecene (left) and 1-tridecene (right) over H-ZSM-5</i>	109
<i>Table A-5. Pressure versus temperature for the reaction of 1-tetradecene over H-ZSM-5</i>	110
<i>Table B-1. Aromatic and aliphatic distribution of the products from the conversion of different mixture of gases (at total pressure of 100 psi and preheating temperature of 220 °C)</i>	115
<i>Table B-2. Aromatic and aliphatic distribution of the products from the conversion of different mixture of gases (at total pressure of 100 psi and preheating temperature of 220 °C)</i>	115
<i>Table B-3. Aromatic and aliphatic distribution of the products from the conversion of different mixture of gases (at total pressure of 100 psi and preheating temperature of 220 °C)</i>	116
<i>Table B-4. Amount of product captured every 20 min during the 3 h of experiment (at total pressure of 100 psi and preheating temperature of 220 °C)</i>	116

List of figures

<i>Figure 1-1. Vision of advanced bitumen processing</i>	2
<i>Figure 1-2. Potential strategies for catalytically converting cracked gas into liquids</i>	3
<i>Figure 2-1. Reaction network of the acid-catalyzed reactions happening during OLI [7]</i>	7
<i>Figure 2-2. (a) Classic Whitmore-type carbocation mechanism (b) ester-based mechanism (typical of phosphoric acid) (c) 1,2-insertion and β-hydride elimination (typical of organometallic catalysis) (d) radical propagation [7]</i>	8
<i>Figure 2-3. Mechanism of propene oligomerisation [9]</i>	20
<i>Figure 2-4. Reaction of propene over H-ZSM-5 [18]</i>	23
<i>Figure 2-5. Morphology of ZSM-5 [15]</i>	25
<i>Figure 3-1. Batch reaction setup</i>	39
<i>Figure 3-2. Sand bath</i>	40
<i>Figure 3-3. NH₃-TPD profile of H-ZSM-5</i>	45
<i>Figure 3-4. NH₃-TPD profile of H-MOR</i>	45
<i>Figure 3-5. NH₃-TPD profile of H-FER</i>	45
<i>Figure 3-6. NH₃-TPD profile of H-Y</i>	45
<i>Figure 3-7. FTIR spectra of adsorbed pyridine for H-ZSM-5 at different outgassing temperatures</i>	46
<i>Figure 3-8. FTIR spectra of adsorbed pyridine for H-MOR at different outgassing temperatures</i>	46
<i>Figure 3-9. FTIR spectra of adsorbed pyridine for H-Y at different outgassing temperatures</i>	46
<i>Figure 3-10. FTIR spectra of adsorbed pyridine for H-FER at different outgassing temperatures</i>	46
<i>Figure 3-11. Pressure changes as the temperature increases for the reaction of 1-hexene over H-ZSM-5</i>	47
<i>Figure 3-12. Pressure changes as the temperature increases for the reaction of 1-heptene over H-ZSM-5</i>	47
<i>Figure 3-13. Pressure changes as the temperature increases for the reaction of 1-octene over H-ZSM-5</i>	48
<i>Figure 3-14. Pressure versus temperature for the reaction of 1-nonene over H-ZSM-5</i>	48
<i>Figure 3-15. Pressure versus temperature for the reaction of 1-decene over H-ZSM-5</i>	48
<i>Figure 3-16. Pressure changes as temperature increases for the reaction of 1-undecene over H-ZSM-5</i>	48

<i>Figure 3-17. Pressure changes as the temperature increases for the reaction of 1-dodecene over H-ZSM-5</i>	49
<i>Figure 3-18. Pressure versus temperature for the reaction of 1-tridecene over H-ZSM-5</i>	49
<i>Figure 3-19. Pressure changes as the temperature increases during the reaction of 1-tetradecene over H-ZSM5</i>	49
<i>Figure 3-20. TG analysis of spent H-ZSM-5 after reacting with ethene</i>	53
<i>Figure 4-1. Continuous reaction setup</i>	59
<i>Figure 4-2. Two positions for pyrolysis gas to liquid conversion as illustrated with a delayed coker process. Only lines pertinent to the discussion are shown on the flow diagram.</i>	62
<i>Figure 4-3. Ethene and propene reacting over acid catalysts</i>	64
<i>Figure 4-4. Adiabatic time-temperature profile in H-ZSM-5 catalyst bed during conversion of a 1:2.4 propene + ethene mixture at 0.7 MPa.</i>	65
<i>Figure 4-5. H-NMR spectrum of the product from the reaction of mixture of propene and butane</i>	68
<i>Figure 4-6. Conversion changes versus time for the reaction of ethene and mixture of propene, ethene, and methane</i>	70
<i>Figure 5-1. TPR profile of 5Ni-Siral 40</i>	78
<i>Figure 5-2. TPR profile of 5Ni-Siral 20</i>	78
<i>Figure 5-3. XRD patterns of (a) NiAl₂O₄(b) 5Ni/Siral-40, and (c) 5Ni/Siral-20</i>	79
<i>Figure 5-4. TPR profile of 5Ni/Silica</i>	80
<i>Figure 5-5. TPR profile of 5Ni/ZSM-5</i>	81
<i>Figure 5-6. NH₃-TPD profile of 5Ni/Siral-20</i>	82
<i>Figure 5-7. NH₃-TPD profile of 5Ni/Siral-40</i>	82
<i>Figure 5-8. NH₃-TPD profile of 5Ni/ZSM-5</i>	82
<i>Figure 5-9. FTIR spectra of adsorbed pyridine for 5Ni/Siral-20 at different temperatures</i>	83
<i>Figure 5-10. FTIR spectra of adsorbed pyridine for reduced 5Ni/Siral-20 at different outgassing temperatures</i>	83
<i>Figure 5-11. FTIR spectra of adsorbed pyridine for reduced 5Ni/ZSM-5 at different outgassing temperatures</i>	84
<i>Figure 5-12. FTIR spectra of adsorbed pyridine for reduced 5Ni/ZSM-5 and H-ZSM-5 (at 25 °C)</i>	84
<i>Figure 5-13. Mass spectrum of the gas products from the reaction of propene over 5Ni/Siral-40 (at 400 °C)</i>	90
<i>Figure 5-14. Thermal gravimetric analysis of spent 5Ni/Siral-40 after the interaction with propene</i>	92

<i>Figure 5-15. Mass spectrum of the gas products from the reaction of butane over 5Ni/SiO₂ (at 450 °C)</i>	93
<i>Figure 5-16. Thermal gravimetric analysis of spent 5Ni/SiO₂ after interacting with ethene</i>	94
<i>Figure 5-17. Thermal gravimetric analysis of spent 5NiO/SiO₂ after interacting with ethene</i>	96
<i>Figure 5-18. Thermal gravimetric analysis of spent 5NiO/SiO₂ after the interaction with propene</i>	96
<i>Figure B-1. Temperature profile of the catalyst bed from the reaction of propene over H-ZSM-5 (at total pressure of 100 psi and preheating temperature of 220 °C)</i>	111
<i>Figure B-2. Temperature of the catalyst bed for the reaction of mixture of propene and methane over H-ZSM-5 (at total pressure of 100 psi and preheating temperature of 220 °C)</i>	111
<i>Figure B-3. Temperature of the catalyst bed for the reaction of ethene over H-ZSM-5 (at total pressure of 100 psi and preheating temperature of 220 °C)</i>	112
<i>Figure B-4. Temperature profile of the catalyst for the reaction of mixture of propene and hydrogen over H-ZSM-5 (at total pressure of 100 psi and preheating temperature of 220 °C)</i>	112
<i>Figure B-5. Temperature profile of the catalyst bed for the reaction of mixture of propene and carbon dioxide over H-ZSM-5 (at total pressure of 100 psi and preheating temperature of 220 °C)</i>	113
<i>Figure B-6. Temperature profile of the catalyst bed for the conversion of mixture of propene and butane over H-ZSM-5 (at total pressure of 100 psi and preheating temperature of 220 °C)</i>	113
<i>Figure B-7. Temperature profile of the catalyst bed for the reaction of the mixture of methane, ethene, and propene over H-ZSM-5 (at total pressure of 100 psi and preheating temperature of 220 °C)</i>	114
<i>Figure C-1. Arrhenius plot for the reaction of propene over reduced 5Ni/Siral-40</i>	117

List of Symbols, Nomenclatures, and Abbreviation

OLI: Oligomerisation

ISO: Isomerisation

HYD: Hydrogenation

deHYD: Dehydrogenation

OX: oxidation

ARO: Aromatization

LPG: Liquid petroleum gas

FCC: Fluid catalytic cracking

SPA: Solid phosphoric acid

MOGD: Mobil olefin to gasoline and distillate

FTS: Fischer-Tropsch

ASA: Amorphous silica-alumina

SAPO: Silico-aluminophosphate

HPA: Heteropoly acid

k: Reaction rate constant

TAP: Trialkylphosphine

FER: Ferrierite

MOR: Mordenite

TOS: Time on stream

E_a: Activation energy

R: Universal gas constant

n: Mole

m: Mass

T: Temperature

P: Pressure

V: Volume

1. INTRODUCTION TO PYROLYSIS GAS CONVERSION

1.1. Background

Upgrading processes of bitumen are energy intensive, and are usually accompanied with more byproducts than refining of conventional crude oil. New upgrading technologies attempt to use new methods to reduce energy intensity, capital cost, and carbon footprint of oil sands-related processes. Many of these methods employ thermal conversion so that these technologies can directly be applied to bitumen upgrading (Figure 1-1), providing hydrogen-enriched liquid products, hydrogen for hydroconversion upgrading processes, and byproducts management.

Bitumen pyrolysis typically has unwanted byproducts including gas wastes and unconverted residues. Utilizing the off gases from pyrolysis to produce more valuable materials can reduce the environmental impacts of the pyrolysis reactions. Furthermore, the off gases from pyrolysis are hydrogen-rich. As liquids, such hydrogen-rich materials have higher value than bitumen or fuel gas. There is an economic incentive to convert the pyrolysis off gases into liquid products, also called “white products” (Table 1-1).

Table 1-1. Price comparison of white products, bitumen and fuel gas.

Product	Product price (\$/GJ)	Product price (\$/bbl)
White products, e.g. naphtha	22	100
Bitumen	15	60
Fuel gas	3.50	33

Catalytic conversion is proposed to be a pathway to make use of these gases. Integration of bitumen upgrading with a pyrolysis gases conversion system can create new opportunities to convert lower value compounds to higher value products.

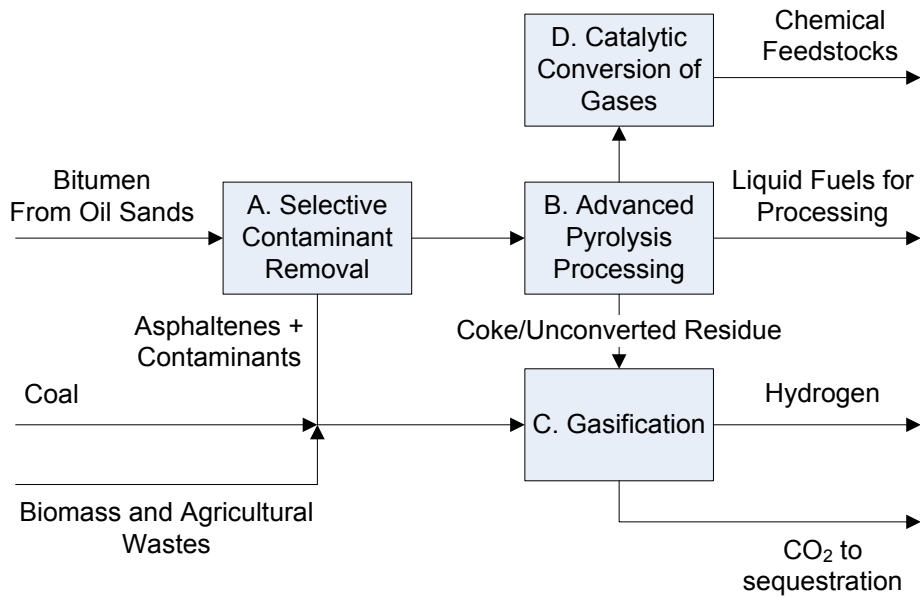


Figure 1-1. Vision of advanced bitumen processing

The present study will investigate the conversion of the light products from cracking of oil sands to more valuable, hydrogen-rich materials to maximize the fuel yield. This step aims to increase the liquid yield from the low temperature pyrolysis processes. The gases obtained from the pyrolysis processes are usually composed of light hydrocarbons including paraffins, olefins, and some aromatics, as well as heteroatom containing species, such as sulphur and nitrogen containing compounds. The task will therefore be the catalyst identification, screening, and evaluation of its potential to convert pyrolysis gas into liquid products. The ultimate goal is application. The key catalytic reactions identified so far are combination of oligomerisation (OLI), hydrogenation (HYD), dehydrogenation (deHYD), oxidation (OX), and aromatization (ARO) (Figure 1-2). These processes are not mutually exclusive and might be required in combination to achieve the maximum yield. The order and combination of these reactions depend on the composition and condition of the gas. In the present study only some of these conversion processes will be studied.

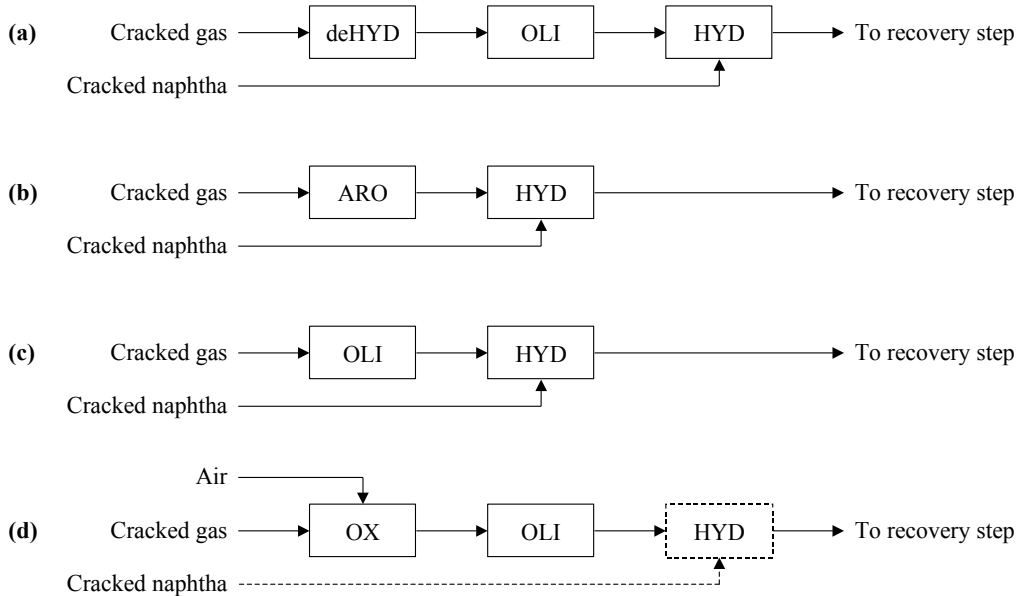


Figure 1-2. Potential strategies for catalytically converting cracked gas into liquids

1.2. Objective/purpose

The project goal is to evaluate multiple catalyst systems for the pyrolysis gas conversion. The focus of the work was on olefin oligomerisation and oligomerisation at conditions where aromatization becomes a significant side-reaction. Some work was also performed that had the potential to combine dehydrogenation with oligomerisation. These are proposals (a), (b) and (c) in Figure 1-2, but excluded the final hydrogenation step.

In the second chapter, with the purpose of catalyst identification, a review was done on all the catalysts, which have already been employed for similar purposes. Typical catalysts to consider are acid catalysts including silica-aluminas, and zeolites. Based on the review, zeolites were selected as candidate catalysts for the investigations as they are robust catalysts, which are active at lower temperatures than amorphous catalysts.

Three experimental investigations were performed:

(1) Catalyst evaluation in batch condition: four types of zeolites were tested in batch reactors, and the most effective one was selected for more detailed analysis in a continuous flow reactor. This work is described in Chapter 3.

(2) Detailed investigation of most promising catalyst in a continuous flow reactor: the catalyst that was identified to have the best performance by batch experiments, was tested for different mixtures of sample gases in a flow reactor. The continuous flow studies were performed since there are plenty of limitations with batch reactor evaluation of catalysts. This work is explained in Chapter 4.

(3) Improving catalyst properties by metal incorporation: based on the outcome of the continuous flow reactor studies, strategies were explored to improve the product by loading metals. Other less acidic supports were also tested in this section. This work is illustrated in Chapter 5.

2. LITERATURE REVIEW ON OLIGOMERISATION

Abstract

In this chapter, the approach is to investigate the current knowledge regarding oligomerisation, catalysts applied for gas to liquid conversion, main application of each class of catalysts, and their optimum reaction conditions. After presenting a brief description of all classes of catalysts in the first section, MFI-type zeolite and its incorporation with metals will be discussed more specifically at the end of the chapter.

Keywords: Oligomerisation, acid catalysts, zeolites, ZSM-5, metal incorporation

2.1. Introduction

In every petrochemical plant, considerable quantities of low chain hydrocarbons are generated [1]. In each fluid catalytic cracking (FCC) unit, a huge amount of low quality liquefied petroleum gas (LPG) is produced due to the intense operating conditions [2]. Ethylene, propylene, C₅-C₇ alkenes, and some heavier olefins are the main olefinic components of the stream coming out of FCC. Oligomerisation of these compounds can produce dimers, trimers, etc., which are valuable compounds in gasoline or diesel fuels [3]. Oligomerisation is usually carried out in the presence of a catalyst, which could be acid catalyst, zeolite, supported phosphoric acid or nickel [4].

Oligomerising by acid catalysts was first used in petroleum industry in 1930's. During these reactions gasoline-range iso-olefins (C₆-C₁₀) were produced by using phosphoric acid impregnated on kieselguhr, a natural silica-rich material. Later zeolites were also studied to be used as catalysts. Shape-selective zeolites (zeolites which control the configuration of the product by their pores) have the advantage of more selectivity in producing liquid products. This resulted to MOGD process (Mobil Olefin to Gasoline and Distillate), which employs ZSM-5

catalysts to convert low molecular weight olefins to higher molecular weight ones [4].

At higher temperatures ($>350\text{ }^{\circ}\text{C}$), reactants may undergo various reactions, such as isomerisation, disproportionation, aromatization, or cracking, which result in a wide spectrum of products. At lower temperatures, these processes also occur, but at lower orders of magnitude. Oligomerisation of low molecular weight alkenes produces liquid fuels, while higher molecular weight ones result in various lube oils. The unsaturated products are then hydrogenated to promote their oxidative stability, or they are consumed in other chemical processes [4].

2.2. Basics of oligomerisation reactions

Oligomerisation is establishing larger molecules from only few monomers, in contrast to polymerization, through which many molecules are combined together. When $n=2$, it is called dimerisation, whereas for $2 < n < 100$ and $n > 100$, it is called oligomerisation and polymerization, respectively [5].

Oligomerisation takes place in the presence of a catalyst, and includes two steps: propagation (chain growth), and elimination (hydrogen transferring from a β carbon to the catalyst center). If k_p and k_e show the rate constants of propagation and elimination, then for polymerization $k_p \gg k_e$, for dimerisation $k_p \ll k_e$, and in case of oligomerisation $k_p \approx k_e$ [6]. Oligomerisation in some cases only means dimerisation. In older texts, the term ‘polymerization’ is also used instead [7].

Oligomerisation reactions are usually accompanied by other processes. In other words, they are not elementary processes, and several reactions may occur in parallel [4]. The reaction network between OLI and other accompanying reactions is shown in Figure 2-1. OLI happens between two molecules, while double bond isomerisation, skeletal isomerisation, and cracking are monomolecular reactions. Hydrogen transfer sometimes attracts less attention since it mainly happens at elevated temperatures. Aromatics are mostly formed at

temperatures above 300 °C by hydrogen transfer from heavy alkenes (heavier than C₇). Hydrogen transfer from short chain olefins will produce dienes [7].

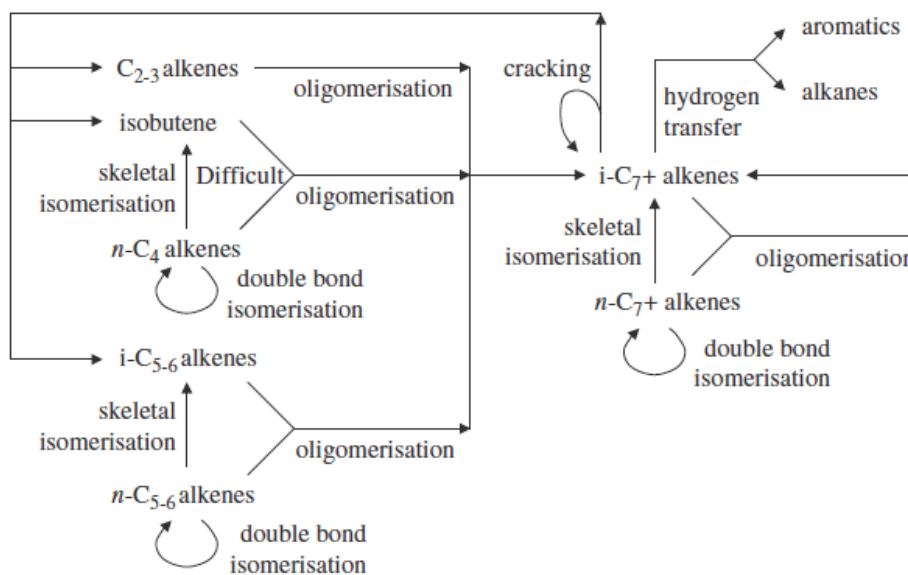


Figure 2-1. Reaction network of the acid-catalyzed reactions happening during OLI [7]

Lack of the information about hydrocarbons makes the prediction of the distribution of the products difficult. As the number of carbon increases, the amount of probable isomers increases drastically [7].

2.3. Mechanism and kinetics of olefin oligomerisation

Type of the catalyst is the main factor that determines the mechanism of the reaction (Figure 2-2). When the process is carried out in the presence of an acidic catalyst, alkene is protonated on the Brønsted acid site. The yielded carbocation is added to another alkene, and possible rearrangements also happen next (Whitemore carbocation mechanism). Solid phosphoric acid (SPA) catalysts behave in a different way. In fact, they form an intermediate phosphoric acid ester when the alkene is adsorbed on the surface of the catalyst. The stability of this intermediate and the transition states control the final products. Some organometallics catalyze the oligomerisation through 1,2-insertion and β-hydride

elimination. Oligomerisation can also take place in the presence of free radicals through non-catalytic pathways [7].

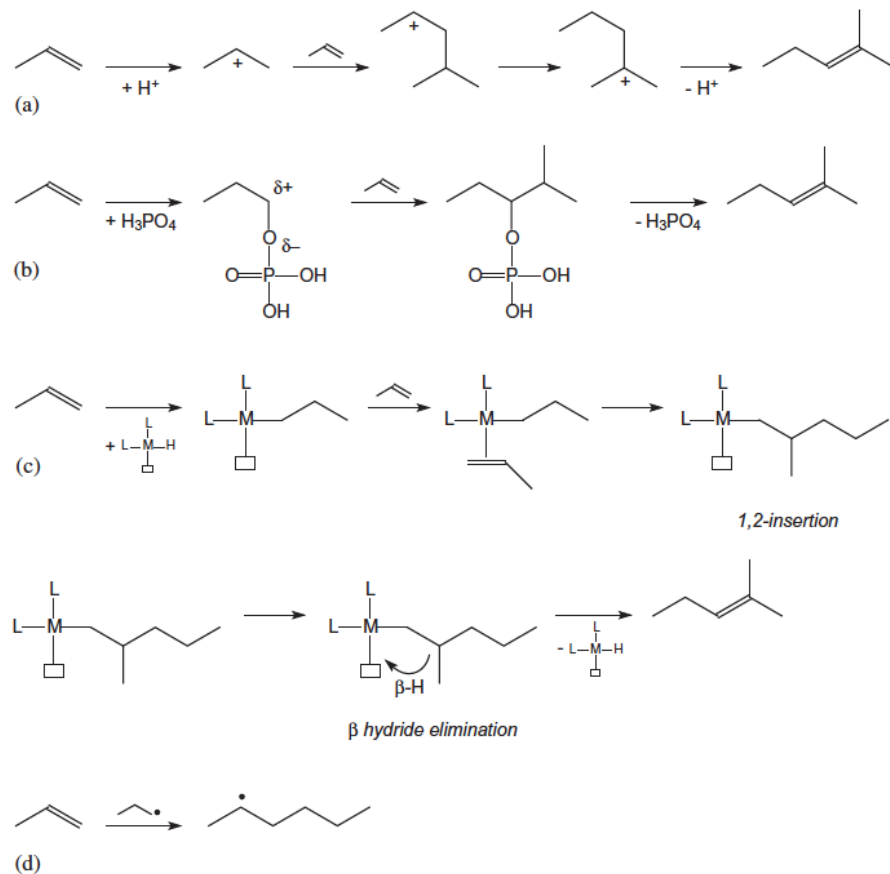


Figure 2-2. (a) Classic Whitmore-type carbocation mechanism (b) ester-based mechanism (typical of phosphoric acid) (c) 1,2-insertion and β -hydride elimination (typical of organometallic catalysis) (d) radical propagation [7]

2.4. Catalysts applied for oligomerisation

2.4.1. Solid phosphoric acid catalysts

Solid phosphoric acid (SPA) catalysts are traditional commercial catalysts used for the OLI of $\text{C}_2 - \text{C}_5$. Operating temperature of these catalysts is normally between 150-245 °C; however lower temperatures have been practised for feed materials containing no C_2-C_3 alkenes. Catalysts usually deactivate with temperature enhancement. In fact, upper temperature tolerance is a function of the stability that catalyst shows for deactivation, while lower temperature limit is set

by formation of stable phosphoric acid esters with the alkenes. Solid phosphoric acid is considered as a very effective catalyst since despite possible fluctuations in the feed; it still produces high-octane olefinic motor gasoline [7].

The biggest deficiency that exists regarding SPA is their short lifetime, which is 6 months and may change with operating conditions [7].

SPA has also been employed mainly for C₃-C₄ oligomerisation. The nature of the feed is an important factor that determines the quality and branching degree of the products. For example, when propene and butene are exposed to the catalysts separately, the products released are different from those obtained from their mixture [7].

It has been reported that during the use of SPA for OLI of C₃-C₄, one can control the catalyst hydration and therefore control the selectivity to diesel range products by changing the water content and temperature of the feed. In order to keep the catalyst activity, a small amount of water should be added to the feed material. Mechanism of the catalyst is not illustrated in terms of Brønsted acid sites; instead the released phosphoric acid ester best describes the mechanism. The reactivity of the alkene is a function of both the stability of the phosphoric acid ester and the stability of the carbocation. For instance, ethene needs high temperature for OLI due to the formation of thermally stable esters (at about 200 °C). When propene is the reactant, the ester tolerates temperatures up to 125 °C. However, this is not true for n-butenes and the process takes place at room temperature. The thermal stability of the esters decreases as the chain length increases [7], [8].

It should be noted that SPA is an environmentally benign catalyst, since only kieselguhr and phosphoric acid which are natural materials are used to produce it, and at the time of disposal it is combined by ammonia which results to the ammonium phosphate fertilizers [8].

In one of the most popular type of non-zeolitic acid catalysts, which are used in olefin oligomerisation, phosphoric acid supported on kieselguhr is used. This process, called Catpoly, has universal application in converting propene/butene to gasoline. Increasing the concentration of the acid improves the conversion of alkene to products. Products' molecular weight increases, as well. In another words, the major fraction of the products changes from trimers to tetramers. In addition, wider distribution of products is observed. However, non-zeolitic acid catalysts are not always applicable for temperatures above 130 °C due to their poor thermal stability [9].

2.4.2. Heteropolyacid (HPA) catalysts

Although there are plenty of heteropolyacid catalysts, the Keggin type is the prominent category. The acidic strength of the most common ones is in this order: $H_3PW_{12}O_{40} > H_4SiW_{12}O_{40} > H_3PMo_{12}O_{40}$. Despite Keggin type catalysts that are thermally stable, other kinds of catalysts are not that stable and therefore cannot be used at temperatures more than 150 °C. OLI of propene, isobutene and mixtures of n-butenes and isobutene have been studied over HPA. Conversion of isobutene takes place at low temperatures (sometimes at -5 °C). The products are lighter at higher temperatures [7].

In order to test the use of HPA in OLI of propene, several kinds of HPA catalysts were employed to yield distillate products. It has been reported that conversion decreases when the feed materials are not dry [7].

2.4.3. Zeolites

Brønsted acid surface sites are the main parts of the zeolites, which initiate oligomerisation. Therefore, the density, acidity and accessibility of these sites are important factors [10]. Among lots of silica-alumina-based materials known for alkene OLI so far, the pentasil zeolite ZSM-5 (MFI) is the most important one. Important parameters in the catalyst performance are: the procedure that one goes

through for the preparation, pre-treatment of the catalyst, and also the reaction condition [7].

The three dimensional structure of ZSM-5 catalyst has sinusoidal ($5.1 \times 5.5 \text{ \AA}$) and straight ($5.4 \times 5.6 \text{ \AA}$) pores. Since it has small pores, it results in low-branched products. Formation of coke precursors and bulky hydrocarbons should be prevented to keep ZSM-5 away from deactivation. The ratio of Si/Al is an important factor that changes selectivity and activity. Ultimately for better yield, one should set a balance between the reaction condition, catalyst's features and type of materials needed from the reaction [7].

Garwood was the pioneer in studying OLI over H-ZSM-5, and after him it was investigated a lot by others. Table 2-1 shows the equilibrated composition of the products at high temperatures [7].

Table 2-1. Equilibrium distribution of the products obtained from the reaction of different alkenes over H-ZSM-5 at 270 - 275 °C and alkene partial pressure of 5-15 kPa (WHSV 0.5 - 0.9 h⁻¹) [7]

Product	Alkene feed material				
	Ethene ^a	Propene	Pentene	1-Hexene	1-Decene
C ₂	0	<0.1	<0.1	<0.1	<0.1
C ₃	11	8	10	9	4
C ₄	20	28	20	20	13
C ₅	21	30	27	23	26
C ₆	13	13	15	16	20
C ₇	12	11	11	10	17
C ₈	8	6	7	8	8
C ₉	8	3	5	6	7
C ₁₀ and heavier	7	1	5	8	5

^a Based on converted ethene; product contained 47.5% ethene.

During OLI over H-ZSM-5, limited cracking happens at low temperatures (usually lower than 230 °C). At higher temperatures, there is equilibrium between distributions of different alkenes (Table 2-1). The reaction has no sensitivity to the distribution of carbon numbers in the feed when feed contents are at equilibrium. Indeed, temperature, pressure and the recycling of the product are key factors in determining carbon number distribution [7].

In general, H-ZSM-5 gives better yield at higher temperatures and higher partial pressure of alkenes. Typically, higher temperatures accelerate parallel reactions, like cracking, copolymerization and disproportionation. These reactions accept no influence from pressure enhancement though. By changing operation conditions of OLI over H-ZSM-5, products can be shifted from mainly naphtha to mostly distillate products. Moderate temperatures (200-220 °C) with the total pressure of 5 MPa can maximize distillate range products, while higher temperatures (up to 300 °C) and lower total pressures of about 3 MPa will lead to naphtha production. Fuel properties gained from OLI over H-ZSM-5 at different process modes are listed in Table 2-2 [7].

The quality of the motor gasoline gained from OLI over H-ZSM-5 improves with catalyst age. As the catalyst deactivates, strong acid sites available for OLI and also cracking decrease, while double bond IS and skeletal IS are not affected. Consequently, C₅-C₆ alkenes in the feed are isomerised instead of oligomerised, and the octane number increases [7].

In the OLI of ethene, propene, and isobutene over template and non-templated H-ZSM-5, it was observed that in the case of ethene, the conversion is greater when non-templated one is used, while for the other two it has opposite order [7].

Table 2-2. Product yielded from C₃-C₆ feed (82% alkenes, 15% alkanes, 1.5% aromatics and 1.8% oxygenates) over H-ZSM-5 [7]

Products	Product yield (mass%)	
	Naphtha mode	Distillate mode
C ₁ -C ₃	4	1
C ₄	5	2
C ₅ -165 °C naphtha	-	15
>165 °C distillate	-	82
C ₅ -200 °C naphtha	84	-
> 200 °C distillate	7	-

The OLI of propene using H-AlMFI at 200-550 °C and absolute pressure of 13 kPa was investigated. It has been reported that conversion increases with

temperature, and the optimal temperature is 300 °C. Hexene is one of the main products in this case [7].

Beside lots of literature found on H-ZSM-5, there are some other zeolites used for OLI, such as H-Y (FAU), H-Mordenite (MOR), H-A (LTA), H-Beta (BEA), H-Offerite (OFF) and H-Omega (MAZ) [7].

Ferrierite (FER) is one of the well-known selective zeolites used for skeletal IS of butene to isobutene, it has a low selectivity for OLI though. One of the suggested mechanism for the isobutene production is that butene dimerises to the C₈, which is later cracked to isobutene. Shape selectivity of the zeolites inhibits migration of C₈ alkenes, so branched alkenes heavier than C₈ cannot be produced, and they are cracked instead [7].

Although zeolite catalysts have strong acidity, they are not usually employed for temperatures below 200 °C. This is because of rapid deactivation in low temperature ranges. This deactivation is due to the formation of heavy oligomers, which are hardly removed from the catalyst surface. At higher temperatures, these heavy alkenes are cracked and moved away [7].

Activity of the catalysts depends on their acid sites. It has been observed that high-silica zeolites with strong Brønsted acid sites can produce linear oligomers. In these reactions, ethoxy groups are intermediates for ethylene oligomerisation. Ethylene over H-ZSM-48 produces shorter chains and also shows lower conversion [4].

Experiments on ethylene and propene oligomerisation show the same product distribution for both of them. The similarity is because for both case the reaction stops after the zeolite pore gets completely filled. The only difference is in the initiation temperature, which is higher for ethylene. Temperature effect is a problem in oligomerisation of ethylene. In order to overcome this problem to some extent, a multistage process in presence of a reducing compound like

hydrogen with a bifunctional metallic zeolite was proposed. Also, co-feeding of water has been used to improve the reaction [4].

At present, MOGD process is one of the most important methods of oligomerisation for small alkenes to liquid fuels, which is mostly used in industry. ZSM-5 type zeolite was tested in this process with the specific molar ratio of silica ammonia. This process was done in two modes: Distillate mode (fixed bed, 190-310 °C, 4-10 MPa, WHSV= 0.5-1), which resulted in a product of 80% distillate fuels with a cetane number of 55. The second mode was gasoline mode (285-375 °C and 0.4-3 MPa); during this mode C₅₊ was yielded with reasonably high octane number. By changing the reaction condition, one can change the gasoline to distillate ratio from 0.12 to 100. Also, viscosity of the lubricant product of light alkenes can be improved by passing them over H-ZSM-5 at low pressure and in the temperature range of 200 to 300 °C. It should be pointed out that the initial reactant has no effect on the degree of branching [9].

If Ni and/or Zn are loaded onto ZSM-5 by using ion exchange or impregnation, the temperature that the reaction is carried out at, can be decreased drastically. Ethene can react over ionic Ni-exchanged H-ZSM-5 at 2.9 MPa and temperature of 100-450 °C. Although Ni makes no effect on the activity of propene, for ethene it can decrease the temperature from 300 °C, temperature needed over H-ZSM-5, to 100 °C [9].

Acid zeolites HY, HM, and H-ZSM-5 have been investigated in oligomerisation of ethene, propene and butenes by UV-vis and infrared. The observations have shown that HY can produce highly branched alkenes. The effect of high temperature on the performance of these catalysts was investigated. The alkenes were converted to coke over HY at high temperatures, and they were transformed to aromatics over H-ZSM-5 and first to aromatics, then to coke over HM. If we calcine them at temperatures higher than 650 °C, much less coke will be formed since at that temperature a large portion of the acid sites are Lewis

sites. Strong Brønsted sites get poisoned, which eliminates the formation of coke and aromatics, letting only oligomerisation proceed [9].

2.4.4. Amorphous silica-alumina (ASA) catalysts

The most significant difference of this kind of catalysts with zeolites is their less regular porous geometry, or in other words, their less crystallinity. There are also some other differences, which make the products yielded from ASA different from those obtained from zeolites. These differences include higher interest in hydrogen transfer, apparent lower acid strength, and the reaction mechanism [7].

During the studies conducted on ASA, it has been observed that these catalysts are useful for Fischer-Tropsch (FTS) feeds, which sometimes include oxygenates. Products obtained from these catalysts usually have higher density than other OLI catalysts. The properties of naphtha depend on the feed components. Short chain alkenes gained from these catalysts show better motor gasoline quality than those captured from the reaction over H-ZSM-5 [7].

In the OLI of C₇-C₁₀ over ASA, the yield is not always constant. It decreases gradually (10% is lost every 50-60 days), as a result of the formation of viscous products and coke, which limits access to the active sites. Thus, the operating temperature should be increased over the time to keep the conversion constant. Other more structured silica-alumina catalysts, such as MCM-41, are also attracting attention for alkene OLI. They have large pores and no geometric restriction. They have not been applied for industrial purposes, yet [7].

There is also some natural clay that can be used as silica-alumina catalysts. Montmorillonite is specifically studied for catalyzing poly-alphaolefin (PAO) lubricants. Particularly, aluminium nitrate-treated montmorillonite has found to be very effective in the OLI of C₁₄. Montmorillonite and Al³⁺-, Zr⁴⁺-, and H⁺-exchanged montmorillonites when operating at high temperatures and low pressures show high activity for the OLI of 1-decene. Their activity is in this

order: montmorillonite-H > montmorillonite-Zr > montmorillonite-Al > montmorillonite-K10 > montmorillonite-Na. Their activity has direct relation with the acidity [7].

Nickel has been applied to improve the properties of silica-alumina in OLI of ethene, propene and butene. It should be noted that these catalysts are so sensitive to moisture. It has been observed that when NiO/SiO₂-Al₂O₃ adsorbs just 0.5% water, it deactivates rapidly. Whereas silica-alumina catalysts show more activity as they are exposed to water [7]. More information about heterogeneous nickel catalysts will be given later in the text.

2.4.5. Silico-aluminophosphate (SAPO) catalysts

This kind of catalyst is not very popular in OLI. The study conducted by Vaughan et al. is one of the rare ones in this area, which has investigated OLI of propene over different formulations of SAPO-11. Results, gained from their work, are presented in the table below. Liquid yield in this table is defined as the product mass collected from the period of maximum conversion to half the catalyst lifetime [7].

Table 2-3. Propene oligomerisation over SAPO-11 (AEL)-based catalysts [7]

Catalyst	Maximum conversion (%)	Liquid yield (g _{cat} ⁻¹)	Product distribution (mass %)		
			Dimer	Trimer	C ₁₂ ⁺
SAPO-11 (powder)	78	702	56.3	22.3	21.2
SAPO-11 (extruded)	84	416	57.5	28.9	13.6
SAPO-11 (pellet)	95	1368	65	27	8
SAPO-11 (mild steaming)	93	1674	53.7	27.7	18.6
SAPO-11 (severe steaming)	89	1762	70.3	19.5	10.1
SAPO-11 (silanised)	33	12	69.8	23	7
SAPO-11 (acid washed)	55	35	47.9	24.4	27.7
Ni-SAPO-11	60	16	56.2	30.4	13.4
Fe-SAPO-11	60	43	60.4	26.2	13.4
Co-SAPO-11	65	47	73.3	20.8	5.8
Mn-SAPO-11	59	680	54.9	20.9	24

There are three forms of unmodified SAPO-11 catalysts: pelleted, extruded, and powdered, from which pelleted one has shown the best activity. Incorporation of Ni, Co and Fe into the catalyst decreases the yield. Silanising and acid washing decrease SAPO-11 activity, as well [7].

SAPO-5 (AFI), SAPO-11 (AEL) and SAPO-34 (CHA) were applied for the skeletal IS of butene. It has been reported that the extent of OLI of butene is affected by the catalyst porosity. Therefore, large pore SAPO-5 becomes important in OLI, medium-pore SAPO-11 attracts attention for double bond IS and skeletal IS. However, SAPO-34, which has small pores, doesn't favor OLI [7].

2.4.6. Sulfated zirconia catalysts

Some sulphated metal oxides, such as sulphated zirconia ($\text{SO}_4^{2-}/\text{ZrO}_2$), are solid catalysts that have the property of superacidity. Thus, they can substitute liquid acid catalysts. Investigations on these catalysts have mostly considered dimerisation of butene and OLI of hexene and heavier alkenes [7].

It has been observed that sulphated zirconia has better activity and stability than several zeolites during the OLI of 1-hexene and 1-octene at 100 °C. Only dimers and trimers can be produced over these catalysts. Reports indicate that sulphated zirconia catalysts are not suitable for polyalphaolefin production [7].

2.4.7. Acidic resin catalysts

These catalysts attracted most attention when the legislation of some regions forbade using of methyl tert-butyl ether (MTBE) as an oxygenated fuel component. MTBE is produced by etherification of isobutene with methanol over acidic resin catalysts. Isobutene is dimerised at the same time as a side reaction. By increasing the ratio of isobutene to methanol, one can enhance the selectivity to isobutene dimerisation. MTBE is also converted to dimerised isobutene, simultaneously. Consequently, use of acidic resin catalysts has two benefits:

reusing MTBE to produce isobutene dimerisation unit, and to improve octane number by adding high-octane isobutene dimers to the motor gasoline. During OLI of isobutene by means of acidic resin catalysts, dimers, trimers and heavier oligomers can be found in the product [7].

Typically acidic resin catalysts react with polar compounds vigorously because sulfonic acid groups have strong polarity. Thus, polar solvents, such as alcohols or water, can be applied to control temperature and selectivity. In fact, these compounds manipulate the acid strength of the catalyst by solvating acid groups [7].

2.4.8. Heterogeneous nickel catalysts

Nickel catalysts have been reported in several cases as useful catalysts for alkene oligomerisation. Nickel supported on aluminosilicates, like silica-alumina, silica, layered alumino-silicates and zeolites such as mordenite, zeolite- Y, and ZSM- 5, is specially applied in dimerising ethene, propene and butene [9].

A solution obtained from mixing sodium silicate with a solution of aluminium and nickel nitrate will result in a catalyst of nickel oxide- silica-alumina, which is a catalyst for ethene and propene oligomerisation. Silica-alumina supports have trimerising activity. Nickel changes this property to dimerisation instead [9].

Montmorillonite and catalysts of the same type, which nickel is comprised with, whether supported or as a constituent are also effective catalysts. Nickel on mica-montmorillonite is among the active catalysts for oligomerising propene and butene [9].

One of the catalysts used for propene and butene oligomerisation is produced by the impregnation of a support, such as alumina, with an aqueous solution of nickel nitrate hexahydrate. After dryness and calcining of the catalyst, it is activated with diethyl aluminum chloride and anhydrous aluminum chloride [3].

Among $\text{NiO-ZrO}_2/\text{SO}_4^{2-}$, $\text{NiO-ZrO}_2/\text{PO}_4^{3-}$ and $\text{NiO-ZrO}_2/\text{BO}_3^{3-}$, which have been studied for the dimerisation of ethene, sulphuric acid treated one was the best. In order to produce these catalysts, nickel chloride-zirconium oxychloride mixture is coprecipitated and then treated with H_2SO_4 , H_3PO_4 and H_3BO_3 . Catalyst will be inactive if they are not treated with acids. Acidity of all $\text{NiO-ZrO}_2/\text{SO}_4^{2-}$, $\text{NiO-ZrO}_2/\text{PO}_4^{3-}$ and $\text{NiO-ZrO}_2/\text{BO}_3^{3-}$ were tested. The acid strength of each was found to be $H_0 \leq -14.5$, $H_0 \leq -8.2$, and $H_0 \leq -5.6$, respectively. Superacid is an acid with $H_0 = -11.93$, which is the strength of a 100% H_2SO_4 . Therefore, $\text{NiO-ZrO}_2/\text{SO}_4^{2-}$ is considered as a solid superacid. Superacidic properties are assigned to the nature of the double bond $\text{S}=\text{O}$ in the complexes formed from the interaction of NiO-ZrO_2 with SO_4^{2-} . In fact, $\text{S}=\text{O}$ bond has inductive effect on the complex which makes both Lewis and Brønsted sites stronger. Acid strength of NiO-ZrO_2 with no anions is so weak to be active enough for the dimerisation reaction at room temperature ($H_0 \leq -3.0$). However, it shows a little activity for polymerization. When it is treated with sulphuric acid, it shows low activity for dimerisation. Generally, it is concluded that a low valent nickel ion interacted with an acid both together can catalyze dimerisation [2], [3].

2.4.9. Homogeneous nickel catalysts

Homogeneous catalysts have been studied a lot for alkene oligomerisation. One of the single-component which is really powerful in oligomerisation of ethene to linear alkenes is sulphonated nickel ylide organometallic complex [9].

PdCl_2 and RhCl_3 are more selective for dimerisation of ethene; however Ni is preferred since it generally shows more activity and also it is cheaper. Ni complexes dimerise alkenes in three stages: initiation, monomer insertion and transfer reaction (chain termination) [9].

The environment, that nickel species are acting in, directly affects the dimerisation reaction. Properties that may influence the process are: donor-

acceptor strength of the surroundings, steric crowding, and electronic charge of the nickel [9].

Figure 2-3 shows the general idea of propene oligomerisation. The first step, which is insertion into Ni-H bond, is mainly depending on the kinetic of the reaction, while the second step is related to the nature of the ligand [9].

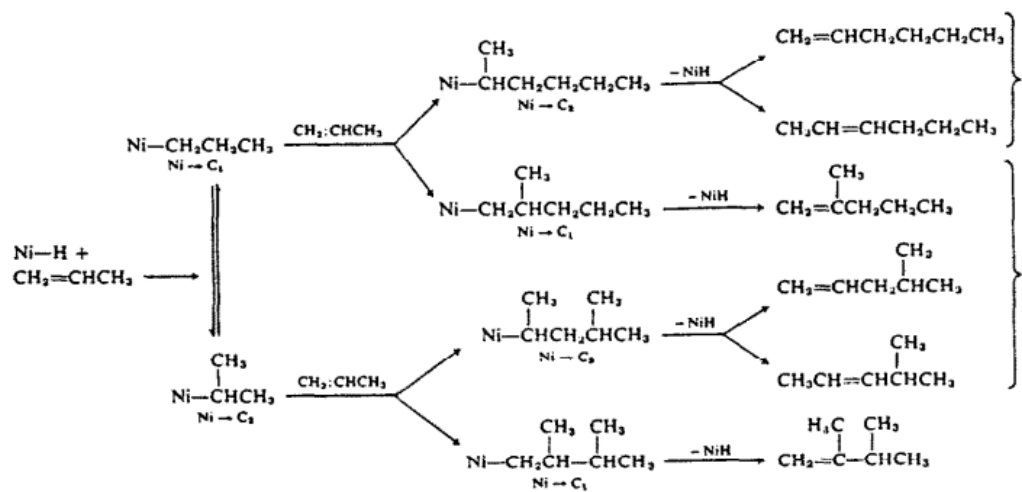


Figure 2-3. Mechanism of propene oligomerisation [9]

The impacts that ligands can have on the nickel based catalysts have been studied in several investigations. Most of the transition metal catalysts make branched-oligomers, that's why a vast part of studies have focused on the effect of ligands on the linearity of the products. Chelate agents have been employed to produce linear α -alkenes. Phosphorous-oxygen and arsine-oxygen are examples of this kind of ligands [9].

Another use of homogeneous nickel catalysts is in catalyzing the reaction between ethene and tri-(C₂₋₂₄) alkylaluminium to produce triethylaluminium and C_{2-C24} α -alkenes [9].

There are many advantages in supporting a homogeneous catalyst on a solid phase without getting the activity lost. One type of the catalyst used in propene and ethene dimerisation is Ni (I) trialkylphosphine (TAP) supported on silica. The

TAP produces the ligands that are needed for oligomerisation. Propene oligomerisation is done only over TAP free monovalent catalysts or those, which have only one ligand. In case of ethene, presence of basic phosphine ligands causes an enhancement in electron density on the nickel, and the primary reaction products can be desorbed much more easier [9].

Dimersol process is one of the fewest processes, which makes use of homogeneous organometallic compounds that is why it is so sensitive to impurities, which are capable of making complexes with Ni. The mechanism of the OLI reaction catalyzed by a nickel-based Ziegler-type catalyst is 1,2-insertion and β -hydride elimination [7].

2.4.10. Metals other than nickel

Nickel is not the only metal that is effective in catalyzing OLI. Trimerisation and tetramerisation of ethene over chromium-based ones have also been reported which are very useful in FTS technologies [7]. Dimerisation of propene is also reported over ReO_3 and WO_3 [9].

Cobalt supported on the activated carbon can produce linear oligomers from alkenes. Carbon is an important ingredient, which cannot be substituted with alumina and kieselguhr. Cobalt concentration is an important factor [9].

Alkali metals may be other potential catalysts. Silicates of alkali, alkaline earth metals, α -aluminas and graphite are possible supports. It's better for the support not to be porous. $\text{K}/\text{K}_2\text{CO}_3$ is a strong propene dimeriser at 150 °C and 10 MPa. 4-methyl-1-pentene makes 79% of the products [9].

Sulphuric acid and phosphoric acid are other catalysts, which were used historically. Sulfuric acid is still applied in aliphatic alkylation of isobutene with other alkenes, but it is not considered as a major one in OLI. Finally, boron trifluoride (BF_3) is another liquid-phase catalyst applied in OLI technologies [7].

2.4.11. Metallocene

Ziegler-Natta catalysts, titanium chloride combined with alkylaluminum, is one of the common catalysts in manufacturing polyolefins. These heterogeneous catalysts are very active and show high specificity in oligomerisation. However, controlling and homogenizing oligomerisation needs definite attention. Metallocenes of group 4 have long been used for olefin oligomerisation. These catalysts are also effective in copolymerization of ethylene with α -olefins. The type of the comonomer can manipulate the length of the side chain. They can also catalyze ethylene to produce linear low-density polyethylene (LLDPE). Propylene and styrene polymerization are other applications of Metallocene [1].

2.5. Oligomerisation over H-ZSM-5

2.5.1. General information

Nowadays, catalysis by zeolites has attracted much attention specially when talking about hydrocarbon formation and conversion [15]. Zeolites generally have vast application in different fields including disproportionation of toluene, conversion of methanol to gasoline and olefins, xylene isomerisation, fluid catalytic cracking (FCC), isomerisation, dewaxing, alkylation, transalkylation, hydrocracking, hydrodecyclisation, and olefin conversion to distillate and gasoline [12], [14].

Zeolite ZSM-5, which was first synthesized in 1970's, has shown good performance in the production of distilled fuels [5], [7]. It is the most known zeolite catalyst applied for the olefin OLI, and in fact, its invention was primarily for the development of the MOGD processes [13], [15].

The major characteristic of ZSM-5, which makes it special, is its product selectivity. This feature leads the feed materials to a well-defined iso-olefinic product in the MOGD process [15].

The distillate to gasoline ratio of the products, obtained from the ZSM-5-catalyzed reactions, can be manipulated by adjusting the temperature. Alkenes go through multiple oligomerisation and recracking steps. Compounds with carbon numbers of six and more are first cracked and then again oligomerised. The nature of the feed has no effect on the skeletal branching based on the work done by Garwood for C₂-C₁₀. Typically, there is a methyl branching for each five carbons in a chain. ZSM-5 has two advantages over other zeolites with wider pores: first, its slower deactivation due to the steric suppression of the bulky coke precursors inside the pores; and secondly, its capability to be synthesized at lower Si:Al ratios and consequently lower acidity, which brings lower deactivation [15], [16].

During the process of propylene conversion over H-ZSM-5, four distinct reactions happen. First, propylene is oligomerised to C₆, C₉, C₁₂, etc. These materials then go through isomerisation and cracking reactions. And finally, they are repolymerized to heavier iso-olefins (Figure 2-4). As a result of having continuous forward (OLI) and backward (cracking) reactions, a specific carbon number distribution of products is formed, which is independent from the starting alkenes. This observation was also reported elsewhere by Garwood [15], [16].

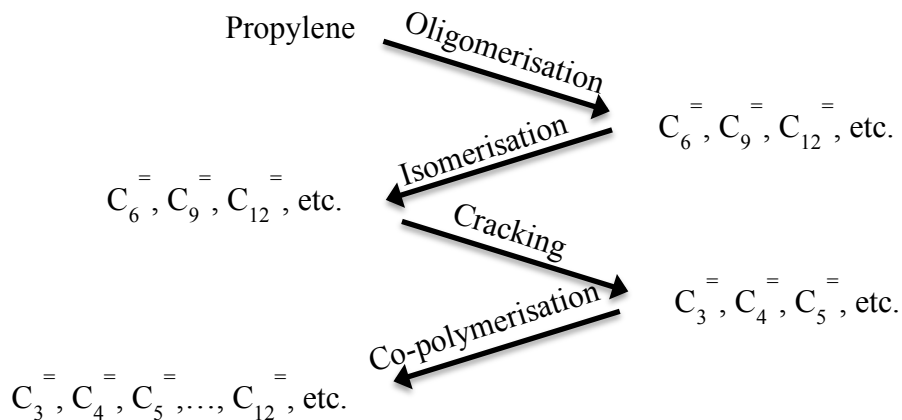


Figure 2-4. Reaction of propene over H-ZSM-5 [18]

Kojima et al. tried to find the optimum condition for ZSM-5 oligomerisation and showed that a Si/Al ratio of 40 and catalyst cycle length before regeneration

of 30 days are the most ideal reaction condition. The product spectrum mostly depends on the reaction temperature. Arranging reactors in series does not affect the products' carbon number distribution [11].

Activity of the ZSM-5 increases with a decrease in the crystallite size, because as the size of the crystallites increases, the bulk of the acid sites will become unavailable. It is based on the fact that the reaction takes place close to the surface of the zeolite. This is due to the probable faster surface adsorption than diffusion into the channels, or the situation of aluminium atoms, which are close to the crystallite surface [11].

Most of the researches, done so far, show a reverse relation between activity and Si/Al ratio. However, in some cases for every specific purpose, such as n-hexane cracking and m-xylene isomerisation, an optimum Si/Al ratio of 25 and 17 is reported, respectively [14].

O'Connor and his co-workers also explored the effect of Si/Al ratio and synthesis time on catalyst activity. According to their research at 300 °C and 50 atm, optimum catalyst performance was observed at Si/Al=40 and synthesis time of 30 days. The relative activity of propene, 1-butene and 1-hexene as feed for ZSM-5 has this order: 1-butene > propene > 1-hexene. The main oligomer formed from the reaction of the all gases was C₁₂ [14].

Beside ZSM-5, other porous acid catalysts, including other zeolites (H-ZSM-22, Al-TS-1, H-ZSM-57), zeotypes (SAPO-11), and mesostructure materials (Al-MCM-41, Al-MTS, Al-SBA-15), and amorphous silica-alumina have also been practised for olefin OLI [13].

2.5.2. Structure

Molecular sieves generally have three-dimensional structures consisting of silicon-oxygen, and metal-oxygen tetra- or octahedral configuration among which the size of the micro-pores changes periodically. Acid sites, which are part of the

structure, are mainly because of the imbalance of the charges of oxygen and metal atoms [12]. Structure consists of a series of channels in two directions. The protonic acid site carries out the reaction. However, shape and diameter of the zeolite influences the product's shape and size [15]. The MFI-type zeolite (ZSM-5) has 10 membered rings with two kinds of microporous channels (0.51×0.55 nm, and 0.54×0.56 nm) (Figure 2-5) [13].

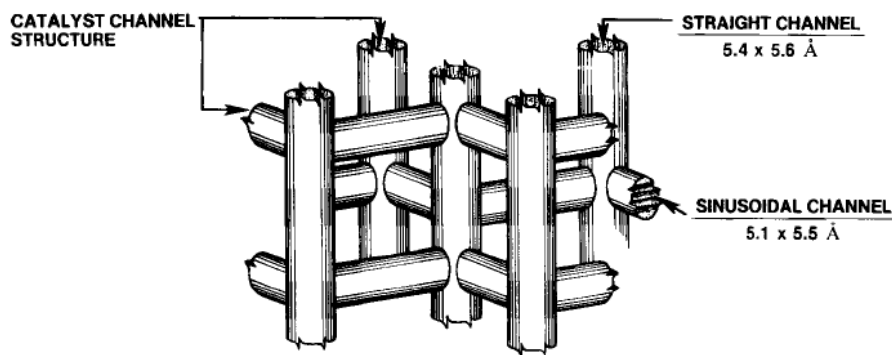


Figure 2-5. Morphology of ZSM-5 [15]

Although product structure is controlled by pore size, the operating condition determines the molecular weight of the products. Considering the reaction from the thermodynamic perspective, increasing pressure always results in higher molecular weights. However, temperature has a different effect. In fact, increasing temperature first leads to higher molecular weights, but at a certain point cracking is the predominant reaction, which cause a decrease in the products' molecular weight [15].

Si/Al ratio has been introduced as a determining parameter in the reaction yield, as the acid site concentration has direct relation with the Al concentration. In the investigation conducted by Amin et al., application of H-ZSM-5 for the conversion of palm oil vapors to liquid hydrocarbons has been studied. Among three ratios of $\text{SiO}_2/\text{Al}_2\text{O}_3$ tested in this study ($\text{SiO}_2/\text{Al}_2\text{O}_3 = 30, 50$, and 70), the ratio of 30 is suggested as the most effective one for the gasoline production [17].

2.5.3. Metal-loaded ZSM-5

In an attempt to improve the properties of H-ZSM-5, ion exchanging of the acidic protons of the catalyst with various metals was conducted [14]. Loading metals on zeolites combines the shape selectivity and high metal dispersion together, and results in an active catalyst, which is highly reactive for hydrogenation and Fischer-Tropsch synthesis [18].

Rare earth zeolites are frequently mentioned in the literature as cracking agents. In a Mobil-study by Owen et al., utilization of rare earth exchanged ZSM-5 for the transformation of olefins into gasoline and distillate is discussed. It is unlikely that incorporating of such element is for the thermal stability improvement, since ZSM-5, itself, has a high stability at high temperatures. In the report from Chen et al. on the rare-earth exchanged zeolite X, the catalyst has shown significant cracking property even at temperatures as low as 250 °C. This implies that one possible reason for the incorporation of these ions into the catalyst might be the ability they bring for the catalyst to crack heavy coke precursors at low temperatures, resulting in the longer lifetime for the catalyst [14].

Loading La on the ZSM-5 has no effect on the free pore volume of the catalyst as well as no influence on the increase in steric hindrances against the passage of linear molecules. TPD results of La-ZSM-5 show that the number of strong sites decreases with La incorporation, and simultaneously weak sites increase. As the La content of the catalyst increases, its activity for propene OLI and hexane cracking decreases. In the case of hexane cracking, increased selectivity towards heavier products is also another effect of La incorporation. However, it doesn't have any effect on the catalyst deactivation. Sodium exchanging also has the same effect as metal exchanging with Al-sites decreases the acid site concentration. Presence of water in the feed causes an increase in the

temperature required for reaction initiation. But, at the same time the degree of OLI activity decreases [11], [14].

In the comparison done on the performance of boron modified and unmodified ZSM-5 for the high pressure OLI of propene, unmodified ZSM-5 showed the longer cycle time. B-ZSM-5 was only active for temperatures above 300 °C. Product distribution was not affected by the presence of boron, and was primarily temperature dependent. Activity of the catalyst was reduced with boron incorporation. Activity was a function of loading method when the boron content was less than 0.4 wt% [5]. With those contents of metal, Boron-ion-exchanging reduces the propene oligomerisation activity, which is due to the pore diffusivity reduction. However, it keeps the acidity constant. Boron-impregnation has no influence on the activity and acidity [11].

Bababeva et al. carried out efforts to make use of by-product hydrocarbons, mainly C₁-C₃ alkanes, produced during refining and oil recovery processes. In order to achieve that, they attempted to convert those by-products to benzene, propene, and alkylarenes. With the purpose of making use of light alkanes, and simultaneously producing valuable hydrocarbons, alkylation of benzene by the lower hydrocarbons was suggested. Three approaches have been reported with this regard: (a) aromatization of methane over molybdenum oxide/H-ZSM-5 at 700-750 °C; (b) C₂₊ alkane aromatization over Ga/Pt/Zn modified ZSM-5 at 550 °C; and (c) benzene alkylation with the same catalysts but at lower temperatures (350-500 °C). One of the catalysts that can facilitate both aromatization of C₂₊ alkanes and benzene alkylation by these light alkanes is alumina-supported catalysts having group VIIIb elements in their structure. In order to make the alkylation of benzene with C₂ and C₃ alkane feasible, the H-form of a zeolite and a component with dehydrogenating property is required. In other words, combination of a dehydrogenating metal with acid sites of a zeolite activates light alkanes reactions [19].

In situ upgrading of vapors yielded from fast pyrolysis of biomass was conducted by applying different catalysts including commercial equilibrium FCC catalyst (E-cat), magnesium oxide, nickel monoxide, zirconia/titania, various ZSM-5 formulations, tetragonal zirconia, titania and silica-alumina. The main purpose of the study was to maximizing the production of high value materials and make use of low value components (similar to the objective of our study). Among all the catalysts, zirconia/titania and ZSM-5 with the highest surface area has been reported to be the most promising catalyst, both for decreasing the amount of oxygenated components and for increasing aromatics. Loading metals (Ni, Co, Fe, Ga) on ZSM-5 increased hydrocarbon yield even more. The worst performance was reported for the FCC catalyst, which resulted in a low carbon to oxygen ratio. This is due to the significant amount of coke that formed on the surface of the catalyst [20]. According to the work done by Kojima et al., cobalt incorporation on ZSM-5 reduces the extent of cracking, but decreases the activity, which is because of the decrease in the pore diffusivity [11].

Production of aromatics by zeolites has been previously suggested as a pathway to convert LPG to liquid materials [12]. Besides the petrochemical value of benzene, toluene, and xylene (BTX), the BTX aromatics are also considered as important industrial materials because of their high octane number. This is the main objective of the study carried out by Guisnet and Gnepp. In their study, they have tried to conduct propane aromatization over Ga/H-MFI. They have shown that Ga reduces the coking/aromatization ratio and makes the removal of coke easier by oxidative treatments. These two, both, depend on the hydrogen pretreatment of the catalyst since Ga species are better dispersed when they are well reduced [21].

Conversion of olefins to aromatics has a complex mechanism, through which all the oligomerisation, cracking, hydrogen transfer, dehydrogenation-cyclization, and trans-alkylation may happen at the same time. Oligomerisation is the predominant reaction, which happens at relatively low temperatures. However,

high temperatures favour aromatization and cracking. With regard to the study by Song et al. done with 1-pentene in a pulse reactor at 360 °C, toluene was the main compound in the aromatic products. After that, benzene, and C₈ aromatics were the main constituents [22].

Chang et al. also explored zinc and gallium-loaded ZSM-5 for the transformation of light alkanes to aromatics (benzene, toluene, xylene). In the same study, it has been observed during NH₄-TPD analysis, that after hydrogen pretreatment, the number of strong acid sites was reduced, while the number of weak ones increased simultaneously. By giving enough time for the pretreatment, all the strong sites can be converted to weak ones. The method employed for loading the metal is also influential in activity and efficiency of the catalyst. ZnO/ZSM-5 has shown better activity and selectivity for the aromatics than Ga/ZSM-5, but during the reaction over ZnO/ZSM-5, the activity decreased over the time due to the reduction of ZnO. In industry, sometimes Ga/ZSM-5 is applied more frequently since it has exhibited good catalytic stability [23].

Aromatization of light alkanes over ZSM-5 goes through three consecutive stages: (a) alkanes are transformed into alkenes (b) alkenes are converted to heavier ones (through olefin isomerisation, oligomerisation, and cracking) (c) aromatization (if it happens over H-ZSM-5, aromatics and alkanes are produced, while on metal-ZSM-5, aromatics and hydrogen are main products) [24].

Aromatization of light alkanes is carried out through different processes. In the most known one, called BP/UOP's CYCLAR process, C₃/C₄ gases are converted to aromatics over Ga/H-ZSM-5. Mobil's M2 forming process, and also other technologies, such as Chevron's AROMAX, that utilize C₆-C₈ gases as feedstock, make use of H-ZSM-5 and Pt/L zeolite, respectively [12].

The positive point about modified H-ZSM-5 is the limited coke formation. Ga, Zn, Ag, Ni, and Pt are the metals that can be loaded on ZSM-5. But, among all, Zn- and Ga/ZSM-5 are the most often used ones [12].

Ihm and his co-workers investigated the effect of CO₂ on the aromatization of propane over metal-loaded ZSM-5. According to their work, during the reaction, CO₂ is reduced into CO and hydrocarbon is converted to aromatics. Cr, Fe, Ni, and Zn were the studied metals, which have shown an improvement in the catalytic activity and selectivity to aromatics [25].

Viswanadham et al. attempted to transform light straight-chain alkanes of C₄-C₇ to liquefied petroleum gas (LPG). They have mentioned these compounds as low octane number materials, which have high Reid vapour pressure, while LPG is a valuable cooking fuel. They tried to crack low-value light naphtha feedstocks, and at the same time, generate aromatics, which are valuable for gasoline blending. This will also co-produce light alkanes for LPG. Nickel-loaded on mildly dealuminated ZSM-5 was suggested as the bifunctional catalyst, which catalyzes cracking and aromatization at the same time. This catalyst has shown better activity in producing LPG when reacting in the presence of N₂. It also makes more aromatics in the presence of H₂. In spite of decrease in pore volume and surface area caused by loading Ni onto the catalyst, some catalytic properties are promoted due to the finely dispersion of the metal in the catalytic pores. Hydrogenation/dehydrogenation activities of the catalysts are among the features, which are improved by metal loading [26].

While Ni acts as a contaminant during heavy oil cracking that causes by-production of undesirable hydrogen and coke in the FCC process, its deposition on the zeolites has found to be effective for NO_x reduction. When the percentage of Ni on Ni-ZSM-5 is up to 0.4% (regardless of the metal loading method), metal is only deposited inside the zeolite channels as charge compensation cations. However, when its portion is increased to 1 wt% (through impregnation), it will locate both inside and outside of the channels. Maia et al., who employed Ni promoted catalysts for n-hexane cracking, reported that the method of nickel introduction can alter the activity and selectivity toward light alkanes [27].

2.5.4. Poisons

Gaseous emissions released from the combustion of fossil fuels typically contain sulphur compounds that inhibit the catalyst activity in the exhaust system [28]. Naphtha feedstock from FCC also has considerable quantity of various sulphur and nitrogen compounds (tiols, thiophenes, amines, etc.) in the stream. Depending on the nature of the crackable material and the operating condition, the sulphur concentration in the stream varies from 500 to 2000 ppm. The inclination of acid sites of the catalyst to adsorb both nitrogen and sulphur compounds leads to rapid catalyst deactivation. Sulphur-containing materials can completely deactivate H-ZSM-22 and H-ZSM-57 during OLI. In fact, it is believed that sulphur compounds are coke precursors in these processes [13].

According to the study done by Saaid et al. on the performance of Pt-Cu-ZSM-5 for the reduction of NO_x , bimetallic catalysts are prone to deactivate in the presence of water vapour and sulphur dioxide [29].

The study made by Van Grieken et al. on the OLI of 1-hexene over nanocrystalline H-ZSM-5 (n-ZSM-5) and two mesostructured silica-alumina (Al-MTS and Al-MCM-41) in the presence of model sulphur (thiophene) and nitrogen (n-butylamine) poisons, either alone or together, indicated that n-ZSM-5 is too sensitive to the poisons. Especially at high concentrations of poisons, the catalyst has more interest in generating lighter oligomers (dimers, $\text{C}_7\text{-C}_8$ isomers). In such conditions, no oligomers heavier than C_{19} were observed (instead of $\text{C}_{36}\text{-C}_{40}$ over Al-MTS and Al-MCM-41). Also, a drastic drop in adiabatic temperature occurs when the poisons are present in the system. It is due to the reduction that happens in the reaction progress at high concentrations of poisons. However, Al-MTS and Al-MCM-41 (specially Al-MTS) were not considerably affected by poisons, even at high concentrations of poisons. This is mainly because of their high surface area and medium acid strength. On the contrary, ZSM-5 possesses strong acid sites, which can be easily deactivated by poison adsorption and heavy oligomer/coke formation on both external surface and in the micropores. Van

Grieken et al. also suggested application of n-paraffin solvents such as n-octane and n-dodecane as a pathway to slowing down the deactivation and increasing the lifetime of zeolite USY. This can be because of the hydrogen that solvent provides for the reaction, which leads to less aromatization [13].

References

- [1] Imanishi, Y.; Naga, N. *Prog. Polym. Sci.* **2001**, *26*, 1147-1198.
- [2] Sohn, J. R.; Kim, H. W.; Kim, J. T. *J. Mol. Catal.* **1987**, *41*, 375-378.
- [3] Sohn, J. R.; Kim, H. J. *J. Catal.* **1986**, *101*, 428-433.
- [4] Sanati, M.; Hornell, C.; Jaras, S. G. *Catalysis* **1999**, *14*, 236-287.
- [5] Janiak, C. *Coord. Chem. Rev.* **2006**, *250*, 66-94.
- [6] Al-Jarallah, A. M.; Anabtawi, J. A.; Siddiqui, M. A. B.; Aitani, A.M.; Al-Sa'doun, A.W. *Catal. Today* **1992**, *14*, 1-121.
- [7] De Klerk, A.; Furimsky, E. *Catalysis in the Upgrading of Fischer-Tropsch Syncrude*; Royal Society of Chemistry: Cambridge, UK, **2010**, pp. 40-164.
- [8] De Klerk, A.; Leckel, D. O.; Prinsloo, N. M. *Ind. Eng. Chem. Res.* **2006**, *45*, 6127-6136.
- [9] O'Connor, C. T.; Kojima, M. *Catal. Today* **1990**, *6*, 329-349.
- [10] Knifton, J. F.; Sanderson, J. R.; Dai, P. E. *Catal. Lett.* **1994**, *28*, 223-230.
- [11] Kojima, M.; Moller, K.; Schwarz, S.; Vogel, A.; Andersen, B.; Parker, T.; Petrik, L.; Wishart, C.; Winter, M. *Catalysis Research Group Report for Sasol*, University of Cape Town, Department of Chemical Engineering: South Africa, June **1988**.
- [12] Stocker, M. *Microporous and Mesoporous Materials* **2005**, *82*, 257-292.
- [13] Van Grieken, R.; Escola, J.M.; Moreno, J.; Rodriguez, R. *Applied Catalysis A: General* **2008**, *337*, 173-183.

- [14] O'Connor, C.T.; Kojima, M.; Petrik, L.; Wishart, C.; Louw, L.A.; Schwarz, S.; Andersen, B.; Vogel, A.; van Niekerk, M.; Hartford, R. Catalysis Research Group Report for Sasol, University of Cape Town, Department of Chemical Engineering: South Africa, September **1989**.
- Pater, J.P.G.; Jacobs, P.A.; Martens, J.A. *Journal of Catalysis* **1999**, *184*, 262-267.
- [15] Tabak, S.A.; Krambeck, F.J.; Garwood, W.E. *AIChE Journal* **1986**, *32*, 1526-1531.
- [16] Garwood, W.E. A.C.S. Symp. Ser. Vol. *218*, **1983**, 383.
- [17] Amin, S.; Aishah, N.; Kasim, F.H. 15th Symposium of Malaysian Chemical Engineers SOMChe **2001**, 78-83.
- [18] Petrera, M.; Gennaro, A.; Gherardi, P.; Gubitosa, G.; Pernicone, N. *Journal of Chemical Society, Faraday Transactions 1: Physical Chemistry in Condensed Phases* **1984**, *80*, 709-720.
- [19] Babaeva, F.A.; Abasov, S.I.; Rustamov, M.I. *Catalysis in Industry* **2010**, *2*, 42-47.
- [20] Stefanidis, S.D.; Kalogiannis, K.G.; Iliopoulou, E.F.; Lappas, A.A.; Pilavachi, P.A. *Bioresource Technology* **2011**, *102*, 8261-8267.
- [21] Guisnet, M.; Gnep, N.S. *Catalysis Today* **1996**, *31*, 275-292.
- [22] Song, Y.; Zhu, X.; Xu, L. *Catalysis Communications* **2006**, *7*, 218-223.
- [23] Chang, C.; Lee, M. *Applied Catalysis A, General* **1995**, *123*, 7-21.
- [24] Nguyen, L.H.; Vazhnova, T.; Kolaczkowski, S.T.; Lukyanov, D.B. *Chemical Engineering Science* **2006**, *61*, 5881-5894.

- [25] Ihm, S; Park Y.; Lee, S. *Applied Organometallic Chemistry* **2000**, *14*, 778-782.
- [26] Viswanadham, N.; Saxen, S.K.; Kumar, M. *Petroleum Science and Technology* **2011**, *29*, 393-400.
- [27] Maia, A.J.; Louis, B.; Lam, Y.L.; Pereira, M.M. *Journal of Catalysis* **2010**, *269*, 103-109.
- [28] Marcilly, C. *Oil and Gas Science and Technology* **2001**, *56*, 499-514.
- [29] Saaid, I. M.; Mohamed, A. R.; Bhatia, S. *Journal of Molecular Catalysis A: Chemical* **2002**, *189*, 241-250.

3. BATCH REACTOR STUDIES

Abstract

The following chapter explains the experiments conducted over four types of catalysts for the oligomerisation of alkenes. ZSM-5, Mordenite, Ferrierite, and zeolite Y were examined in batch condition in order to compare their performances for the oligomerisation of ethylene. Before performing oligomerisation reactions, cracking of C₆-C₁₄ alkenes was investigated in the presence of H-ZSM-5 in order to get the temperature range that cracking may take place. Monitoring the pressure changes in the reactor while the temperature was increasing gradually showed that 300 °C is the optimum temperature where almost no cracking happens in the reactor. Oligomerisation of ethene over zeolite catalysts was carried out at that temperature and with the pressure of 100 psi. The pressure drop happened in the reactor for all the zeolites indicated that acid form ZSM-5 is the most efficient catalyst for our specific purpose.

Keywords: Zeolites, oligomerisation, micro-reactor, Brønsted acid sites

3.1. Introduction

As stated in the first chapter, the main purpose of the present work is to evaluate different catalysts for the conversion of the pyrolysis gases. Since olefins are the major constituents of pyrolysis gases, attempts were performed to convert these gases to more useful liquid products through oligomerisation. There are several classes of catalysts used for this purpose. But, many studies have emphasized the capability of zeolites for the oligomerisation of alkenes. Yarlagadda et al. have described acid catalysts, such as zeolites, as potential catalysts for the polymerization of lower alkenes [1]. Bellussi et al. have employed zeolite-based catalysts for the production of high quality diesel fuels from light olefins [2]. In another study, ZSM-5 with strong Brønsted acid sites is proposed as an effective catalyst to transform ethylene into propylene. In the same

work, performance of different molecular sieves including SBA, MCM, Y, X, MOR, Beta, and SAPO for the conversion of ethylene to propylene was investigated and ZSM-5 was reported as the most efficient one [3]. All these studies along with those summarized in chapter 2 lead us to choose zeolites as the candidate catalysts for our purpose.

In the following section, performance of four types of zeolites (ZSM-5, Y, Mordenite, and Ferrierite) for the conversion of gas olefins is investigated in batch reactors. Conducting reactions in batch reactor gives us the opportunity to simply compare different catalysts and their activity before performing a more detailed analysis of the products in the flow reactor (Chapter 4). It also brings us the chance to compare efficiency of the reaction in batch condition with the one in the continuous condition.

The temperature for the onset of cracking of the products was determined by performing the reaction with heavy alkenes as feed in the presence of catalyst at different temperatures, while the pressure was being monitored. The temperature obtained in that way was assigned as a threshold for the oligomerisation reactions.

Synthetic gases were used as sample gases for oligomerisation. Ethylene was the reactant for batch analysis since it is the least reactive olefin. Based on the pressure drop that happens in the reactor due to the gas consumption, ZSM-5 was selected as the most efficient catalyst.

3.2. Experimental

3.2.1. Materials

Ethylene, with the purity of 99%, provided by Praxair, was used as feed material for the reactions. Four types of zeolites including ZSM-5, Mordenite, Ferrierite, and zeolite Y, purchased from Zeolyst International (United States), were used as catalysts for the batch reactions. Their properties provided by the supplier are listed in Table 3-1. The catalysts were converted into acid form by

calcining at 650 °C for 5 h in air. All types of zeolites were purchased in ammonium form and with the highest ratio of Si/Al available in the company. The reason for choosing the highest of Si/Al was based on the work, which has been done in the literature. It can be implied from these studies that high percent of Al restricts the growth of oligomers due to the crowding of species at the active sites. Aromatic formation will also increase as the Si/Al ratio is decreased since the Brønsted sites get closer together [4].

Table 3-1. Properties of the zeolites provided by supplier

Zeolite	SiO ₂ /Al ₂ O ₃	Nominal Cation Form	Na ₂ O Weight %	Surface Area, m ² /g	Unit Cell Size, Å
ZSM-5	280	Ammonium	0.05	400	-
Zeolite Y	12	Ammonium	0.05	730	24.35
Mordenite	20	Ammonium	0.08	500	-
Ferrierite	20	Ammonium	0.05	400	-

1-hexene (purity 97%), 1-heptene (purity 97%), 1-octene (purity 98%), 1-nonene (purity 96%), 1-decene (purity 94%), 1-undecene (purity 99%), 1-dodecene (purity 95%), 1-tridecene (purity 96%), 1-tetradecene (purity 92%) provided by Sigma-Aldrich, were utilized to measure the cracking temperature of long-chain olefins.

3.2.2. Equipment

A stainless steel micro-reactor, with 1" (2.54 cm) nominal diameter, made from 316 L seamless pipe and Swagelok fittings was used as the batch reactor. It was attached to a holder via ¼" (0.635 cm) nominal diameter stainless steel tubing. A thermocouple and a pressure gauge were used to monitor the internal temperature and pressure. The thermocouple tip was aligned with the center of the micro-reactor. Swagelok fittings were employed to transfer the gas reactants to the micro-reactor. In each run, 0.5 g of pretreated catalyst was placed in the micro-reactor. The reactor was filled with the feed gas to the total pressure of 100

psi. After doing the leak test, it was placed in the sand bath with pre-assigned temperature (Figure 3-1).

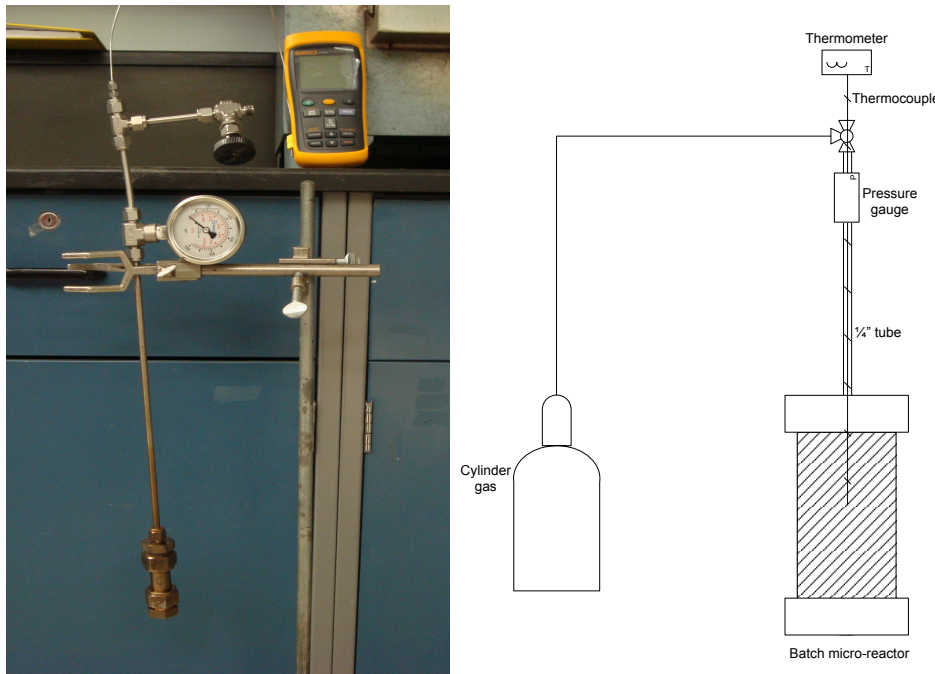


Figure 3-1. Batch reaction setup

Sand bath, provided by TECHNE was used to heat the micro-reactor (Figure 3-2). Type K thermocouple connected to Fluke 54IIB thermometer was monitoring the internal temperature of the micro-reactor. Pressure gauge with the 1000 psi pressure restriction, was provided by Swagelok to monitor the pressure of the micro-reactor during the experiments. Since all the zeolites were in ammonium form, they needed to be turned into acid form by calcination. Thus, they were calcined at 650 °C for 5 h in air in a Carbolite CWF 11/13 muffle furnace.



Figure 3-2. Sand bath

3.2.3. Analyses

Liquid products were quantified using an Agilent 7890A gas chromatograph with a flame ionization detector (GC-FID) and nitrogen as carrier gas. It is supplied with Agilent 7693 autosampler. Column model is Agilent HP-PONA, and its specifications are: 50 m long, 200 μm ID, and film thickness of 0.5 μm . It is programmed to ramp up from 40 to 300 °C at a rate of 10 °C /min and stay at that temperature for 5 min.

Gas products were identified and quantified by an Agilent 7890A gas chromatograph with a flame ionization detector (GC-FID) and helium as carrier gas. It was accompanied by a HayeSep R stainless steel column 80/100 (3.048 m \times 3.175 mm OD). The oven is programmed to hold the temperature at 70 °C for 7 min before ramping to 250 °C with the rate of 10 °C/min. It remains at 250 °C for 2 min, and finally cools it to 70 °C and stays at that temperature for 8 min.

Density and strength of the acid sites were determined by performing ammonia temperature programmed desorption (NH₃-TPD) of calcined catalyst

with a ChemBET TPR/TPD Chemisorption Analyzer purchased from Quantachrome. The instrument is equipped with a thermal conductivity detector (TCD). The oven is programmed to heat up to 250 °C with the rate of 20 °C /min and hold for 1 h to remove all the physisorbed species while Helium is passing over the catalyst with the flow rate of 70 mL/min. The sample was then cooled to 50 °C, and gas was switched to NH₃ (70 mL/min) for 60 min before switching back to He. Keeping the He flow over the sample for 60 min removes all the physisorbed ammonia from the surface of catalyst. TPD analysis was then performed under the He flow while the oven heats up to 900 °C with the rate of 10 °C/min and the released ammonia is monitored continuously. The detector current during analysis was 150 mA, with attenuation of 16, and carrier gas flow of 70-75 mL/min. About 70 mg of sample is analyzed in each run. Acid site density of the catalysts were measured by calibrating the TCD for the desorption of a known amount of ammonia.

FTIR spectra of adsorbed pyridine were recorded using ABB MB3000 FTIR with a Pike DiffuseIR attachment, and nitrogen as carrier gas. Its environmental chamber, which is temperature controlled, can go up to 500 °C. Infrared measurements were performed on wafers of catalysts formed by pressing the powder in the sample cell. Pyridine vapor was adsorbed at room temperature on the activated sample. Prior to the collection of the data, pyridine was admitted to the sample for 1 h at room temperature to get all the sites completely saturated by the probe gas. The sample was then purged with nitrogen at the same temperature for 1 h to remove all the physisorbed pyridine. The sample was then outgassed at various temperatures [5]. Spectra were recorded at a resolution of 16 cm⁻¹ and the average of 120 scans, and the spectral region monitored was between 1400 cm⁻¹ to 1800 cm⁻¹.

Thermal gravimetric (TG) analysis of the spent catalyst was performed to measure the amount of carbon deposited on the catalyst. The analysis was carried out by TG 409A (NETZSCH) and with air as carrier gas. The TG analyzer is

programmed to hold the temperature at 100 °C for 5min prior to heating up. It helps the baseline to stabilize. Then, it ramps up to 900 °C with a rate of 10 °C/min while the analysis is performed.

3.2.4. Calculations

For the gas GC analyses, the external standard (ESTD) report was selected, and the mole % of the component x was calculated using equation below (Equation 3-2):

$$Mol\ \% \ of \ x = \frac{Response_x \cdot RF_x \cdot 100}{\sum(Response \cdot RF)} \quad (3-2)$$

For liquid GC analyses, “Percent” report was selected, and the equation below was applied (Equation 3-3):

$$Norm\ \% \ of \ x = \frac{Response_x \cdot RF_x \cdot 100}{\sum(Response \cdot RF)} \quad (3-3)$$

$Response_x$ is the area of the peak x. Response factors (RF) are obtained from the calibration for the known compounds.

Areas under the peaks of the TPD profiles were integrated order to determine the total acidity of the catalyst. A semi-quantitative comparison of the strength distribution was achieved by LogNormal deconvolution of the peaks. Weak and strong acidities were defined as the areas under the peaks at lower and higher temperatures, respectively. Peak area represented by desorption that happen at temperatures lower than 350 °C are classified as weak acid sites, while those at higher than 350 °C belong to the strong sites.

The relative heights of the peaks observed in FTIR spectra of the catalysts, determines the relative Brønsted to Lewis acidity of the catalysts. Considering total acidity, obtained from TPD, and the ratio of B/L acid sites, from FTIR, the amount of the acid sites was calculated through the equation below (Equation 3-1).

$$\text{Concentration of Lewis sites} = \frac{H_l}{H_l + H_B} \cdot C \quad (3-1)$$

H_l and H_B are the height of Lewis and Brønsted bands in FTIR spectra, respectively, and C is the total concentration of acid sites obtained from TPD analysis. Density of the Brønsted sites can be calculated using the same equation as mentioned above. For a catalyst that has been treated with pyridine, the band at around 1545 cm^{-1} is a signature of Brønsted acid sites, while the one at 1455 cm^{-1} is attributed to Lewis sites. The absorption at 1485 cm^{-1} is an indicator for both acid sites [6], [7].

3.3. Results and discussion

3.3.1. Catalyst characterization

NH_3 -TPD was conducted to measure and compare the total acidity and strength of the acid sites of the zeolites. The TPD thermograms of NH_3 desorption from ZSM-5 (MFI), mordenite (MOR), ferrierite (FER), and zeolite Y (FAU) are shown in Figure 3-1 to 3-4. The acidity measurements were complemented with FTIR analysis of the catalysts with adsorbed pyridine to determine the nature of the acid sites (Lewis or Brønsted), and also their relative proportion. As can be seen from the NH_3 -TPD data (Figure 3-3 to Figure 3-6), the acid sites can be divided into two groups, namely, weak acid sites and strong acid sites. The acid site concentration, acid site strength distribution (weak and strong) and classification of the acid sites (Brønsted or Lewis) are listed in Table 3-2.

Table 3-2. Acid site strength and density of each zeolite (at 25 °C)

	Y	ZSM-5	Mordenite	Ferrierite
Desorption temperature 1 (°C)	214	264	224	191
Desorption temperature 2 (°C)	437	505	557	463
Weak B* sites (μmol/g)	102	77	153	173
Strong B sites (μmol/g)	61	133	49	58
Weak L* sites (μmol/g)	249	267	248	250
Strong L sites (μmol/g)	147	457	79	83
L/B	1.9	3.4	1.6	1.4

*“B” and “L” stand for Brønsted and Lewis acidity, respectively.

Figures 3-7 to 3-10 show the IR spectra of pyridine desorption for the zeolites. Pyridine is chemisorbed in two modes: on Brønsted acid sites by transfer of the proton from the acid site to the nitrogen of the pyridine, and on Lewis sites (electron-pair acceptor or coordinatively unsaturated sites) by coordination of nitrogen lone pair of electrons. For the zeolites, studied in the present work, the bands were observed at the ranges 1440-1460 cm⁻¹ and 1540-1560 cm⁻¹ for Lewis and Brønsted sites, respectively.

In order to combine the TPD and FTIR data together, it was assumed that ammonia and pyridine have the same basic property; however, pyridine is a weaker base [9]. FTIR spectrum baseline was obtained by recording the spectrum for empty cell.

There's some scattering in the frequency of IR bands, which is unavoidable for every zeolite because of the secondary influence of counterions or uneven distribution of Al atoms in the framework. As the Si ratio of the zeolite increases, it inclines to behave non-linearly and out of the regular frameworks, which is due to the reduction that takes place in the collective interactions between negatively charged Al centers [6].

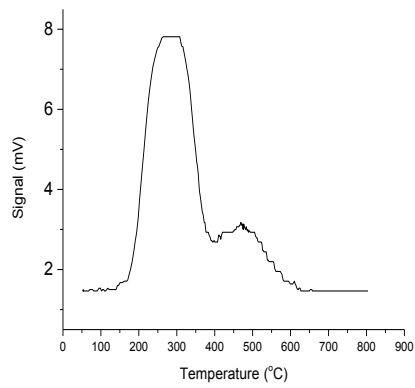


Figure 3-3. NH₃-TPD profile of H-ZSM-5

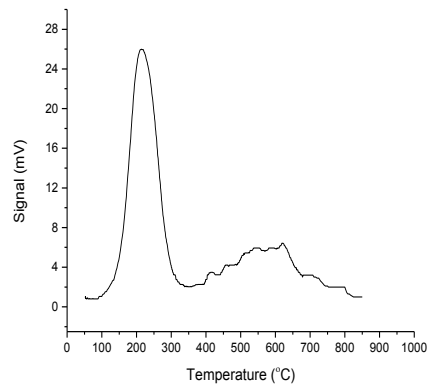


Figure 3-4. NH₃-TPD profile of H-MOR

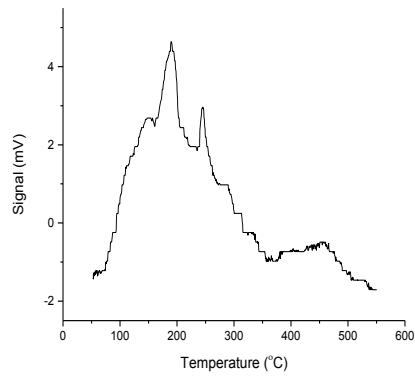


Figure 3-5. NH₃-TPD profile of H-FER

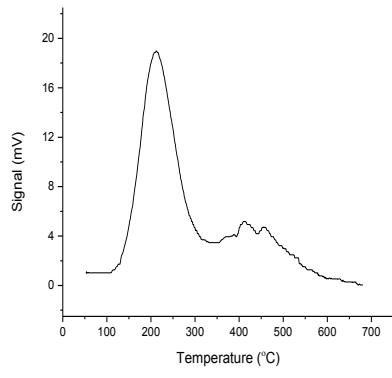


Figure 3-6. NH₃-TPD profile of H-Y

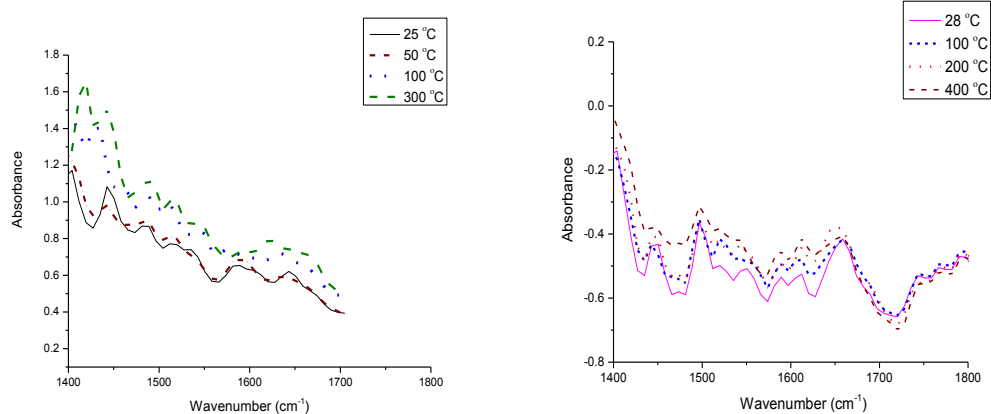


Figure 3-7. FTIR spectra of adsorbed pyridine for H-ZSM-5 at different outgassing temperatures

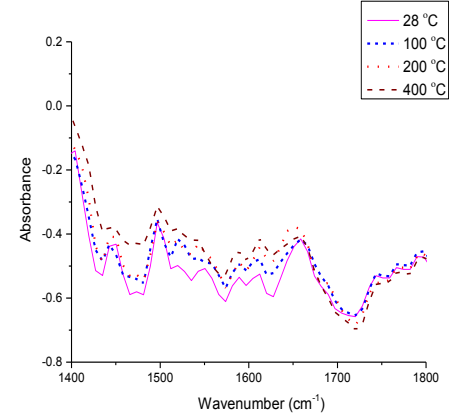


Figure 3-8. FTIR spectra of adsorbed pyridine for H-MOR at different outgassing temperatures

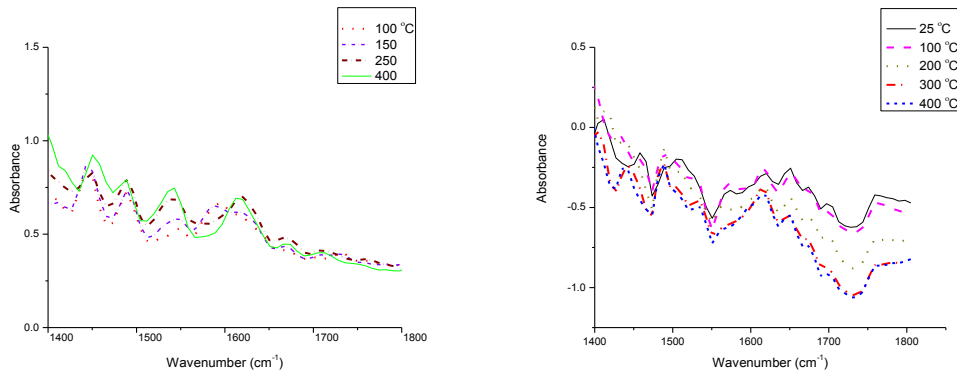


Figure 3-9. FTIR spectra of adsorbed pyridine for H-Y at different outgassing temperatures

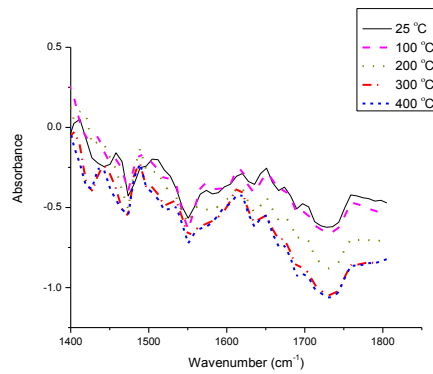


Figure 3-10. FTIR spectra of adsorbed pyridine for H-FER at different outgassing temperatures

For H-ZSM-5, as it can be seen, there's a shoulder next to the band at 1450 cm^{-1} when the sample is outgassed at 100 °C and 300 °C. The peak at 1450 cm^{-1} can be because of the vibrations of pyridine coordinately bounded to Lewis sites. The shoulder is associated with the pyridine bound to residual Na^+ species. It has previously reported that Na^+ cations have weak Lewis acidity properties [10], which have appeared in the spectrum at temperatures above 100 °C for this case.

3.3.2. Measuring the cracking temperature of long-chain olefins over H-ZSM-5

In order to get an idea about the temperature that cracking of the oligomerisation products may become significant, a series of experiments were carried out on the high-chain alkenes in the presence of H-ZSM-5. Alkenes in the range of C₆ - C₁₄ were the selected chemicals. In each run, 0.5 g of the alkene was placed in the micro-reactor in the presence of 0.5 g calcined ZSM-5. Temperature of the sand bath was increased gradually, while the pressure was being recorded. The temperature, at which a significant jump in the pressure was seen, was the moment when cracking started becoming significant. The pressure versus temperature for the reaction of each alkene is plotted in the graphs below (Figures 3-11 to 3-19). The temperatures, reported here, are sand bath temperature, which is around 50 °C higher than reactor internal temperature.

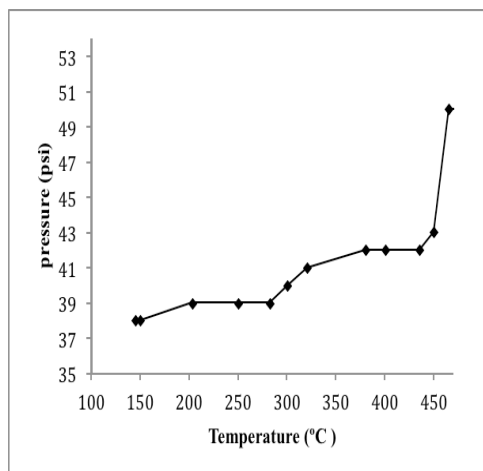


Figure 3-11. Pressure changes as the temperature increases for the reaction of 1-hexene over H-ZSM-5

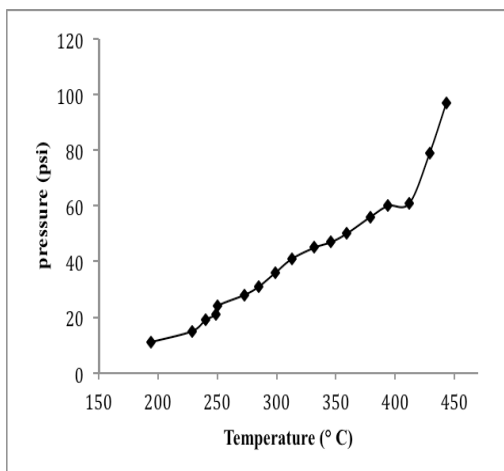


Figure 3-12. Pressure changes as the temperature increases for the reaction of 1-heptene over H-ZSM-5

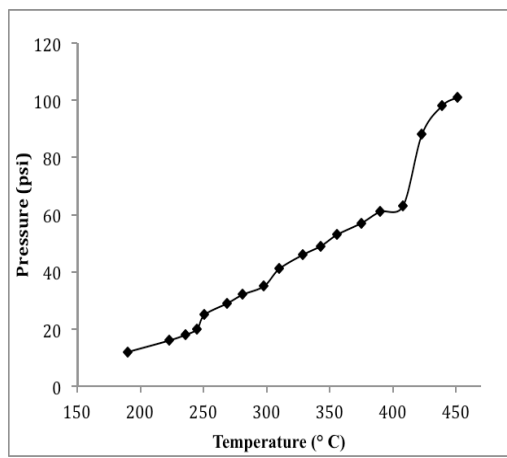


Figure 3-13. Pressure changes as the temperature increases for the reaction of 1-octene over H-ZSM-5

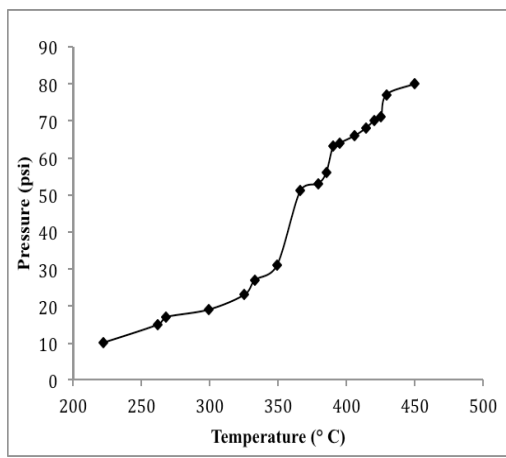


Figure 3-14. Pressure versus temperature for the reaction of 1-nonene over H-ZSM-5

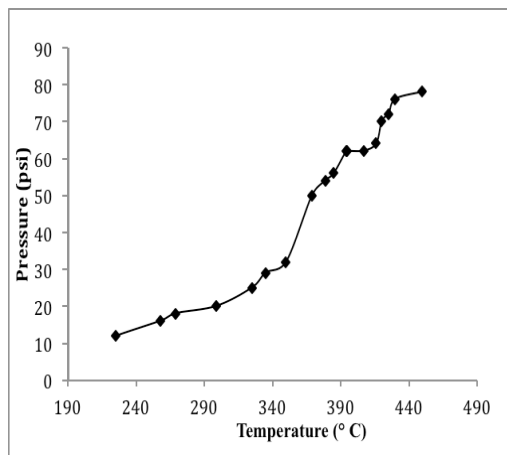


Figure 3-15. Pressure versus temperature for the reaction of 1-decene over H-ZSM-5

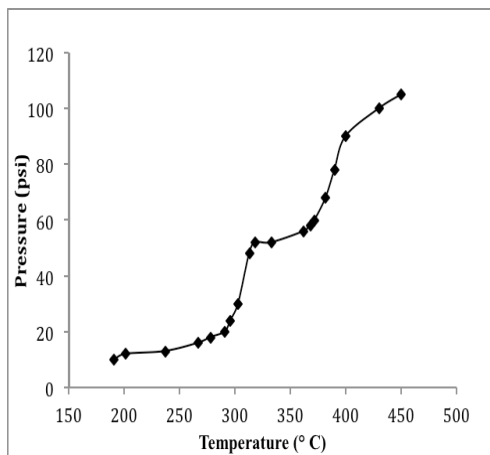


Figure 3-16. Pressure changes as temperature increases for the reaction of 1-undecene over H-ZSM-5

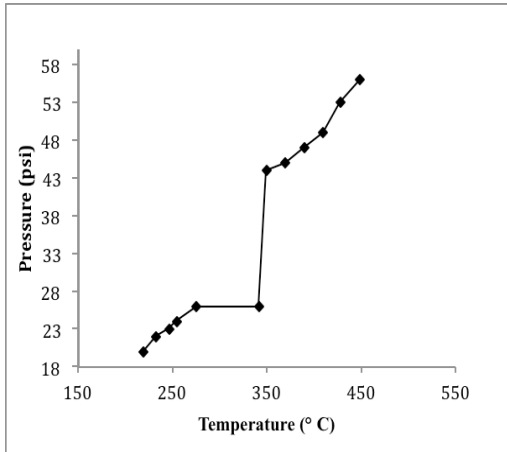


Figure 3-17. Pressure changes as the temperature increases for the reaction of 1-dodecene over H-ZSM-5

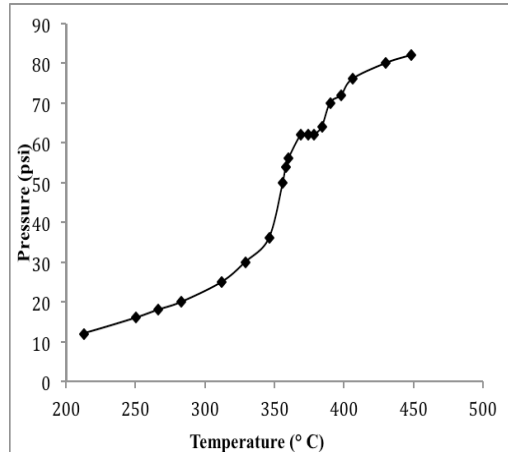


Figure 3-18. Pressure versus temperature for the reaction of 1-tridecene over H-ZSM-5

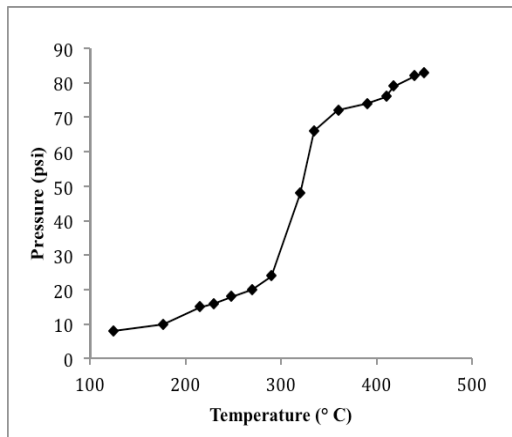


Figure 3-19. Pressure changes as the temperature increases during the reaction of 1-tetradecene over H-ZSM5

Temperatures where cracking start to take place for every alkene are listed in Table 3-3. As one may consider the lightest hydrocarbon has the lowest cracking temperature. As the chain length increases, the cracking temperature decreases. This can be due to the carbocations, which are formed during the cracking of the olefins. As the length of the carbon chain increases, the carbocations generated

from their cracking will also become longer and more stable, so the olefins can be cracked with lower activation energy, and consequently at lower temperatures. It has already reported that hexene cracking over H-ZSM-5 goes through a dimerisation-cracking pathway, while the alkenes heavier than hexene have a monomolecular reaction. That is why they can easily crack at lower temperatures than hexene [11]. The lowest temperature in the table belongs to 1-tetradecene, which is the heaviest hydrocarbon. The pressure jump for 1-tetradecene has happened at 305 °C, which is the temperature that cracking started to happen. So in order to avoid cracking in our experiments, and according to the data in the table, the experiments were performed at 300 °C.

Table 3-3. Cracking temperature of C₆ - C₁₄ alkenes measured from the reaction of 0.5 g alkene in the presence of 0.5 g H-ZSM-5, and atmospheric pressure

Alkene	Cracking temperature (°C)
1-hexene	465
1-heptene	420
1-octene	408
1-nonene	372
1-decene	355
1-undecene	308
1-dodecene	346
1-tridecene	348
1-tetradecene	305

Some of the numbers in the Table 3-3 are outliers. The temperature observed for 1-dodecene is supposed to be less than the one observed for 1-undecene. It is also true for 1-tridecene. Unfortunately, no logical reason could be find to explain the observing trend in the table. Similar thing is true for the numbers listed in Table 3-4. In this table, the distribution presented for the products obtained from the reaction of 1-dodecene over H-ZSM-5 is not in agreement with the other alkenes. The distribution is in such a ways that the percentage of the products starting from C₁ increases to some extent and then decreases to zero. 1-dodene is not following this trend. Instrumentation or experimental errors might be the reasons for the deviation observed in the results. No liquid was observed. The

analyses of the gases produced from the reaction of each alkene are listed in the table below.

Table 3-4. Carbon number distribution from the reaction of different alkenes over H-ZSM-5 (atmospheric pressure, 0.5 g H-ZSM-5, 0.5 g reactant, and temperature of 450 °C)

Reactant	C ₁	C ₂	C ₃	C ₄	C ₅	C ₆
1 - hexene	25	19	52	5	0	0
1 - heptene	22	23	48	6	0	0
1 - octene	27	24	43	6	0	0
1 - nonene	26	33	35	5	0.4	0
1 - decene	23	37	33	7	0	0
1-undecene	21	29	41	8	0.3	0
1 - dodecene	50	21	28	2	0	0
1 - tridecene	24	33	39	4	0	0
1-tetradecene	20	44	31	4	0	0

3.3.3. Reaction of ethene over zeolite catalysts

Catalytic oligomerisation of ethene in the presence of different zeolites will be discussed in this section. In the last section, 300 °C was found to be the ideal temperature for oligomerisation reactions in the presence of H-ZSM-5. Therefore, the reactions were conducted at 300 °C, with 0.5 g catalyst, and pressure of 100 psi (the highest pressure available from gas cylinder), the reactor was kept at this condition for 3 h.

Ethylene is the least reactive alkene because it produces an unstable primary carbocation when reacting over acid catalysts. Therefore, first attempts were made to oligomerise this gas.

Pressure change happening in the reactor after the 3 hours of reaction is an indicator of the gas consumed during the reaction. Table 3-5 shows the pressure drops happened during the reaction of ethene over different zeolites. As one may consider, H-ZSM-5 has the highest pressure drop, indicating that the catalyst has had the most activity among all the catalysts and the reaction has proceeded the most. Sadly, the products were not sufficient to be analyzed with the typical analysis techniques. There can be several reasons for the low conversion observed

in the batch reactor. First of all, the volume of the micro-reactor was not much (only 20 mL), so even for 100 % conversion, the liquid produced is not remarkable. In addition, the contact area of the catalyst and gas is not enough. Lack of mixing in the reactor restricts the interaction of the catalyst and gas. The sand bath temperature is also not constant during the reactions. All these restrictions explain the low conversion observed for the batch reactions.

Table 3-5. Pressure drops observed during the reaction of ethene over different zeolites (at 300 °C, 100 psi, and 0.5 g catalyst)

Catalyst	Pressure drop (%)
H-ZSM-5	6
H-Y	2
H-MOR	5
H-FER	4

However, the TG analysis of the spent H-ZSM-5 after its reaction with ethene shows almost 3 % reduction in the sample weight (Figure 3-20). As the figure shows, there are two weight losses for the sample. The first stage, which starts from the beginning of the analysis and continues to 230 °C, is ascribed to moisture and volatiles evaporation. The second stage, at temperature ranging from 230 °C to 450 °C, corresponds to combustion of some heavier products. No weight loss was observed at temperatures higher than 500 °C, indicating that no coke has been formed on the catalyst [13].

The data of the TG plot are given in Table 3-6. As the table shows, the ratio of heavy products is higher than volatile ones, indicating that oligomerisation has preceded more than cracking.

Table 3-6. TG results of spent H-ZSM-5 after reacting with ethene

	Temperature		Amount (%)
	Original (°C)	End (°C)	
Dehydration and release of volatiles	28	230	1.3
Heavy products combustion	230	450	2

For the reaction studied here the activity can be ascribed to Brønsted sites, as H-ZSM-5, which possesses the highest ratio of each, has shown the most conversion.

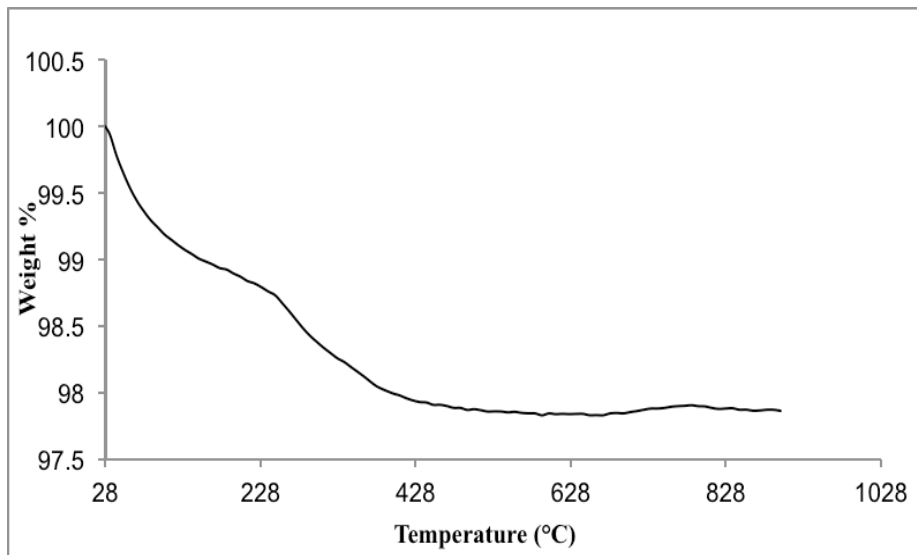


Figure 3-20. TG analysis of spent H-ZSM-5 after reacting with ethene

3.4. Conclusion

In this chapter, performance of four types of zeolite for the oligomerisation of ethene was investigated. Among all the acid-form catalysts, ZSM-5 showed the highest pressure drop in the reactor, indicating that it is the most active zeolite.

Temperature of 300 °C was found to be the effective temperature at which no naphtha range alkene would crack.

Maximum ethylene conversion achieved (from H-ZSM-5) was only 6%. Products were not considerable due to the restrictions with the batch reactor. Continuous reactor was suggested to improve the reaction condition, which will be investigated thoroughly in the next chapter.

References

- [1] Yarlagadda, P.; Lund, C. R. F.; Ruckenstein, E. *Applied Catalysis* **1990**, *62*, 125–139.
- [2] Bellussi, G.; Mizia, F.; Calemma, V.; Pollesel, P.; Millini, R. *Microporous and Mesoporous Materials* **2012**, *164*, 127–134.
- [3] Lin, B.; Zhang, Q.; Wang, Y. *Industrial & Engineering Chemistry Research* **2009**, *48*, 10788–10795.
- [4] Mlinar, A. N.; Zimmerman, P. M.; Celik, F. E.; Head-Gordon, M.; Bell, A. T. *Journal of Catalysis* **2012**, *288*, 65–73.
- [5] Védrine, J.; Auroux, A.; Bolis, V.; Dejaifve, P.; Derouane, E. G.; Nagy, J. B. *Journal of Catalysis* **1979**, *262*, 248–262.
- [6] Topsoe, N. *Journal of Catalysis* **1981**, *70*, 41–52.
- [7] Rodríguez-González, L.; Hermes, F.; Bertmer, M.; Rodríguez-Castellón, E.; Jiménez-López, A.; Simon, U. *Applied Catalysis A: General* **2007**, *328*, 174–182.
- [8] Rajagopal, S.; Grimm, T. L.; Collins, D. J.; Miranda, R. *Journal of Catalysis* **1992**, *137*, 453–461.
- [9] Xia, Y. *Acid catalyzed aromatic alkylation in the presence of nitrogen bases*; M.Sc. thesis, University of Alberta, Edmonton, Canada, 2012.
- [10] Mihályi, R. M.; Lázár, K.; Kollár, M.; Lónyi, F.; Pál-Borbély, G.; Szegedi, Á. *Microporous and Mesoporous Materials* **2008**, *110*, 51–63.
- [11] Buchanan, J. S.; Santiesteban, J. G.; Haag, W. O. *Journal of Catalysis* **1996**, *287*, 279–287.

- [12] Van Den Berg, J.P.; Wolthuizen, Van Hooff, J.H.C. *Journal of Catalysis* **1983**, *144*, 139–144.
- [13] Mochizuki, H.; Yokoi, T.; Imai, H.; Namba, S.; Kondo, J.N.; Tatsumi, T. *Applied Catalysis A: General* **2012**, Article in Press.

4. FLOW REACTOR STUDIES WITH H-ZSM-5

Abstract

The batch reactor experiments performed in chapter 3 indicate that H-ZSM-5 was the most active of the zeolites tested. In this chapter, the main focus is on the industrial application of H-ZSM-5 for the conversion of light olefins to liquid products. In order to decrease preheating, and to make use of heat of the reaction, experiments were carried out under adiabatic condition. Different mixtures of gases were tested over H-ZSM-5. Propene was the most reactive gas tested ($74.6 \text{ g}_{\text{liquid}} \cdot \text{g}_{\text{cat}}^{-1} \cdot \text{h}^{-1}$), while its mixture with other gases resulted in lower activity. Beside olefins, aromatic compounds such as benzene, and alkyl benzenes were also observed in the liquid products, while C₄ alkenes were the main components in the outlet gas.

Keywords: Propene, ZSM-5, oligomerisation, aromatics, adiabatic

4.1. Introduction

As stated before, the main purpose of the whole study is to find effective catalysts for the conversion of pyrolysis gases to more useful liquid products. Since light olefins are the most reactive part of the pyrolysis gases, as first step oligomerisation of olefins was proposed as a pathway to transform them to more valuable products. In the first attempts, conversion of ethene was tested over four types of zeolite in a batch reactor. Among all catalysts tested, ZSM-5 showed the highest activity.

However, the batch reaction has some drawbacks, including accumulation of heavy products in the reactor, issues related to mixing in the reactor, and reactor volume restrictions. The limited reactor volume gets more important when the reactant is in gas form. In such a small reactor, even for 100% conversion, which is hardly achievable in catalytic reactions, the yielded product would not be considerable. This made the accurate analysis and quantification difficult. In order

to overcome these restrictions, and to develop a better understanding of the time-on-stream behavior for the catalyst, a fixed-bed continuous reactor was commissioned. This reactor provides a steady state flow with continuous inlet of feed gas and outlet of products [1].

Previous studies have also outlined other disadvantages that a batch reactor can have during the oligomerisation of ethylene. It is reported that the temperature needed in the batch reactor for gas phase conversion of ethylene is much higher than in a slurry reactor (continuous stirred tank reactor type). This high temperature leads to the rapid deactivation of the catalyst [2].

In this section, a study was conducted over the acid-form of ZSM-5 to evaluate its performance for the conversion of different mixtures of gases. Propene was the major component in most of the mixtures and showed the highest conversion when it was the only reactant in the absence of other gases.

4.2. Experimental

4.2.1. Materials

In addition to ethylene, mentioned in section 3.2.1, methane (purity of 99%), butane (purity of 99%), hydrogen (purity of 99.995%), and carbon dioxide (purity of 99%), provided by Praxair, were also used as feed materials for the flow reactor. ZSM-5, with the same features as described in section 3.2.1, was used as catalyst for the continuous reactions.

Two sizes of silicon carbide (#16 and #80 mesh), supplied by Kramer Industries, were used for the fixed bed reactor. #80 mesh was used to dilute the catalyst, while #16 mesh was employed to pack the catalyst in the reactor tube.

3 mm glass beads, as provided by Fisher Scientific, were employed in the packed bed reactor as bed support. Glass beads were also used to help the inlet gas be mixed completely before reacting over catalyst, as well as to make a

consistent heat flow throughout the tube. Quartz wool, purchased from Fisher scientific, was used to separate the packs in the reactor tube.

4.2.2. Equipment

Figure 4-1 shows a whole view of the experimental setup. 316 L stainless steel tube, provided with the proper fittings by Swagelok, was used as the tubular reactor. The length and the diameter of the tube are 45 cm and 1.27 cm, respectively. In order to pack the fixed-bed reactor, a piece of quartz wool is placed at the bottom of the tube while glass beads are loaded over that, so that half of the tube is filled with the glass beads. The catalyst bed consists of two layers of carborundum (#16 mesh) along with a mixture of catalyst and #80 mesh silicon carbide, which is packed between the two layers. Similar thermocouple and thermometer, as described in section 3.2.2, were employed to monitor the temperature. The thermocouple tip should be placed close to the bed in order to monitor its temperature changes. A pressure gauge, similar to the one described in section 3.2.2, was used to monitor the reactor pressure. Glass beads fill the rest of the tube to the top, and quartz wool covers the whole packing, so that there's no mixing of layers in the catalyst bed. Two pieces of quartz wool separate the silicon carbide from the glass beads [3]. Reactant gases were fed from top to the bottom after passing through mass flow meters. Lindberg Blue M tube furnace, supplied with controller by Thermo Fisher, is used as heating mantle for the tubular reactor.

Mass flow meters, purchased from Brooks, measure and control the flow rate of the inlet gases. A Brooks mass flow controller (model: 0254) controls the flow rate of the flow meters. Each flow meter is calibrated for a specific gas. However, in practice it was found that the flow rates indicated are not always accurate. Therefore, an Agilent ADM2000 gas meter, provided by Fisher Scientific, was used to measure the outlet flow rate at the same time.

Glass condenser, provided by Fisher Scientific, was used to cool the outlet products. Liquid products were captured in a flask after passing through the condenser, while the outlet gases were either collected for analysis or vented through the fume hood. Julabo F25 chiller circulated the cooling water (at a temperature of 5 °C) between condenser and chiller.

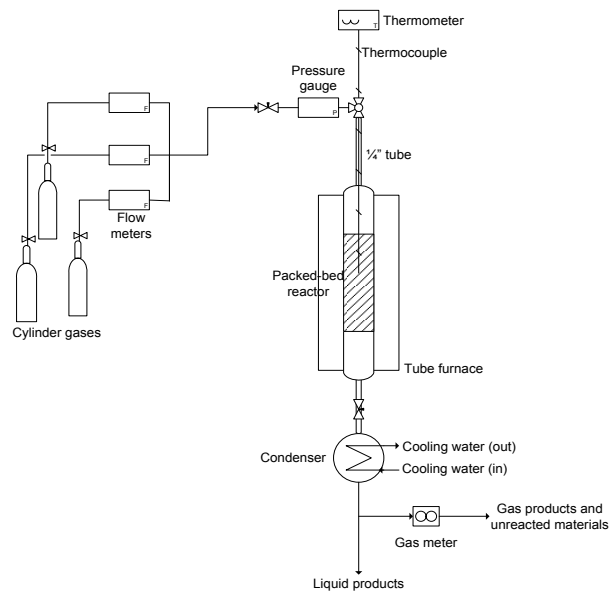


Figure 4-1. Continuous reaction setup

The furnace, described in section 3.2.2, was used to calcine the catalyst. Before running the experiments, the catalyst was pretreated in the same way as explained before (5h at 650 °C in air).

4.2.3. Analyses

Other than all the equipment mentioned in section 3.2.3, Gas chromatography with mass spectrometry (GC-MS) and proton NMR were also used to analyze the products.

Thermo fisher DSQ II gas chromatograph with mass spectrometer (TR-1 column; 30 m × 0.25 mm × 0.5 µm) was employed to identify the liquid products. It was programmed to keep the temperature at 40 °C for 2 min before ramping up to 290 °C at the rate of 5 °C/min. It holds the temperature at 290 °C for another 3 min. Helium was used as carrier gas.

A Varian Mercury 400 MHz spectrometer operating at 400.393 MHz, was used at 27 °C to distinguish types of hydrogen in the liquid products. Samples were diluted with chloroform 99.8 atomic % D, provided by Sigma-Aldrich. 16 scans were performed for each proton spectrum and the residual chloroform (CHCl_3) peak resonance at 7.26 ppm was the reference peak.

4.2.4. Calculations

- GC calculations**

GC calculations were conducted in the same way as explained in section 3.2.4. Catalyst deactivation rate was calculated using equation below:

$$\text{Catalyst deactivation (\%)} = 1 - \frac{\text{Final yield}}{\text{Maximum yield}} \quad (4-1)$$

In order to carry out the mass balances, the reactant gas was assumed to be an ideal gas. Thus, the ideal gas law can be utilized.

$$PV = nRT \quad (4 - 2)$$

$$m = n \times \text{Molecular weight of the gas} \quad (4 - 3)$$

Where P is the pressure (Pa), V is volume (m^3), n is mole, R is universal gas constant ($8.314 \text{ J.mol}^{-1}.\text{K}^{-1}$), T is temperature (K), and m is the weight of the reactant gas. Having the flow rate of the gas going inside, the total mass of the reactant can be calculated from the formula above. In that equation, V is assigned to be the flow rate of the reactant gas, P would be the pressure of the cylinder, and T is room temperature (25°C). n, calculated in this way, will be the mole of reactant gas per unit time. Multiplying this number to the molecular weight of the gas gives us the mass of the inlet gas. Amount of liquid, captured from the reactor, is subtracted from the mass of inlet gas, which is the total mass of the gas going out of the reactor. This gas contains both converted, and unconverted reactant gas. The portion of each compound in the product and the unconverted gas in the outlet stream can be calculated from the GC analysis, and therefore masses of the components in the product can be measured. Liquid yield can be calculated using equation below.

$$\text{Product yield} = \frac{\text{Mass of product}}{\text{Time} \cdot \text{Amount of catalyst}} \quad (4 - 4)$$

4.3. Results and discussion

4.3.1. Background - Conceptual design for applied study

In a typical thermal upgrader there are two positions for pyrolysis gas to liquid conversion. The first is after the pyrolysis reactor/coker drum before the vapor product enters the fractionator (Figure 4-2 stream 1) and the second is after the overhead drum (Figure 4-2 stream 2).

The second position (Figure 4-2) is preferred, because some of the H₂S and most of the NH₃ will be absorbed in the sour water. Furthermore, it restricts conversion to the light gases, which is really important for the present work. The disadvantage is that the pyrolysis gas is no longer hot and it must be preheated before conversion can take place. However, oligomerisation is exothermic. If sufficient preheating can be achieved for conversion at a reasonable rate, the adiabatic temperature rise in the catalyst bed will further heat the pyrolysis gas, until it is balanced by aromatization, which is endothermic. This conceptual design proposal formed the basis for the catalytic investigation in the present work [4].

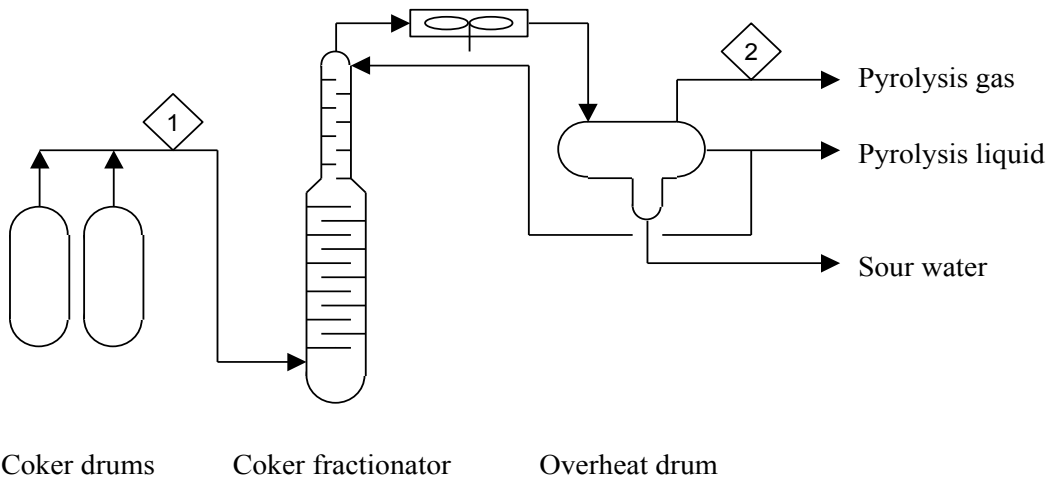


Figure 4-2. Two positions for pyrolysis gas to liquid conversion as illustrated with a delayed coker process. Only lines pertinent to the discussion are shown on the flow diagram.

4.3.2. Catalytic investigations

- **Product yield**

The investigation was limited to low pressure conversion (max. 0.7 MPa), as one can expect in a pyrolysis gas system. Preheating was limited to max. 220 °C for most of the experiments, instead of the lower limit of 300 °C as indicated previously based on the batch reactor test work. This inlet temperature can be easily achieved with steam, which is an advantage for commercialization.

Different synthetic gas mixtures were used to simulate the impact of changes in pyrolysis gas composition on conversion when the temperature was allowed to increase adiabatically (Table 4-1).

On this point it is worthwhile noting that for the most productive conversions, adiabatic heating stabilized at a bed temperature of around 300 °C (i.e. confirming the outcome of the batch reactor studies). Productivity depended on the adiabatic temperature, as one would expect, with a significant self-heating found for concentrated olefinic feeds. In real pyrolysis gas the olefin content is lower, as represented by olefin-paraffin mixtures. The productivity is much lower, but the results are still encouraging. For example, for the catalyst employed for the M- and M₂-forming processes, developed in the 1980's, a liquid productivity of ~1.5 g. g_{cat}⁻¹.h⁻¹ was reported at 260 °C and 5 MPa [6], [7]. This is the same order of magnitude as found during the present work (~2.5 g. g_{cat}⁻¹.h⁻¹), albeit at less severe condition.

Table 4-1. Conversion of pyrolysis gas mixtures to liquids over H-ZSM-5 with inlet at 190-200 °C and 0.6 MPa

Experiment code	Gas mixture	Flow rate (L·g _{cat} ⁻¹ ·h ⁻¹)	Conversion (g liquid·g _{cat} ⁻¹ ·h ⁻¹)
A	Propene	33	74.6
B	1:2.4 propene + ethene	101	53.5
C	1:1.2 propene + methane	70	20.8
D	1:1.9 propene + hydrogen	95	16.8
E	1:1 propene + butane	66	2.5
F	1:1.8 propene + Carbon Dioxide	92	15
G	1:2.2:1.2 propene+ethene+methane	142	10.7
H	ethene	142	16.4

The data were gathered from 3 h of time on stream (TOS). The products were captured every 20 min.

In case of ethene, because of its low reactivity, and for the mixture of propene, methane and ethene, because of the low partial pressure of the propene, the reaction was conducted at higher temperature (furnace temperature of 300 °C).

The reason that conversion of ethene was low compared to propene is that ethene makes primary carbocation when reacting over acid catalysts, while propene produces a secondary carbocation, which is more stable (Figure 4-3).

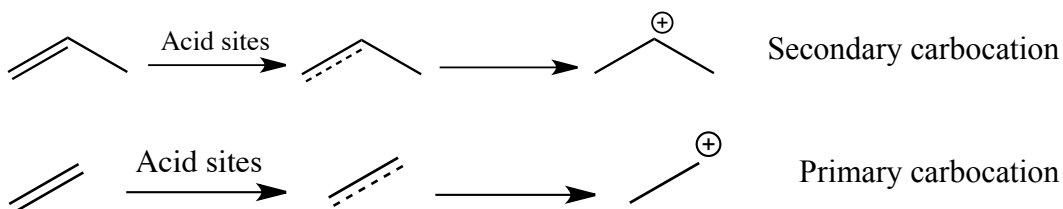


Figure 4-3. Ethene and propene reacting over acid catalysts

Propene, as the reactant gas, gives less conversion when mixed with other gases. It is because of the reduction of its partial pressure. As one might realize, for the mixture of propene, ethene, and methane, where propene has the lowest partial pressure, the lowest conversion is also observed.

Carbon dioxide was mixed with propene only as a diluent, which means that it doesn't have any effect on the mechanism of the reaction. Despite of mixing propene and carbon dioxide with the ratio of 1:2, the yield decreased by 50% instead of 67%, which indicates that the conversion doesn't have linear relation with pressure. Assuming the rate constant of the reaction (k) to be constant, the order of the reaction (n) can be calculated:

$$-r_A = k \cdot C_A^n \quad (4 - 5)$$

$$\frac{-r_{A_2}}{-r_{A_1}} = \left(\frac{C_{A_2}}{C_{A_1}}\right)^n \quad (4 - 6)$$

$$\log \left(\frac{-r_{A_2}}{-r_{A_1}}\right) = n \cdot \log \left(\frac{-r_{A_2}}{-r_{A_1}}\right) \quad (4 - 7)$$

$$\log(0.5) = n \cdot \log\left(\frac{0.3333}{1}\right) \rightarrow n = 0.63 \quad (4 - 8)$$

Experiments were not isothermal tests and the conversions cannot be compared in the normal way. The conversion rate depended much on whether the

gas mixture enabled sufficient conversion to result in a significant adiabatic temperature increase or not. A typical time-temperature history is shown in Figure 4-4.

There is an “initiation” period during which the bed temperature increases slowly before a threshold temperature is reached. After reaching the threshold temperature there is a rapid increase in temperature to reach aromatization conditions. At these conditions, a temperature drop begins to take place, which is because of two reasons: Firstly, catalyst deactivation due to the coking; and secondly, hydrocarbon aromatization, which is an endothermic reaction.

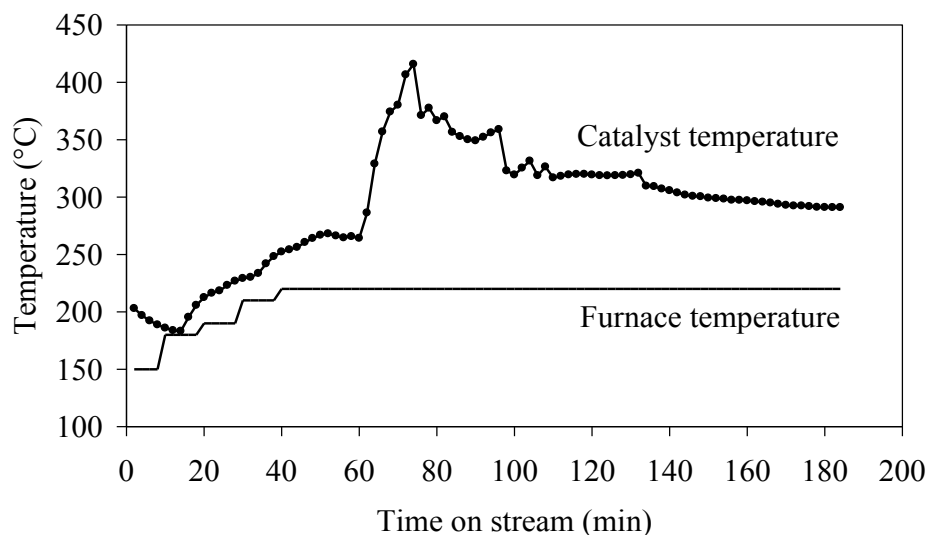


Figure 4-4. Adiabatic time-temperature profile in H-ZSM-5 catalyst bed during conversion of a 1:2.4 propene + ethene mixture at 0.7 MPa.

- **Product composition**

The liquid product composition reflects the bed temperature (Table 4-2). More aromatics are found in the liquid product of higher bed temperature conversion.

The amount of aromatics observed for the reaction of propene over H-ZSM-5 is close to what has been reported by Guisnet et al., although their reaction condition is slightly different [5]. For all cases, toluene, different types of alkyl

benzenes including xylene, trimethyl benzene, and diethyl benzene are prominent aromatic compounds. Little benzene was detected in the products, though. The carbon number distribution of the liquid products is presented in

Table 4-2. Amount of aliphatics and aromatics in the liquid products from the conversion of different mixture of gases over H-ZSM-5

Experiment	Aliphatics	Aromatics
A	79	21
B	78	22
C	65	35
D	70	30
E	76	24
F	72	28
G	56	44
H	62	38

It was not possible to correlate the composition to the anticipated equilibrium composition, because the temperature changed over the reaction period (Figure 4-4). Overall, the typical liquid product composition is similar to that previously reported for the M-forming processes of Mobil [6], [7]. This is hardly surprising considering the same catalyst is employed.

Table 4-3. Carbon number distribution of the products from the conversion of different gas mixtures

Exp	Selectivity (wt. %)							
	A	B	C	D	E	F	G	H
C ₁	0.03	0.2	-	0.04	0.003	0.006	-	0.9
C ₂	0.9	1.6	1.8	1.1	0.01	0.97	1	4.2
C ₃	3.5	8.7	5.8	3.6	0.25	2.8	4	35.5
C ₄	25.5	37.3	34.1	34.4	89.1	40.4	48.6	31
C ₅	18.1	12.7	12.4	10	0.9	10.4	10.5	5
C ₆	15.1	12.1	12.5	19.3	4.1	19.7	23.1	8.1
C ₇	9.9	6.5	7	6.4	1.1	6.8	3	2.7
C ₈	12.8	8.3	11.3	10	1.8	8.7	4.8	5.6
C ₉	8.1	5.4	7.3	7.7	1.4	5.8	2.9	4.2
C ₁₀	3.7	3.3	3.9	4.2	0.8	3.6	1.1	1.5
C ₁₁₊	2.3	4.1	3.9	3.3	0.5	1.2	1	1.5

Branched products were at higher quantities compared to straight-chain ones, which is due to the operating temperature. Van Den Berg et al. [12] have reported

that oligomerisation of short alkenes at low temperatures (<300 K) mostly occur inside the intracrystalline pores, and consequently more linear products will be observed. However, as the temperature increases (300 K $<$ T $<$ 500 K), the reaction rate increases, and heavy products cause pore-mouth blockage. In this case, the outer surface sites will become important for the reaction. Therefore, more branched products will be observed. When the temperature goes even higher, cracking is predominant, and there is no more pore blockage. Two types of products will be the major parts in this situation: short chain compounds (e.g. C₃) and highly branched compounds. Since the temperature of the catalyst increased during our reactions (to more than 500 K), it could be expected to see such spectra for the products.

It has been previously reported that light alkanes, such as methane, ethane, propane, and butane are capable of producing aromatics at high temperatures and fairly low pressure (530 °C, and 1bar). The alkanes first go through a cracking step. The oligomerisation of the products yielded from the first step will result in aromatic compounds by hydrogen disproportionation. For the mixture of propene and butane, in our experiments, it seems that for butane, cracking step hasn't proceeded significantly. The low rate of cracking can be due to the lower operating temperature compared to what has been employed in Guisnet et al. experiments [5]. Therefore, n-butane in the presented work has most probably had no contribution in the aromatics production. The high percentage of dehydrogenated C₄ products that have been observed is more likely due to propene oligomerisation and cracking.

For the reaction of propene and butane, there's also a possibility of hydride transfer for n-butane. In this case, the obtained carbocation may interact with propene or other alkenes present in the system to generate paraffins. In order to check this hypothesis, proton NMR was conducted on the liquid products (Figure 4-5).

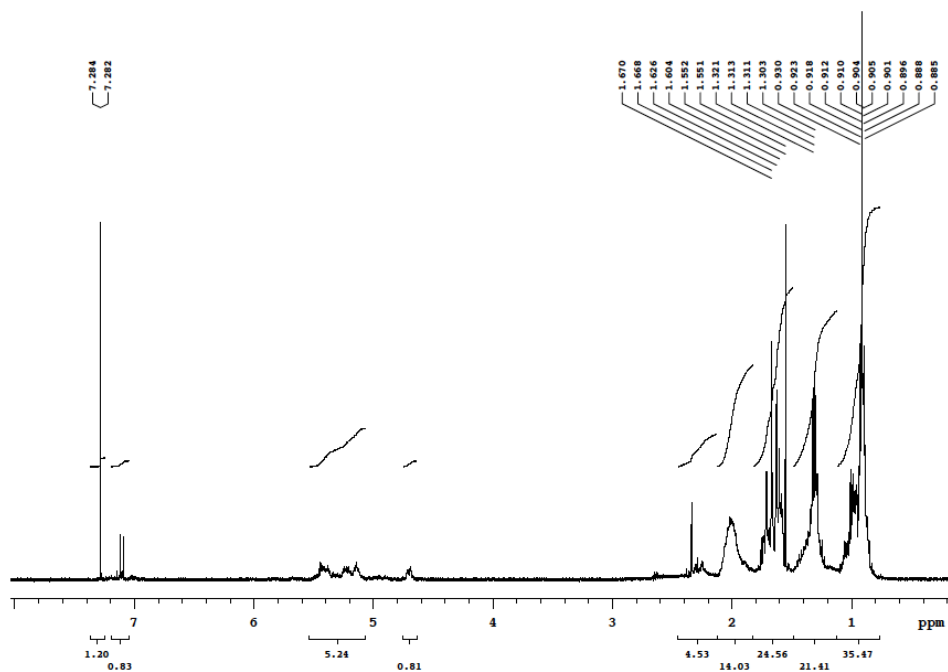


Figure 4-5. H-NMR spectrum of the product from the reaction of mixture of propene and butane

Peaks at around 1.2 and 1.8 are respectively assigned to highly mobile CH₂ and CH₃. All alkane hydrogens are in this area. Those at ~2-3 ppm belong to hydrogen adjacent to sp² carbon which have reduced mobility [9]. Those include the ones on single bound carbon, which is itself connected to a double-bound carbon. In the range of 4.5-6.5 ppm, alkene protons, directly attached to double-bound carbon, show up. And finally at the range of 6.5-8.5 ppm, aromatic protons appear. Table 4-4 shows the portion of each type of hydrogen in the liquid products captured from the reaction of mixture of propene and butane over H-ZSM-5.

Considering both the data obtained from H-NMR analysis and the results listed in Table 4-4, it can be concluded that alkenes are predominant species in the product. Only a small portion of the product contains paraffinic compounds. This means that the primary hypothesis that paraffins might have reacted over the catalyst, did not happen in practice.

Table 4-4. Summary of the $^1\text{H-NMR}$ analysis for the products obtained from the reaction of mixture of propene and butane over H-ZSM-5

Type of hydrogen (%)	Alkane (1.2-1.8)	Alkene (2-6.5)	Aromatic (6.5-8.5)
Mixture of propene and butane as reactant	75.3	22.8	1.9

Product, obtained from the reaction of ethene, has a higher ratio of light hydrocarbons ($\text{C}_1\text{-C}_3$) compared to those captured from other reactants. Further, heavier components have a lower ratio. These are because of the higher temperature employed to get the ethene react, which leads to a higher cracking rate.

- **Catalyst deactivation**

As it was mentioned before, ethene and also mixture of propene, ethene, and methane was converted at higher temperature compared to other mixtures. The higher temperature caused the conversion to decrease over the time. The conversion and other percentages, mentioned in this chapter, all belong to the maximum amount of the product captured at the first minutes, i.e. initial conversion. For the reaction of ethene, the catalyst completely deactivated after 100 min of reaction. In case of propene, ethene, and methane, as reactants, the conversion decreased by 57% after 3 h of operation. The rate of liquid production versus TOS for both cases is plotted in Figure 4-6. Reaction starts with a low rate of products before reaching its maximum value, and then the yield decreases again. For other mixture of gases, deactivation was not remarkable; leading to the conclusion that temperature is a determining factor for the catalyst deactivation.

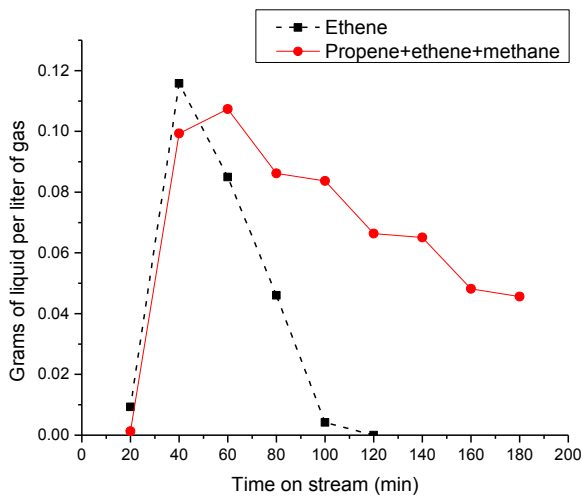


Figure 4-6. Conversion changes versus time for the reaction of ethene and mixture of propene, ethene, and methane

4.4. Conclusion

It was demonstrated that catalyst selected for the conversion was capable of converting the olefinic products in the pyrolysis gas into liquid products at a rate that is comparable with typical refinery process technology. Although catalyst stability must still be confirmed in the presence of all the potential heteroatom-containing gases present in pyrolysis gas, the initial prognosis is encouraging.

Using the reaction heat as the driving force for the reactions facilitates an operating condition with a limited preheating, which is of value from economical perspective.

Reaction condition is the determining factor to modify the product spectrum. Therefore, the operating condition should be strictly controlled, should one intend to limit the product composition to a specific range. Catalyst deactivation is mainly a function of reaction temperature. Temperatures of higher than 400 °C cause a rapid deactivation of the catalyst.

References

- [1] Lallemand, M.; Finiels, A.; Fajula, F.; Hulea, V. *Chemical Engineering Journal* **2011**, *172*, 1078–1082.
- [2] Zhang, Q.; Dalla Lana, I. G. *Chemical Engineering Science* **1997**, *52*, 4187–4195.
- [3] Ding, X.; Li, C.; Yang, C. *Energy & Fuels* **2010**, *24*, 3760–3763.
- [4] Shamaei, L., De Klerk, A. *Prepr. Pap.-Am. Chem. Soc., Div. Energy Fuels* **2012**, *57* (2), 1005–1006.
- [5] Guisnet, M.; Gnep, N. S.; Aittaleb, D.; Doyemet, Y. J. *Applied Catalysis A: General* **1992**, *87*, 255–270.
- [6] Chen, N. Y.; Yan, T. Y. *Ind. Eng. Chem. Process Des. Dev.* **1986**, *25*, 151–155.
- [7] Chen, N. Y.; Garwood, W. E.; Heck, R. H. *Ind. Eng. Chem. Res.* **1987**, *26*, 706–711.
- [8] Van Den Berg, J.P.; Wolthuizen, Van Hooff, J.H.C. *Journal of Catalysis* **1983**, *144*, 139–144.
- [9] Helms, J. R.; Kong, X.; Salmon, E.; Hatcher, P. G.; Schmidt-Rohr, K.; Mao, J. *Organic Geochemistry* **2012**, *44*, 21–36.

5. FLOW REACTOR STUDIES WITH SUPPORTED NICKEL CATALYSTS

Abstract

Loading nickel onto an acidic support material was proposed as a pathway to improve the products obtained from the oligomerisation of pyrolysis gas. H-ZSM-5 and two kinds of amorphous silica-alumina with Si/Al ratios of 20 and 40 wt%, called Siral 20 and Siral 40, were selected as supports. Two loadings of Ni, 0.5 wt.% and 5 wt.%, were tested. Lower loading (0.5 wt.% Ni) didn't change the support properties much. The higher loading (5 wt.%) on H-ZSM-5 resulted in less aromatics and more oligomers and cyclohydrocarbons than observed before at similar conditions. The role of Ni in dehydrogenation was confirmed by reaction of butane over Ni/SiO₂, which is a non-acidic support. A similar strategy was employed to evaluate the contribution of NiO to oligomerisation and it was found that NiO/SiO₂ was inactive for oligomerisation of both propene and ethene. The conversion over the catalysts employing Siral 20 and 40 as support were lower than that over the catalysts employing H-ZSM-5 as support. In fact, Siral 20 didn't show any activity due to the strong interaction of metal species with the support, leading to the formation of nickel aluminate, which made it difficult to reduce the NiO to Ni.

Keywords: Nickel, silica-alumina, dehydrogenation, dimerisation, ZSM-5

5.1. Introduction

Catalysts, such as zeolites, which possess Brønsted acid sites, are so common for catalyzing olefin oligomerisation at moderate reaction condition; however, their selectivity to oligomers is not significant. This can be due to the presence of Brønsted acid sites, which are capable to crack the products and generate aromatics through skeletal isomerisation mechanism. Brønsted acid catalysts show high activity for the oligomerisation of C₃-C₅ Olefins due to the formation

of stable carbenium ions; however, their activity for ethene oligomerisation is much lower and it can only happen at high temperatures. Acid-catalyzed oligomerisation generally has less selectivity as many side reactions happen at the same time, which lead to a complex mechanism and a broad range of components in the product. In some studies, Ni-based acidic catalysts are proposed as a substitution for unpromoted Brønsted acid catalysts, as they have a higher selectivity to olefins [1], [2].

Oligomerisation of light olefins over acid-form ZSM-5 was investigated in the last chapter. The products, as mentioned before, had a plenty of aromatic compounds. In this chapter, in order to improve the product spectrum as well as the operating condition of the ZSM-5 catalyzed reactions, Ni incorporation was suggested. In addition to the highly acidic ZSM-5, three other supports (with less or no acidity), including Siral 20, Siral 40, and silica were also examined for the oligomerisation of alkenes in combination with Ni and NiO.

5.2. Experimental

5.2.1. Materials

Among the cylinder gases mentioned in section 3.2.1 and 4.2.1, ethylene, propylene, butane, hydrogen, and nitrogen were used in this part. In addition to the materials mentioned in section 4.2.1, two types of silica-alumina, silica, as well as Nickel (II) nitrate hexahydrate were also used in this set of experiments.

Silica-aluminas, as purchased from Sasol Germany, were used for metal support. The specifications, provided by the company, are listed in table below. Other than silica-aluminas, silica with the purity of 99.8%, provided by Sigma-Aldrich, was also used as nickel support material.

Nickel (II) nitrate hexahydrate was used as Ni source for catalyst metal function on the various supports. It was provided by Sigma-Aldrich with the purity of 99.999%.

Table 5-1. General properties of silica-aluminas provided by supplier

Catalyst	Al ₂ O ₃ : SiO ₂	C (%)	Fe ₂ O ₃ (%)	Na ₂ O (%)	Loose bulk density (g/L)	Particle size (d ₅₀) (μm)	Surface area (BET) (m ² /g)	Pore volume (mL/g)
Siral 20	80:20	0.2	0.02	0.005	300-500	50	420	0.75
Siral 40	60:40	0.2	0.02	0.005	250-450	50	500	0.9

5.2.2. Equipment and procedure

The equipment and procedure are identical to those employed previously for flow reactor, except that the diameter of the tube reactor was increased to 0.75" in order to reduce temperature changes in the catalyst bed during reactions. All the reactions were conducted at near atmospheric pressure. Operating temperature varied depending on the reactant. Temperatures presented in this chapter, unless otherwise stated, belong to the furnace temperature. The difference of the internal reactor temperature with furnace is ±20 °C along the tube. In cases where the catalyst needed to be reduced, the reducing gas, which was employed, was a mixture of hydrogen and nitrogen with the volume ratio of 1:9. The reducing temperature was determined based on the TPR profiles in such a way that the reducing temperature will be more than the temperature of the last reduction peak in the TPR analysis.

Nickel was loaded on the support using the "dry impregnation" technique. Prior to the impregnation, ZSM-5 was calcined at 550 °C for 3 h to be transformed into the acid form. 1 cm³ of impregnating solution per gram of support was added drop by drop to the supports at room temperature while the mixture was being stirred thoroughly. The excess solution was allowed to dry at room temperature for several days, while it was stirred periodically. Finally the catalysts were calcined in air at 550 °C for 3 h [4].

5.2.3. Analyses

GC-MS analyses were performed by a Varian CD-3800 GC supplied with a 220 GC-MS. It was equipped with FID, autosampler, and a Varian FactorFour Capillary type column (VF-5ms) with the length of 30 m, inner diameter of 0.25 mm and film thickness of 0.25 μm . The samples were diluted with carbon disulfide prior to injection. It was programmed to hold the temperature at 50 °C for 10 min before ramping to 320 °C with the rate of 10 °C/min. Temperature eventually remained constant for an additional 10 min. Nitrogen was used as carrier gas. Mass spectrometry of the gas products were carried out using OMNI star™ Gas Analysis System, supplied with a PFEIFFER vacuum system.

NH₃-TPD and FTIR analyses of the catalysts were performed to determine the strength, abundance, and nature of the acid sites. Tests were performed with the same instrument and method as described in section 3.2.3.

Temperature-programmed reduction (TPR) thermograms were recorded using the same apparatus used for TPD analyses. TPR measurements were carried out by passing 10 vol. % H₂/He gas mixture (10 mL/min) over the sample while it was heated at a constant rate of 10 °C/min from room temperature to 950 °C. Since the samples were already calcined, TPR analyses were directly conducted without any further pretreatment of the samples. The instrument was programmed to wait for 15 min before ramping up, so that the baseline stabilized. Helium is the carrier gas with the flow rate of 70 mL/min. The machine was run with the detector current of 150 mA, and attenuation of 16. In order to get the amount of hydrogen consumed during the reduction of the catalyst, the instrument was calibrated with the same gas used for the reduction of the catalyst.

X-Ray Diffractometry (XRD) was also used to characterize the catalyst. Powder X-ray diffraction patterns collected on an Intel diffractometer equipped with a curved position-sensitive detector (CPS 120) and a Cu K α 1 radiation source. The XRD patterns were recorded with the scan speed of 0.029 °/min, λ =

1.54056 Å in the 2θ range of 0.28 – 113.78°. Samples were ground evenly before running the tests.

Thermal gravimetric analyses of spent catalysts were conducted by TGA/DSC1 LF FRS2 MX5 ($5\text{g} \pm 1\mu\text{g}$) supplied with sample robot. Samples were analyzed under air. The oven was programmed to ramp from 25 °C to 900 °C with the rate of 10 °C/min.

5.2.4. Calculations

The quantity of the metal salt, needed to be dissolved in the distilled water, was calculated through the equation 5 - 1. Molecular weights of Ni and $\text{Ni}(\text{NO}_3)_2$ are 58.7 and 290.7 g/mol, respectively.

$$\begin{aligned}\text{Amount of } \text{Ni}(\text{NO}_3)_2 \cdot 6\text{H}_2\text{O} = & \text{ Metal loading (either 0.5% or 5%)} \times \text{support weight} \\ & \times \text{Molecular weight of } \text{Ni}(\text{NO}_3)_2 / \text{Molecular weight of Ni}\end{aligned}\quad (5 - 1)$$

GC, NH_3 -TPD and FTIR calculations were carried out using the same method as explained in section 3.2.4 and 4.2.4. In order to calculate the amount of hydrogen consumed during TPR measurements, LogNormal deconvolution of the peaks was employed.

In the cases that both liquid and gas products were observed, mass balances were performed using the same method as illustrated in section 4.2.3. But, for those that only gas products were captured, for conversion calculations, it was assumed that the unconverted gas coming out of the reactor has the same quantity as the gas going inside the reactor. In other words, the conversion is calculated from the equation below:

$$\text{Conversion (\%)} = \frac{\text{Mass of products. 100}}{\text{Mass of unreacted gas}} \quad (5 - 2)$$

In order to get the conversion (%) by means of GC software, “percent” mode was chosen for the report type. Pure reactant gas was primarily analyzed by GC, and the conversion % for each run of the experiment was calculated by subtracting the percent of unreacted gas from the percent of the pure gas.

5.3. Results and discussion

5.3.1. Catalyst Characterization

- Metal content characterization**

TPR analyses of the catalysts were performed to test the reducibility of the Ni species deposited on the substrates. In the first set of experiments, 0.5 wt.% nickel was loaded over ZSM-5, Siral 40, and Siral 20. Unfortunately, TPR profiles of the 0.5 wt.% loaded supports didn't show any signal to indicate that reduction took place. Also, the catalysts didn't show any activity during the experiments (which will be explained later in the text). It was therefore concluded that 0.5 wt.% loading is not sufficient to make big changes in the support features. 5 wt.% loading was suggested as the adequate loading for the metal, and interestingly the TPR profiles changed thoroughly after loading enhancement. ZSM-5, Siral 40, Siral 20, and silica containing 5 wt.% of nominal Ni content will be respectively referred to as 5Ni/ZSM-5, 5Ni/Siral-40, 5Ni/Siral-20, and 5Ni/Silica hereafter.

Figure 5-1 and Figure 5-2 show the TPR profiles of 5Ni/Siral-40 and 5Ni/Siral-20. As one might consider, the profile of 5Ni/Siral-40 has a minor negative peak at around 300 °C, which is originating from the reduction of nickel oxide species. Ni^{2+} species are usually reduced without forming any intermediate oxides, so bulky NiO is reduced at 300 °C. It can be inferred that nickel on Siral 40 resembles bulk nickel oxide. The main reduction, which happens at higher temperature (750 °C) is associated with the strong interaction of the metal content with the support. Table 5-2 presents the data obtained from the catalysts

characterization. Results in this table show that the ratio of Ni species that incorporated as NiO to those deposited as nickel aluminate is 1:3.5.

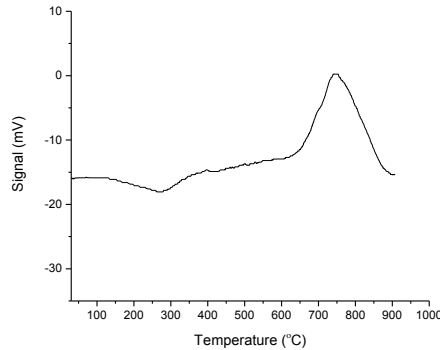


Figure 5-1. TPR profile of 5Ni-Siral 40

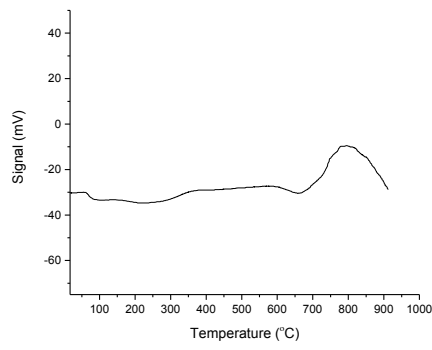


Figure 5-2. TPR profile of 5Ni-Siral 20

In case of 5Ni/Siral-20, there's only a broad peak at fairly high temperature (800 °C), indicating that no nickel oxide exists in the framework, and cationic form of nickel is formed on the support. According to the literature, nickel aluminate reduction profile has a single peak at high temperatures. Thus, most probably NiAl_2O_4 is the major compound in the framework of both 5Ni/Siral-20 and 5Ni/Siral-40.

For 5Ni/Siral-20 the disappearance of the minor negative peak, which showed up in 5Ni/Siral-40 TPR profile, is because of the presence of more Al species in the Siral 20 framework. The broad peak has shifted to higher temperatures for 5Ni/Siral-20, which is again as a result of high concentration of Al species in the framework [5], [6]. In order to confirm the presence of NiAl_2O_4 in the support structure, 5Ni/Siral-20 and 5Ni/Siral-40 were analyzed by XRD. Figure 5-3 shows the XRD results for the samples. As it can be seen from the figure, the diffractograms best match the pattern of NiAl_2O_4 . The amorphous structure of the supports has broadened the peaks appeared in the XRD diffractograms.

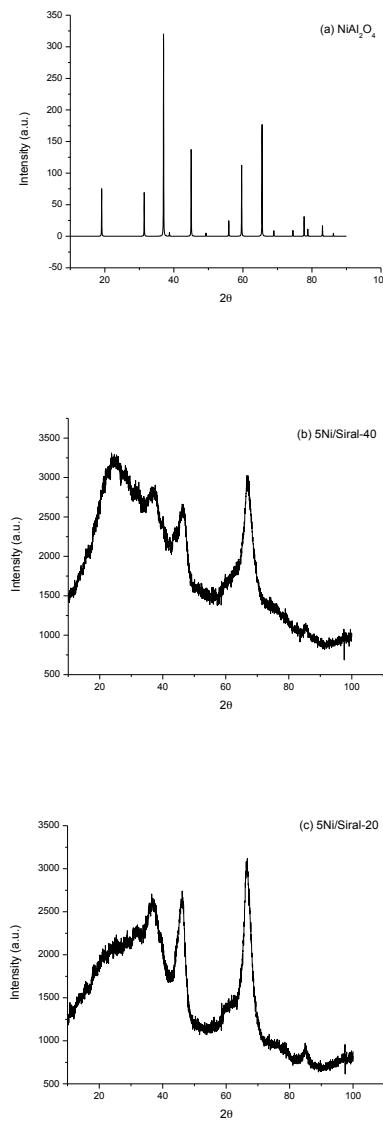


Figure 5-3. XRD patterns of (a) NiAl_2O_4 (b) 5Ni/Siral-40, and (c) 5Ni/Siral-20

In order to overcome the interaction of metal oxide particles and support, which is due to the high density of Al species in the support structure, attempts were made to modify the support. Silica was suggested as the substitution since it has no Al content to interact with the metal. 5% nickel was loaded in the same way as described before. Interestingly, TPR analysis of 5% nickel containing silica indicates that support modification has been successful, as the peaks all appeared at temperatures less than 600 °C (Figure 5-4). The great peak at 450 °C,

which has a shoulder at ~390 °C, corresponds to the reduction of bulky well-dispersed NiO species. The shoulder at lower temperature could be ascribed to large NiO particles having weak interactions with the surface of the support. The last overlapping peak at ~550 °C can be assigned to the reduction of Ni species on the pore wall surface and in the silica framework [8], [9].

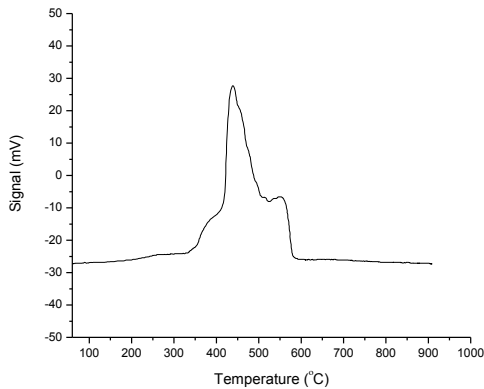


Figure 5-4. TPR profile of 5Ni/Silica

Figure 5-5 shows the TPR profile of 5Ni/ZSM-5. In general, peaks in TPR profiles of nickel-loaded zeolites, which happen at low temperature (<500 °C) correspond to the Ni^{2+} species localized in the sodalite and/or supercage cavities. Those appearing at high temperatures (>400 °C) are associated with the nickel content deposited in the hexagonal cavities. For 5Ni/ZSM-5, there's one clearly resolved maximum at 400 °C, which is attributed to the reduction of NiO species having very low interaction with the support. It can be also due to the reduction of NiO formed on the outer surface of the crystal. The smaller peak observed at ~540 °C can be assigned to the reduction of NiO species, which are strongly interacting with the support. The TPR profile is in agreement with the one previously reported in the literature [7]. Table 5-2 summarizes the data obtained from the TPR analyses.

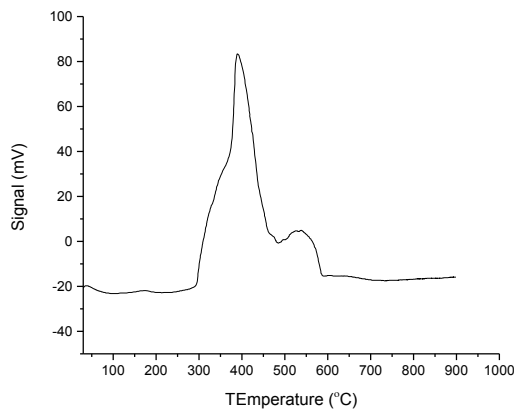


Figure 5-5. TPR profile of 5Ni/ZSM-5

Table 5-2. Peak temperatures and amount of hydrogen consumed for the reduction of each catalyst

Catalyst	Temperature of 1 st peak (°C)	Temperature of 2 nd peak (°C)	Amount of H ₂ consumed for the 1 st peak (μmol/g)	Amount of H ₂ consumed for the 2 nd peak (μmol/g)
5Ni/Siral-40	266	748	341	1210
5Ni/Siral-20	-	799	-	1620
5Ni/ZSM-5	384	538	1615	408
5Ni/Silica	451	543	2690	1250

- Acid sites characterization**

Reduced catalysts were analyzed by NH₃-TPD after their reduction during the TPR measurements. The graphs below show the TPD profiles and FTIR spectroscopy of adsorbed pyridine for 5Ni/Siral-40, 5Ni/Siral-20, and 5Ni/ZSM-5. 5Ni/Silica didn't show any acid sites in the TPD profile, which was expected, as it has no Al and consequently no acid sites in its framework. The TPD profiles of the nickel-loaded silica-aluminas show a broad distribution of acid strength. The distribution is arbitrarily divided into three regions for silica-alumina supports, and two regions for ZSM-5. Three temperature ranges include: 200-300 °C for weak, 300-450 °C for medium, and 450-550 °C for strong sites. For ZSM-5, these regions include 200-300 °C for weak, and 300-500 °C for strong sites. In case of

5Ni/Siral-20, the first and second peaks have merged, and hardly can be distinguished.

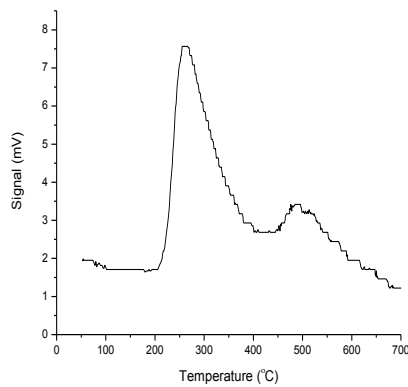


Figure 5-6. NH₃-TPD profile of 5Ni/Siral-20

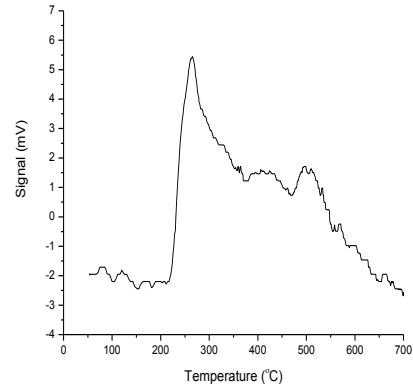


Figure 5-7. NH₃-TPD profile of 5Ni/Siral-40

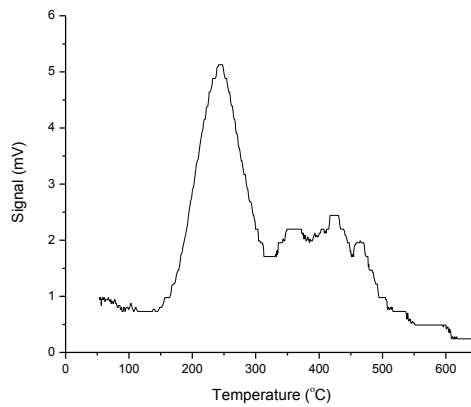


Figure 5-8. NH₃-TPD profile of 5Ni/ZSM-5

Infrared spectra of pyridine desorption were also recorded for the reduced catalysts. Figures below show the spectra for 5Ni/Siral-20, 5Ni/Siral-40, and 5Ni/ZSM-5 (Figures 5-9 to 5-11). Table 5-3 summarizes the concentration and

strength of the sites for each catalyst. As it can be seen, the Brønsted site concentration increases with silica content, as 5Ni/Siral-40 has more Brønsted acidity than 5Ni/Siral-20. The table also indicates that the acidity of ZSM-5 has decreased with nickel loading [10].

Table 5-3. Concentration and distribution of acid sites for different catalysts

	5Ni/Siral-40	5Ni/Siral-20	5Ni/ZSM-5
1 st peak (°C)	263	264	245
2 nd peak (°C)	411	348	-
3 rd peak (°C)	506	515	411
Lewis 1* (μmol/g)	484	739	175
Lewis 2 (μmol/g)	115	123	-
Lewis 3 (μmol/g)	451	619	364
Brønsted 1* (μmol/g)	44	18	59
Brønsted 2 (μmol/g)	11	3	-
Brønsted 3 (μmol/g)	41	15	121

* Lewis 1 and Brønsted 1 correspond to Lewis and Brønsted sites of the first peak.

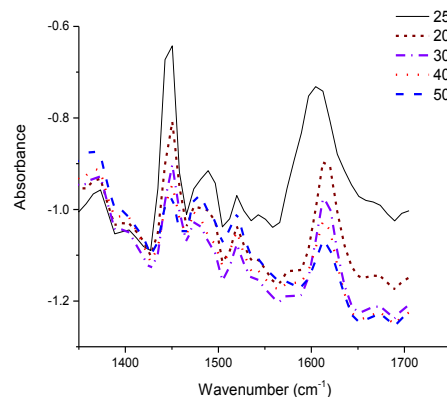


Figure 5-9. FTIR spectra of adsorbed pyridine for 5Ni/Siral-20 at different temperatures

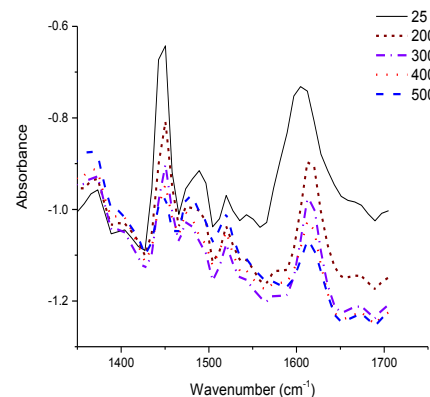


Figure 5-10. FTIR spectra of adsorbed pyridine for reduced 5Ni/Siral-20 at different outgassing temperatures

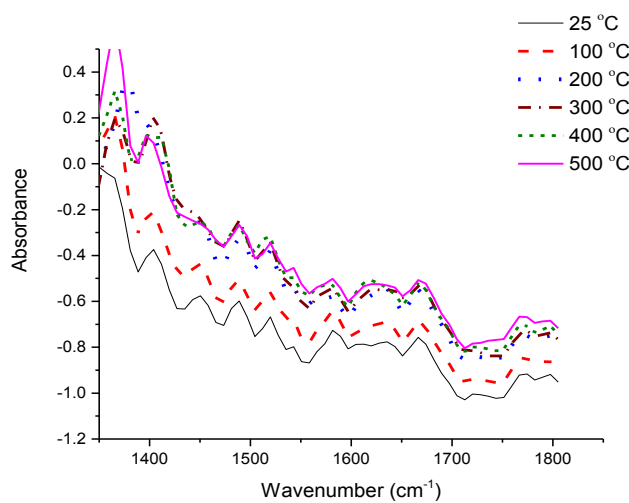


Figure 5-11. FTIR spectra of adsorbed pyridine for reduced 5Ni/ZSM-5 at different outgassing temperatures

The spectrum of 5Ni/ZSM-5 shows the same trend as H-ZSM-5, indicating that the metal incorporation has equally decreased the Lewis and Brønsted sites so that their ratio has remained constant (Figure 5-12).

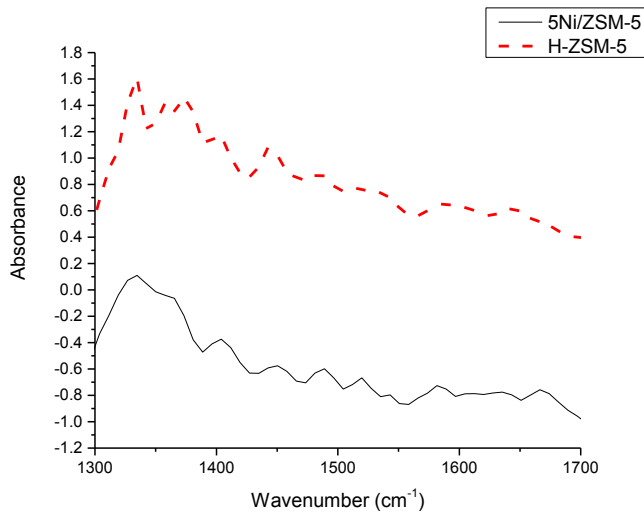


Figure 5-12. FTIR spectra of adsorbed pyridine for reduced 5Ni/ZSM-5 and H-ZSM-5 (at 25 °C)

5.3.2. Catalyst screening in the presence of light hydrocarbons

- 0.5% nickel-loaded catalysts**

Prior to the experiments, the catalysts were pretreated in situ by reducing gas at 400 °C for 1 h. As it was mentioned before, TPR analysis didn't detect any metal reduction. Thus, the reducing temperature was selected arbitrarily at 400 °C.

Reactivity of 0.5% nickel loaded Siral 40, Siral 20, and ZSM-5 was tested for the oligomerisation of propene. Since ionic Lewis sites of Ni combined with acid sites give dehydrogenation properties to the catalysts, they were also tested in the presence of butane, but the catalysts didn't show any reactivity for dehydrogenation or oligomerisation of the butane [11].

Efforts for the oligomerisation of propene and also dehydrogenation of butane at the temperature range of 200-400 °C over 0.5Ni/silica-aluminas were not successful, which perfectly confirms the TPR analyses. The TPR profile didn't show any reduction, which indicates that the amount of metal loading has not be sufficient to have catalytic activity.

However, the oligomerisation of propene over 0.5Ni/ZSM-5 was successful (Table 5-4). Operating pressure was lower than the one applied for H-ZSM-5 reactions. Thus, the reaction temperature was higher (furnace temperature of 300 °C). Temperature of the catalyst bed had the same trend as the one reported for H-ZSM-5 in the previous chapter. Because TPR profile of 0.5Ni/ZSM-5 didn't have any signal, the oligomerisation activity observed for propene might be associated with the acid sites of the zeolite.

Conversion rate is lower than the one observed for H-ZSM-5, which can be due to the decrease in the catalyst acidity caused by metal incorporation. 0.5Ni/ZSM-5 didn't show any activity for butane at 400 °C, which confirms that the catalyst was not active for dehydrogenation. The oligomerisation activity observed for propene is mostly due to the acid sites of the support, and nickel

didn't have any contribution. 0.5Ni/ZSM-5 didn't show any activity for butane at 400 °C, indicating that the catalyst doesn't have dehydrogenating property. Acid sites of the support have most probably resulted in the oligomerisation, observed for propene, and nickel didn't have any contribution.

Table 5-4. Flow rate and conversion rate for the reaction of propene over 0.5Ni/ZSM-5 (at furnace temperature of 300 °C and atmospheric pressure)

Catalyst	Conversion ($\text{g}_{\text{L}} \cdot \text{g}_{\text{cat.}}^{-1} \cdot \text{h}^{-1}$)	Flow rate ($\text{L} \cdot \text{g}_{\text{cat.}}^{-1} \cdot \text{h}^{-1}$)	Grams of liquid per liter of reactant
0.5Ni/ZSM-5	51	60	0.85

Table 5-5 shows the carbon number distribution of the products obtained from the propene oligomerisation over 0.5Ni/ZSM-5. Similar to the product obtained from the reaction of propene over H-ZSM-5, aromatics, such as xylene, ethyl-methyl-benzene, and methyl-propyl-benzene, are considerable constituents of the product.

0.5Ni/ZSM-5 didn't show any activity for butane conversion at temperatures up to 400 °C, which confirms that the catalyst was not active for dehydrogenation. The oligomerisation activity observed for propene is mostly due to the acid sites of the support, and nickel didn't have any contribution.

Table 5-5. Carbon number distribution of the products obtained from the reaction of propene over 0.5Ni/ZSM-5 (at furnace temperature of 300 °C and atmospheric pressure)

Product components	C ₁	C ₂	C ₃	C ₄	C ₅	C ₆	C ₇	C ₈	C ₉	C ₁₀₊
Selectivity (wt.%)	0.1	0.5	0	21	18	31	10	13	5	2

- **5Ni/ZSM-5**

As stated before, in order to increase the contribution of nickel, metal loading was increased to 5 wt.%, and its performance for the conversion of propene was investigated. Prior to the reaction, catalyst was reduced in situ at 400 °C for 1 h. Table 5-6 and Table 5-7 show the conversion and product distribution for the reaction of propene over 5Ni/ZSM-5 at furnace temperature of 300 °C. Changes

of the catalyst temperature had the same trend as the one observed for the reaction over H-ZSM-5.

Table 5-6. Conversion rate of the reaction of propene over 5Ni/ZSM-5 (at furnace temperature of 300 °C and atmospheric pressure)

Catalyst	Flow rate (L·g _{cat} ⁻¹ ·h ⁻¹)	Conversion (g _L ·g _{cat} ⁻¹ ·h ⁻¹)	Grams of liquid per liter of gas
5Ni/ZSM-5	97	38	0.39

Comparing the conversion reported in table above, with the numbers obtained from the reaction over H-ZSM-5 and 0.5Ni/ZSM-5 reveals that increasing the metal incorporation decreases the activity of the support. However, nickel compounds have improved the dimerisation properties of the catalysts. Therefore, an increase in the portion of C₆ compounds is observed in the products obtained from the reaction of propene over 5 wt.% loaded nickel catalysts. However, high amount of C₆ compounds can also be associated with the lower conversion, which make the primary products highlighted. Low valent nickel compounds combined by acid sites are proposed to be the active dimerising sites. It should be noted that acidity of the support is also influential in the oligomerising nature of the catalyst [12].

Table 5-7. Carbon number distribution of hydrocarbon compounds in the product of the reaction of propene over 5Ni/ZSM-5 (at furnace temperature of 300 °C and atmospheric pressure)

Carbon number	C ₁	C ₂	C ₃	C ₄	C ₅	C ₆	C ₇	C ₈	C ₉	C ₁₀₊
Selectivity (wt. %)	0.2	1	0.02	28	18	29	7	12	2	1

A portion of the product captured from the reaction of propene over 5Ni/ZSM-5 consists of alkyl cyclo-pentenes, including methyl cyclo-pentene, ethyl cyclo-pentene, and trimethyl cyclo-pentene. It implies that Ni has dehydrogenated the ring. Table 5-8 shows the amount of alkyl cyclo-pentenes observed in the liquid product.

Table 5-8. Amount of alkyl-cyclopentene compounds in the liquid product captured from the reaction of propene over 5Ni/ZSM-5

	Cyclo-pentene	Methyl-cyclo-pentene	C ₂ -cyclo-pentene	C ₃ -cyclo-pentene	C ₄ -cyclo-pentene
Selectivity (wt. %)	1.8	4.8	4.7	6.4	0.8

- **5Ni/Silica-alumina**

To confirm the TPR analysis, activity of the pretreated 5Ni/Siral-20 (reduced at 380 °C for 1h) was tested in the presence of propene and butane. Both reactions were conducted at temperatures of up to 450 °C. The catalyst didn't show any activity, which is hardly surprising, as the TPR of the catalyst could not detect any reduction and the XRD detected nickel aluminates.

However, for 5Ni/Siral-40 almost 22% of the nickel species were detected in the form of metal oxides. This portion of metal compounds might have oligomerising capabilities. In order to test the probable activity, the catalyst was tested with propene in two modes. In the first mode, metal was pretreated by reducing gas at 380 °C For 1 h. The reduced catalyst was tested with propene at different temperatures. Catalyst started to show activity at 275 °C (flow rate of 0.5 L/min). As the temperature increased, more conversion was also observed. Dimerisation seemed to be the major reaction. At low temperatures, selectivity towards dimers is higher than at elevated temperatures. One can definitely say that at 275 °C only dimerisation has happened. The selectivity to C₆ is comparable to the one reported previously by Spinicci and Tofanari (78.3% at 300 °C, atmospheric pressure, 4 wt.% NiO, and 6 wt.% alumina) [16]. As the temperature increases, the product spectrum shifts towards lighter components (Table 5-9).

The increase in the amount of C₂ and C₄ compounds, and also simultaneous reduction of C₆ species at 400 °C might be associated with the cracking of C₆ compounds. In other words, C₆ breaks down to C₄ and C₂ at that temperature.

The existence of propane at 400 °C can be assigned to the hydrogen transfer to propene due to aromatization.

Table 5-9. Conversion and distribution (vol. %) of the products from the reaction of propene over reduced 5Ni/Siral-40 (flow rate of 60 L_{C3}·g_{cat}⁻¹·h⁻¹)

Temperature (°C)	Conversion (g _{prod} ·g _{cat} ⁻¹ ·h ⁻¹)	C ₁	C ₂	C ₃	C ₄	C ₅	C ₆
275	0.2	0.005	0.1	-	1.2	0.4	98
300	0.6	0.1	0.6	-	6.2	2.0	88
350	1.0	0.3	2.7	-	5.6	3.2	88
400	1.2	1.1	9.7	1.7	18.2	8.1	61.7

Since, nickel is also present on the catalyst, dehydrogenation of the products is also probable. In such case, hydrogen should be present in the gas stream. However, since thermal conductivity of helium, the carrier gas of our GC, is so close to hydrogen, the GC was not able to detect the hydrogen. In order to check the presence of hydrogen, mass spectrometry of the gas product was performed (Figure 5-13). As it can be seen, there is a band at 2 amu. This band can be assigned to hydrogen, as hydrogen spectrum has only one band at 2 amu. The big band at 44 amu is most probably due to the presence of propane.

Activation energy of the reaction (E_a) can be calculated using Arrhenius equation.

$$k = A e^{-E_a/RT} \quad (5 - 3)$$

Where A is the pre-exponential factor, k is rate constant, R is the universal gas constant, and T is the absolute temperature in kelvin. By plotting $\ln k$ versus $1/T$, activation energy is measurable. The activation energy for the reaction of propene over 5Ni/Siral-40 would be 22.5 kJ/mol (Calculations can be found in Appendix III).

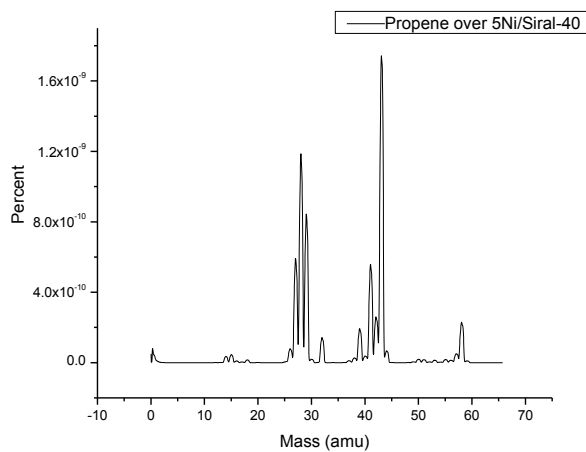


Figure 5-13. Mass spectrum of the gas products from the reaction of propene over 5Ni/Siral-40 (at 400 °C)

In the second mode, the oligomerisation activity of the metal oxide on the support was tested. The reaction of propene was carried out with the flow rate of 0.5 L/min and onset temperature of 200 °C. At 200 °C, catalyst didn't show any activity. At 300 °C, minor conversion was observed. The product mainly contained C₆ compounds, indicating that dimerisation has been the predominant reaction. No liquid and minor cracking was observed. Increasing temperature to 400 °C, enhanced both conversion and the cracking rate. However, increasing the temperature to 500 °C reduced the conversion markedly. When the temperature was reduced back to 400 °C and then to 300 °C, the catalyst was completely deactivated, and no conversion was observed. Temperature of the catalyst bed didn't change throughout the reaction, and it was only 20 °C higher than the furnace temperature.

Table 5-10. Distribution (vol. %) of the products of the reaction of propene over 5NiO/Siral-40 (flow rate of 60 L_{C3}·g_{cat}⁻¹·h⁻¹)

Temperature (°C)	Conversion (g _{prod} ·g _{cat} ⁻¹ ·h ⁻¹)	C ₁	C ₂	C ₃	C ₄	C ₅	C ₆
200	-	-	-	-	-	-	-
300	0.9	0.1	0.6	0.4	2.9	2.3	93.6
400	1.2	1.5	9	2	13	4	71
500	0.1	8	9	10	9	2	61

Thermal gravimetric analysis of the spent catalyst was performed to measure the amount of coke formed on the catalyst. As Figure 5-14 shows, three weight losses were observed in the TG profile. First weight loss, happening at temperatures less than 450 °C, is due to the evaporation of light and volatile hydrocarbons. The second weight loss takes place at the range of 450 to 700 °C, which is ascribed to the thermal decomposition of heavy products. The one that shows up at temperatures higher than 750 °C is associated with the coke formed on the catalyst. Table 5-11 shows the summary of the TG analysis for the spent 5Ni/Siral-40 after the reaction with propene.

Table 5-11. TG results of spent 5NiO/Siral-40 after the reaction with propene

	Temperature		Amount (%)
	Original (°C)	End (°C)	
Dehydration and release of volatiles	28	450	3
Heavy products combustion	450	700	3
Coke decomposition	750	900	3

Compared to the similar investigations, which have reported higher conversions, it can be inferred that pressure and the silica to alumina ratio are important factors in the conversion and selectivity. Low pressure and high density of Al species are the unfavorable parameters in the current study, which have resulted in low conversion [13], [14]. According to the study done by Spinicci and Tofanari on propene oligomerisation over Ni-loaded silica-aluminas, both low valent nickel species and alumina acid sites are mandatory for the catalytic activity. However, the portion of alumina employed in their study was less than 12 wt.%. It can be inferred from their study and the present work that there should be a balance between Al and Si content of the catalyst. High concentration of Al species might lead to the formation of nickel aluminates, while lack of alumina decreases the catalytic activity [16].

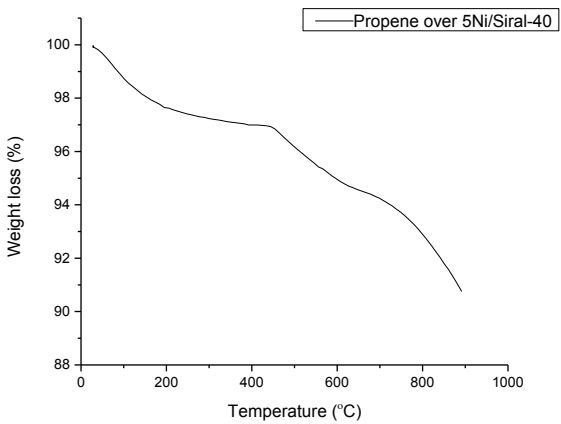


Figure 5-14. Thermal gravimetric analysis of spent 5Ni/Siral-40 after the interaction with propene

- **5Ni/SiO₂**

Silica inherently doesn't have any acid sites. Its contribution to the employed catalyst is only the enhancement of the surface area. Indeed, nickel particles play the major catalytical role in the reactions.

5Ni/SiO₂ was tested in two mode: reduced, and oxide form of the metal. In the first mode, the catalyst was reduced at 600 °C for 1 h. The reduced catalyst didn't show any oligomerisation activity for ethene and propene at temperatures of up to 400 °C. However, it exhibited dehydrogenating properties when interacting with butane. The reaction was conducted with a mixture of nitrogen and butane (1.1 L/min nitrogen, and 250 mL/min butane). Reaction started to happen at 400 °C. The conversion rate remained constant with temperature increasing to 500 °C. But, a significant increase was observed when the temperature increased to 575 °C. Cracking is the major reaction at this temperature. Dehydrogenation also decreased by 70%. No liquid was obtained for all the cases. At 575 °C, no component heavier than C₅ was observed.

Activation energy of the reaction of butane with 5Ni/SiO₂ can be calculated using Arrhenius equation (as illustrated before). The activation energy calculated

in this way was 177 kJ/mol. This activation energy is much higher than the one obtained for the reaction of propene with 5Ni/Siral-40, which is not surprising as the reaction of butane over 5Ni/SiO₂ started to happen at a higher temperature.

Table 5-12. Conversion and carbon number distribution (vol.%) of butane over 5Ni/SiO₂ at different temperatures and atmospheric pressure (flow rate of 30 L_{C4}.h⁻¹.g_{cat}⁻¹)

Temperature (°C)	Conversion (g _{prod} .g _{cat} ⁻¹ .h ⁻¹)	Conversion (g _{prod} .g _{Ni} ⁻¹ .h ⁻¹)	C ₁	C ₂	C ₃	C ₄	C ₅	C ₆
350	0	0	-	-	-	-	-	-
400	0.14	2.8	7	10	4	77	3	0.5
450	0.14	2.8	2	4	7	82	4	0.8
500	0.14	2.8	5	5	7	50	11	0.5
575	1.6	32.6	30	32	31	6	1	-

Since the dehydrogenation has been the major reaction during the experiment, hydrogen was supposed to be one of the main components in the product stream. MS was carried out to check the presence of hydrogen in the gas product (Figure 5-15). Same as propene over 5Ni/Siral-40, the band at 2 amu can be assigned to hydrogen, so the dehydrogenation most probably has taken place.

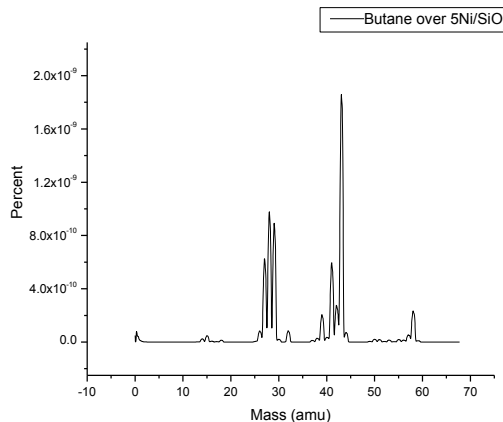


Figure 5-15. Mass spectrum of the gas products from the reaction of butane over 5Ni/SiO₂ (at 450 °C)

TG analysis of the spent catalyst was performed to measure the coke formation (Figure 5-16). As the figure shows, weight loss happens in three stages. First, the volatile and light compounds, deposited on the catalyst, evaporate at

temperatures of up to 550 °C. Heavier products are decomposed at the range of 550 to 700 °C, in the second stage. Finally, coke is combusted at 700 to 900 °C. Table 5-13 shows the summary of the TG results for the reaction of butane over 5Ni/SiO₂.

Table 5-13. TG results of spent 5Ni/SiO₂ after the reaction with butane

	Temperature		Weight loss (%)
	Original (°C)	Original (°C)	
Volatile products evaporation	28	550	2
Heavy products combustion	550	700	3
Coke decomposition	700	900	2

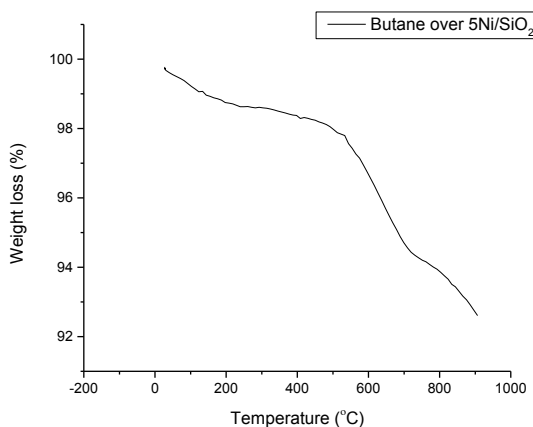


Figure 5-16. Thermal gravimetric analysis of spent 5Ni/SiO₂ after interacting with ethene

In the second mode, oxide form of nickel species was tested with ethene, propene, and butane. However the catalyst in this form was not effective for the dehydrogenation of butane, reaction of ethene and propene over 5Ni/SiO₂ showed different trend. Ethene started to react at 650 °C (flow rate of 1 L/min). No liquid phase was captured. Considering the numbers listed in Table 5-14, one can realize that only thermal cracking of the olefins has occurred during the reaction, and NiO particles didn't exhibited any oligomerising activities.

Table 5-14. Conversion and product distribution (vol.%) of the reaction of ethene over 5Ni/SiO₂ at different temperatures and atmospheric pressure (flow rate of 120 L_{C2}.h⁻¹.g_{cat}⁻¹)

Temperature (°C)	Conversion (g _{prod} .g _{cat} ⁻¹ .h ⁻¹)	Conversion (g _{prod} .g _{Ni} ⁻¹ .h ⁻¹)	C ₁	C ₂	C ₃	C ₄	C ₅	C ₆
600	-	-	-	-	-	-	-	-
650	0.96	19.2	17	29	18	26	5	5

Similar to the reaction of ethene, the only reaction happened during the interaction of propene with 5Ni/Silica has been thermal cracking of the olefins. High temperature of the reactions also confirms that the interaction should be something other than oligomerisation. This observation has already been reported in the literature. Chauvin et al. has demonstrated that nickel nitrate (the impregnating salt used in the present work) when deposited on alumina or silica makes a catalyst, which is almost inactive for oligomerisation reactions [15].

Table 5-15. Product distribution of the reaction of propene over 5Ni/SiO₂ at different temperatures and atmospheric pressure (flow rate of 41 L_{C3}.h⁻¹.g_{cat}⁻¹)

Temperature (°C)	Conversion (g _{prod} .g _{cat} ⁻¹ .h ⁻¹)	Conversion (g _{prod} .g _{Ni} ⁻¹ .h ⁻¹)	C ₁	C ₂	C ₃	C ₄	C ₅	C ₆
500	-	-	-	-	-	-	-	-
600	0.56	11.2	39	29	3	11	3	15
650	1.04	20.9	32	32	3	14	5	15

The trend of TG profile for nickel-supported silica is different from the one for Ni/silica-alumina. Two stages can be observed in the TG profile. In case of ethene, they are so close together that can be hardly distinguished. Both the weight losses happen at temperatures higher than 600 °C, indicating that no volatile or light compounds have been produced. The loss at the range of 600 to 700 °C corresponds to the heavy products, while the one from 700 to 900 °C is ascribed to the coke deposition. Having no weight loss at temperatures less than 600 °C in the TG profiles also confirms that no oligomerisation has happened during the interaction of propene and ethene with the 5Ni/Silica (Figure 5-17 and Figure 5-18). Table 5-16 shows the summary of TG analyses of spent 5Ni/silica after reacting with ethene and propene.

Table 5-16. TG results of spent 5Ni/SiO₂ after the reaction with ethene and propene

	Temperature		Weight loss (%) after the reaction with ethene	Weight loss (%) after the reaction with propene
	Original (°C)	End (°C)		
Heavy products	600	700	1	1.5
Coke	700	900	2	2

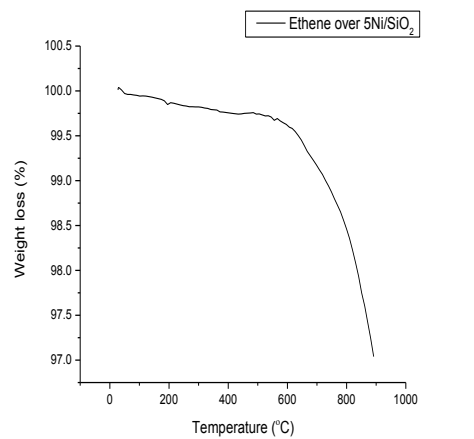


Figure 5-17. Thermal gravimetric analysis of spent 5NiO/SiO₂ after interacting with ethene

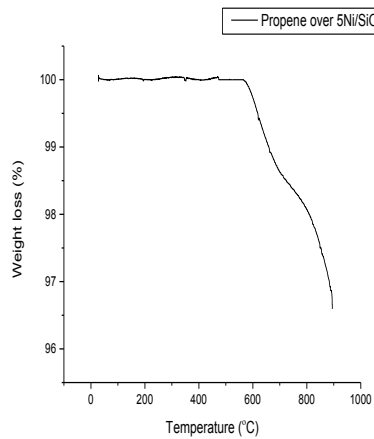


Figure 5-18. Thermal gravimetric analysis of spent 5NiO/SiO₂ after the interaction with propene

5.4. Conclusion

The interaction of a couple of catalysts with light hydrocarbons was investigated. For 0.5% loaded catalysts, Ni didn't have any contribution.

In case of 5% Ni supported catalysts: Siral-20 formed mostly metal aluminates, which is as a result of high density of Al species in the framework. Siral-40, which has less alumina in its structure, also partially formed nickel aluminates. But, still a portion of the metal was in oxide form. That part of metal, in both oxide and reduced form, exhibited dimerising activities for propene as reactant gas.

Ni incorporation on ZSM-5 gives it the capability of making cyclo-hydrocarbons, when the metal is reduced. Ni-promoted silica exhibited good dehydrogenating properties when it is reduced. However, nickel oxide doesn't have any catalytic activity for light hydrocarbons.

References

- [1] Mlinar, A. N.; Baur, G. B.; Bong, G. G.; Getsoian, A. B.; Bell, A. T. *Journal of Catalysis* **2012**, *296*, 156–164.
- [2] Heveling, J.; Nicolaides, C. P.; Scurrell, M. S. *Applied Catalysis A: General* **2003**, *248*, 239–248.
- [3] Rivolta, M. *Solvent extraction of coal: Influence of solvent chemical structure on extraction yield and product composition*; M.Sc. thesis, University of Alberta, Edmonton, Canada, 2012.
- [4] Subramanian, S.; Schwarz, J.A. *Applied Catalysis* **1990**, *61*, 15–19.
- [5] Pawelec, B.; Castaño, P.; Arandes, J. M.; Bilbao, J.; Thomas, S.; Peña, M. a.; Fierro, J. L. G. *Applied Catalysis A: General* **2007**, *317*, 20–33.
- [6] Leal, E.; Neiva, L. S.; Sousa, J. P. L. M. L.; Argolo, F.; Andrade, H. M. C.; Costa, A. C. F. M.; Gama, L. *Materials Science Forum* **2010**, *660-661*, 916–921.
- [7] Luengnaruemitchai, A.; Kaengsilalai, A. *Chemical Engineering Journal* **2008**, *144*, 96–102.
- [8] Infantes-Molina, A.; Merida-Robles, J.; Braos-Garcia, P.; Rodriguez-Castellon, E.; Finocchio, E.; Busca, G.; Maireles-Torres, P.; Jimenez-Lopez, A. *Journal of Catalysis* **2004**, *225*, 479–488.
- [9] Liu, Z.; Zhou, J.; Cao, K.; Yang, W.; Gao, H.; Wang, Y.; Li, H. *Applied Catalysis B: Environmental* **2012**, *125*, 324–330.
- [10] Rajagopal, S.; Grimm, T. L.; Collins, D. J.; Miranda, R. *Journal of Catalysis* **1992**, *137*, 453–461.

- [11] Hoang, D. L.; Berndt, H.; Miessner, H.; Schreier, E.; Vijlter, J.; Lieske, H. *Applied Catalysis A: General* **1994**, *114*, 295–311.
- [12] O'Connor, C. T. ; Kojima, M. *Catalysis Today* **1990**, *6*, 329–349.
- [13] Heveling, J.; Nicolaides, C. P.; Scurrell, M. S. *Applied Catalysis A: General* **1998**, *173*, 1–9.
- [14] Heveling, J.; Nicolaides, C. P.; Scurrell, M. S. *Applied Catalysis A: General* **2003**, *248*, 239–248.
- [15] Chauvin, Y.; Commereuc, D.; Hugues, F. *Applied Catalysis* **1988**, *42*, 205–216.
- [16] Spinicci, R.; Tofanari, A. *Materials Chemistry and Physics* **1990**, *25*, 375–383.

6. CONCLUSIONS AND SIGNIFICANCE

6.1. Introduction

The research was conducted through Helmholtz-Alberta initiative as part of the Theme 1 “Advanced Processes for Bitumen and Coal Upgrading and Conversion Technologies” under Task 4 “Conversion of pyrolysis gases”. The objective was to investigate the potential of pyrolysis gases, obtained from the thermal processing of bitumen, to be converted to liquid fuels. In order to achieve the target, the catalyzed conversion of model gaseous feed mixtures were investigated.

Three approaches were taken:

- 1) Catalyst screening. Candidate catalysts were identified from literature and evaluated by conversion of model gas mixtures over the candidate catalysts in a batch reactor. The catalysts evaluated were ZSM-5, Ferrierite, Mordenite, and Zeolite Y.
- 2) Detailed study of H-ZSM-5. A detailed study of the most promising candidate catalyst (H-ZSM-5) was conducted in a continuous flow reactor. This study was based on the potential application that it might have for industrial purposes. The reactions were therefore performed at adiabatic condition to investigate the use of the reaction heat to decrease the preheating of the reactants in industrial plants.
- 3) Catalyst modification. Investigation of the effect of metal incorporation on the catalyst performance. Both reduced Ni and NiO phases were investigated for dehydrogenation and heterogeneous Ni-catalyzed oligomerisation as suggested in literature.

An excerpt of the main outcomes of each approach is given in this chapter.

6.2. Main conclusions

The key points, which can be highlighted from the study, are as follow.

- a. In an effort to find the most suitable reaction temperature for pyrolysis gas conversion, where cracking is not considerable compared to oligomerisation, C₆-C₁₄ alkenes were catalytically tested at an increasing temperature and over H-ZSM-5. These studies were conducted in a batch reactor. Hexene showed the highest resistance against cracking, while tetradecene was the easiest to crack (cracking became significant at 305 °C). A temperature of 300 °C was therefore selected as the optimum operating temperature for evaluation.
- b. Due to the limited volume of gas that can be contained in a batch reactor, no liquid was collected and the progress of conversion was monitored by the decrease in reactor pressure. During the testing of four types of zeolite (acid forms of ZSM-5, Mordenite, Ferrierite, and Zeolite Y), H-ZSM-5 showed the maximum pressure drop (i.e. highest gas conversion), indicating that it has the most activity. A more detailed analysis of the conversion behaviour of H-ZSM-5 was conducted in a continuous flow reactor.
- c. Throughout the applied studies carried out in the flow reactor, H-ZSM-5 was highly active for the conversion of olefins, especially propene. Conversion ranged from 2.5 to 75 g_{liquid·g_{cat}}^{-1·h⁻¹ under adiabatic conditions with external temperature ranging from 220 to 300 °C. Although mixing propene with other gases reduced the conversion to some extent, the yield was still promising compared to literature values. Only olefinic gases were converted and the liquid products consisted of mainly olefins and a portion of aromatics.}

- d. The H-ZSM-5 deactivation rate was mainly a function of operating temperature. For ethylene, due to its reaction-resistant nature, and for the mixture of propene, ethene, and methane, because of the low partial pressure of the propene, a higher temperature (furnace temperature of 300 °C) was employed for the reactions, compared to most of the conversion studies that were performed at 220 °C. Under such conditions, the catalyst was completely deactivated after 100 min in case of ethene, and partially deactivated for the mixture of propene, ethene, and methane within the time on stream of hours. Subsequent analysis of the catalyst revealed that deactivation was due to the formation of carbonaceous deposits on the catalyst.
- e. Acidic catalyst support materials modified by 0.5 wt.% of nickel impregnation didn't affect the catalytic performance measurably. 0.5Ni/ZSM-5 behaved similar to H-ZSM-5 for the conversion of propene.
- f. Amorphous silica-alumina catalyst support materials modified by Ni incorporation at higher percentage (5 wt.%) had limited success. During calcination of the Ni modified catalysts, the NiO formed nickel aluminates with the Al₂O₃ in the support. Nickel aluminates are not readily reducible and require reduction temperatures of 900 °C and higher. In amorphous silica-alumina with 20% silica and 80% alumina (Siral 20), there was no catalyst activity for dimerisation after impregnation with Ni. Some dimerisation activity was found in amorphous silica-alumina with 40% silica and 60% alumina (Siral 40) after Ni impregnation.
- g. It was found that 5 wt.% Ni on H-ZSM-5 was capable of producing aliphatic cyclo-hydrocarbons from propene at external temperature of 300 °C and atmospheric pressure.

h. The oxide form of the metal species on silica (NiO/SiO_2) didn't exhibit any catalytic activity, while the reduced metal (Ni) was highly active for the dehydrogenation of butane. This can give us the idea of employing both Ni and H-ZSM-5 to convert paraffins (alkanes) and olefins (alkenes) at the same time.

6.3. Significance of this work

Applying this work for the industrial uses can be beneficial from two perspectives: First, from economical aspect by producing liquid fuels with a higher value than fuel gas. And second, from environmental point of view by reducing the environmental impacts of the pyrolysis off gases, by making post-pyrolysis clean-up more efficient.

However, application of this work in the larger industrial scale is premature. First of all, it should still be confirmed whether or not H-ZSM-5 shows activity in the presence of catalyst inhibitors (mainly carbon monoxide, nitrogen and sulfur compounds), and if it does, to what level each poison is tolerable, i.e. maximum poison concentration at which the zeolite keeps working sufficiently well for industrial use. In case of metal-supported acid catalysts, a few modifications should be applied to some of the catalyst supports. Silica-aluminas with higher levels of silica are more favorable to be used as catalyst support. Although the reactions were conducted at low pressures due to the low pressure of the pyrolysis gas, higher pressure can be a suggestion to improve the reaction condition.

6.4. Future work

One of the potential areas that can be considered for more investigation in the future is the performance of catalysts in the presence of poisons, and the level of poisons, that the catalysts can tolerate. For this purpose, catalysts' activity can be tested in the presence of different concentrations of model sulfur and nitrogen compounds. Finally, they can be directly examined for the conversion of the gases released from the pyrolysis of bitumen.

Another potential area of study might be testing the performance of mixture of H-ZSM-5 and Ni-promoted silica for the oligomerisation of alkenes and alkanes. We could realize from the presented study that H-ZSM-5 has good oligomerising activities for olefins, while reduced Ni/silica has dehydrogenating properties, which makes it suitable for paraffin conversion. Combination of these two catalysts can therefore be effective for simultaneous conversion of both olefins and paraffins.

6.5. Presentations and publications

The nature of the project required regular formal updates on progress, as well as opportunity to present aspects of the work to a broader audience at conferences.

"Catalytic conversion of pyrolysis gases", Ladan Shamaei, Arno de Klerk, poster presentation: HAI 1st Science Forum, Edmonton, Canada, September 28 - 30, 2011.

"Catalytic conversion of pyrolysis gases", Ladan Shamaei, Arno de Klerk, oral presentation: CSChE 2011 London, Ontario, October 23 - 26, 2011.

"Catalytic conversion of pyrolysis gases", Ladan Shamaei, Arno de Klerk, poster presentation: 3rd HAI annual meeting, Edmonton, Canada, May 9 - 11, 2012.

"Catalytic conversion of pyrolysis gases", Ladan Shamaei, Arno de Klerk, poster presentation: 3rd Faculty of Engineering Graduate Research Symposium (FEGRS 2012), Edmonton, Alberta, June 21, 2012.

"Catalytic conversion of pyrolysis gases", Ladan Shamaei, Arno de Klerk, oral presentation: 244th ACS National Meeting, Philadelphia, Pennsylvania, August 19 - 23, 2012.

Shamaei, L., De Klerk, A. Pyrolysis gas to liquid conversion. *Prepr. Pap.-Am. Chem. Soc., Div. Energy Fuels*, 57:2 (2012) 1005-1006.

"Catalytic conversion of pyrolysis gases", Ladan Shamaei, Arno de Klerk, oral presentation: HAI 2nd Science Forum, Potsdam, Germany, September 10 - 11, 2012.

Appendices

A. Appendix I

The additional data for chapter 1 is presented in this section.

Table A-1. Pressure changes as temperature increases for the reaction of 1-hexene (left) and 1-heptene (right) over H-ZSM-5

Temperature (°C)	Pressure (psi)	Temperature (°C)	Pressure (psi)
145	38	224	11
150	38	259	15
203	39	270	19
250	39	279	21
282	39	280	24
300	40	303	28
320	41	315	31
380	42	329	36
400	42	343	41
435	42	362	45
450	43	376	47
465	50	389	50
488	50	409	56
		424	60
		342	61
		459	79
		473	97

Table A-2. Pressure changes as temperature increases for the reaction of 1-octene (left) and 1-nonene (right) over H-ZSM-5

Temperature (°C)	Pressure (psi)	Temperature (°C)	Pressure (psi)
190	12	222	10
223	16	262	15
236	18	268	17
245	20	299	19
251	25	325	23
269	29	333	27
281	32	349	31
298	35	366	51
310	41	379	53
329	46	385	56
343	49	390	63
356	53	395	64
375	57	406	66
390	61	414	68
408	63	420	70
423	88	425	71
439	98	429	77
451	101	450	80

Table A-3. Pressure changes as the temperature increases for the reaction of 1-decene (left) and 1-undecene (right) over H-ZSM-5

Temperature (°C)	Pressure (psi)	Temperature (°C)	Pressure (psi)
225	12	191	10
258	16	201	12
269	18	237	13
299	20	267	16
325	25	278	18
335	29	291	20
350	32	296	24
369	50	303	30
379	54	313	48
385	56	318	52
394	62	333	52
395	62	362	56
407	62	368	58
416	64	372	60
420	70	382	68
425	72	390	78
430	76	400	90
450	78	430	100
		450	105

Table A-4. Pressure versus temperature for the reaction of 1-dodecene (left) and 1-tridecene (right) over H-ZSM-5

Temperature (°C)	Pressure (psi)	Temperature (°C)	Pressure (psi)
220	20	213	12
233	22	250	16
247	23	266	18
255	24	283	20
276	26	312	25
342	26	329	30
350	44	346	36
370	45	356	50
390	47	358	54
410	76	360	56
418	79	369	62
440	82	374	62
450	83	378	62
		384	64
		390	70
		398	72
		406	76
		430	80
		448	82

Table A-5. Pressure versus temperature for the reaction of 1-tetradecene over H-ZSM-5

Temperature (°C)	Pressure (psi)
125	8
177	10
215	15
230	16
248	18
270	20
290	24
320	48
335	66
360	72
390	74
410	76
418	79
440	82
450	83

B. Appendix II

Additional experimental data pertaining to chapter 4 are presented here.

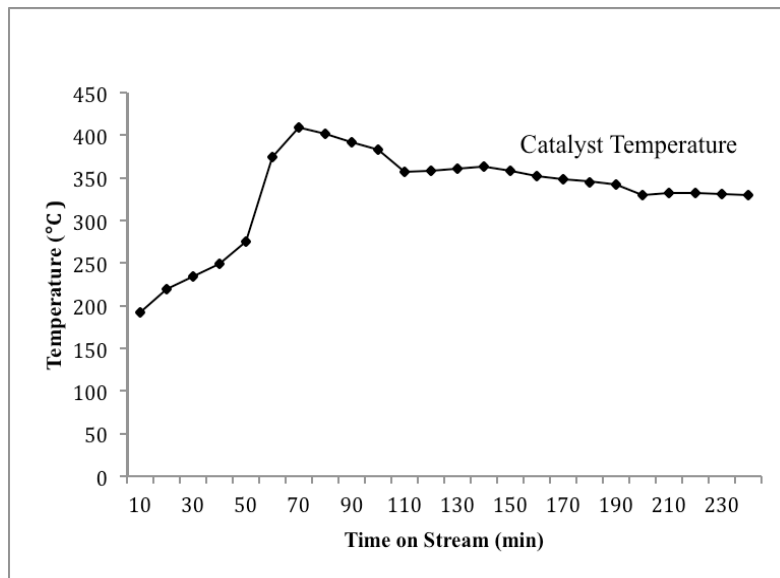


Figure B-1. Temperature profile of the catalyst bed from the reaction of propene over H-ZSM-5 (at total pressure of 100 psi and preheating temperature of 220 °C)

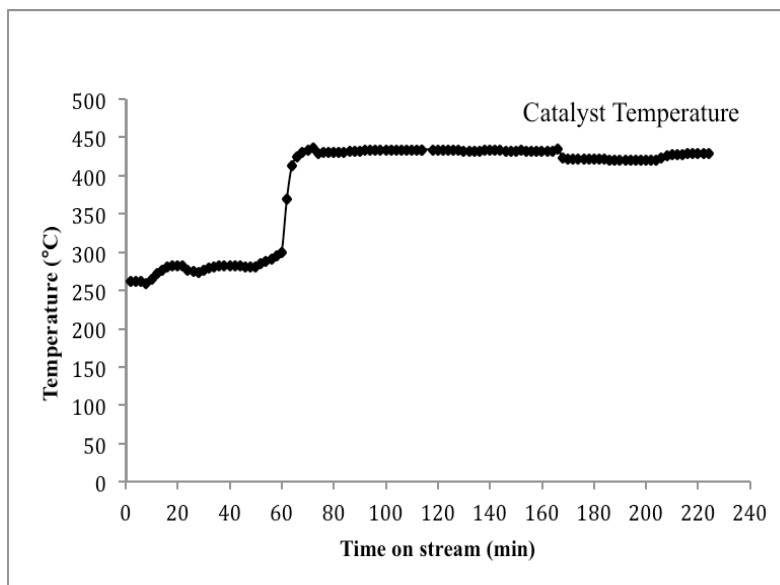


Figure B-2. Temperature of the catalyst bed for the reaction of mixture of propene and methane over H-ZSM-5 (at total pressure of 100 psi and preheating temperature of 220 °C)

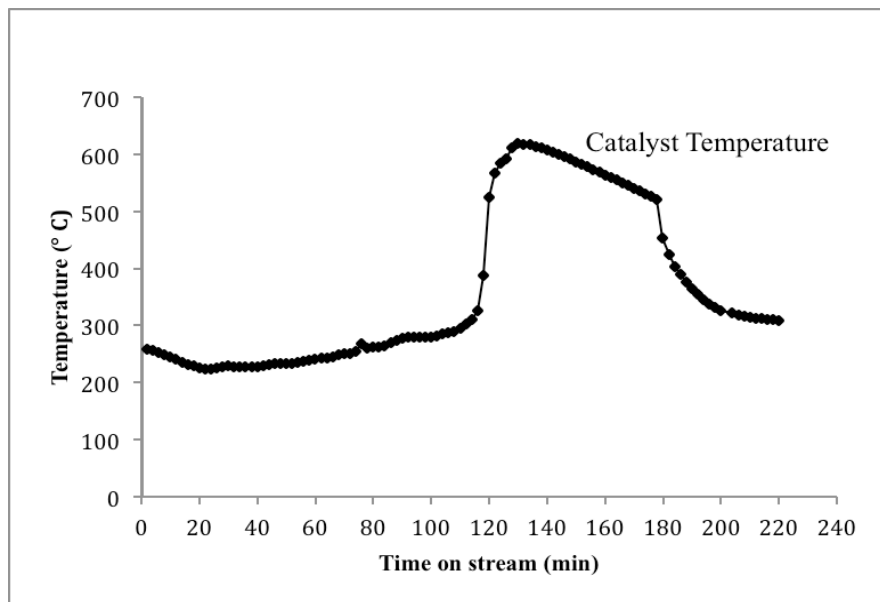


Figure B-3. Temperature of the catalyst bed for the reaction of ethene over H-ZSM-5 (at total pressure of 100 psi and preheating temperature of 220 °C)

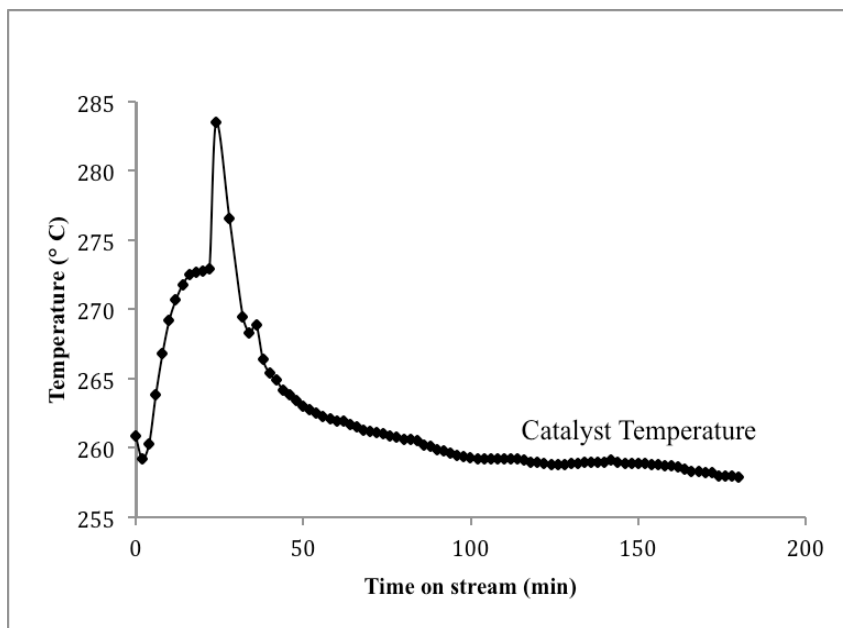


Figure B-4. Temperature profile of the catalyst for the reaction of mixture of propene and hydrogen over H-ZSM-5 (at total pressure of 100 psi and preheating temperature of 220 °C)

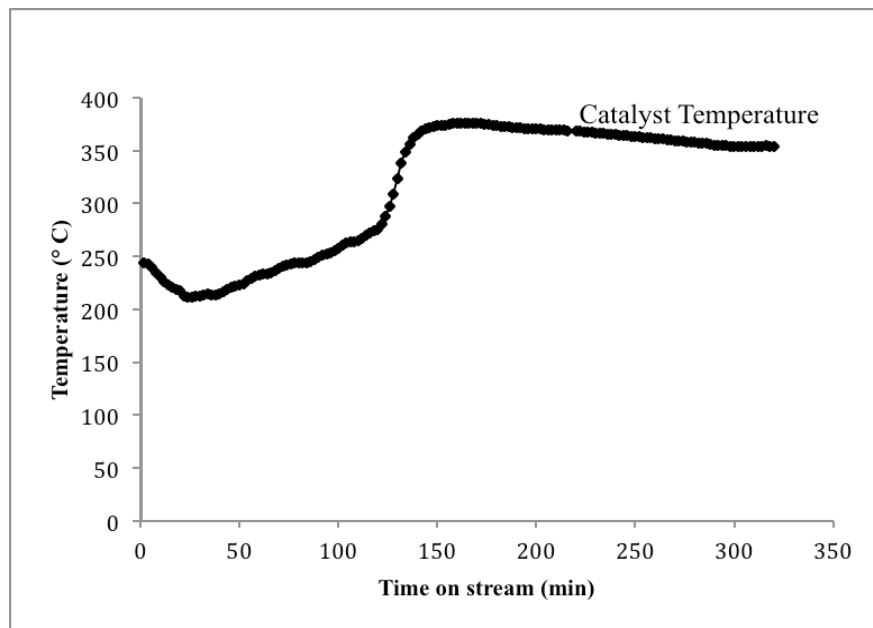


Figure B-5. Temperature profile of the catalyst bed for the reaction of mixture of propene and carbon dioxide over H-ZSM-5 (at total pressure of 100 psi and preheating temperature of 220 °C)

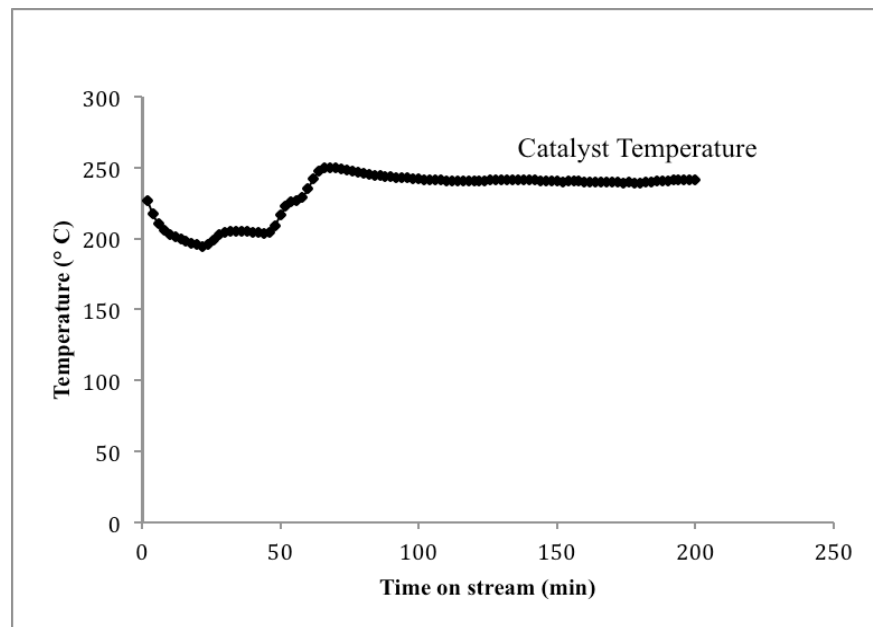


Figure B-6. Temperature profile of the catalyst bed for the conversion of mixture of propene and butane over H-ZSM-5 (at total pressure of 100 psi and preheating temperature of 220 °C)

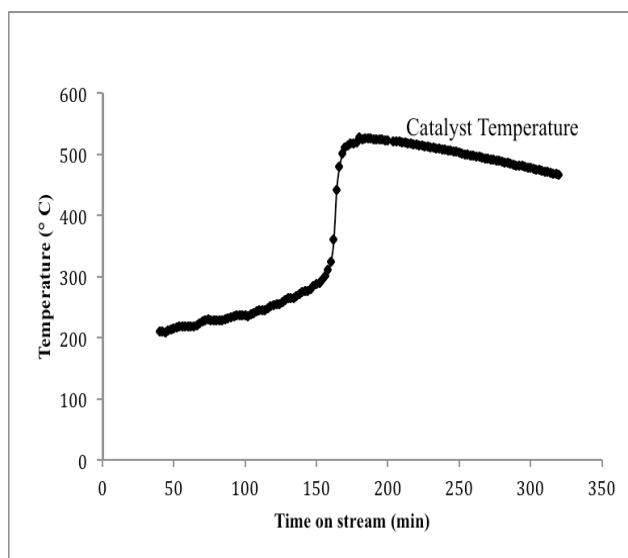


Figure B-7. Temperature profile of the catalyst bed for the reaction of the mixture of methane, ethene, and propene over H-ZSM-5 (at total pressure of 100 psi and preheating temperature of 220 °C)

Table B-1. Aromatic and aliphatic distribution of the products from the conversion of different mixture of gases (at total pressure of 100 psi and preheating temperature of 220 °C)

Exp.	A		B		C	
	Aliphatics	Aromatics	Aliphatics	Aromatics	Aliphatics	Aromatics
C ₁	0.03	0	0	0	0.01	0
C ₂	0.9	0	1.8	0	1.8	0
C ₃	3.5	0	5.8	0	5.8	0
C ₄	25.5	0	34.1	0	34.1	0
C ₅	18.1	0	12.4	0	12.4	0
C ₆	14.9	0.1	12.5	0.0004	12.5	0.0004
C ₇	9.9	1.5	6.0	0.01	6.0	0.01
C ₈	12.8	5.6	6.6	0.05	6.6	0.05
C ₉	8.1	4.4	3.4	0.04	3.4	0.04
C ₁₀	3.7	1.9	1.8	0.02	1.8	0.02
C ₁₁₊	0	1.5	0	0.04	0	0.04

Table B-2. Aromatic and aliphatic distribution of the products from the conversion of different mixture of gases (at total pressure of 100 psi and preheating temperature of 220 °C)

Exp.	D		E		F	
	Aliphatics	Aromatics	Aliphatics	Aromatics	Aliphatics	Aromatics
C ₁	0.04	0	0.004	0	0.006	0
C ₂	1.1	0	0.014	0	1.0	0
C ₃	3.6	0	0.2	0	2.7	0
C ₄	34.4	0	89.1	0	40.3	0
C ₅	10.0	0	0.9	0	10.3	0
C ₆	19.2	0.0006	4.2	0.02	19.6	0.1
C ₇	6.0	0.004	1.1	0.07	6.5	0.3
C ₈	6.8	0.03	1.4	0.33	5.9	2.6
C ₉	4.8	0.03	0.9	0.51	3.6	2.6
C ₁₀	2.2	0.02	0.5	0.3	1.9	1.7
C ₁₁₊	0	0.03	0	0.5	0	1.2

Table B-3. Aromatic and aliphatic distribution of the products from the conversion of different mixture of gases (at total pressure of 100 psi and preheating temperature of 220 °C)

Exp.	G		H	
	Aliphatics	Aromatics	Aliphatics	Aromatics
C ₁	0	0	0.85	0
C ₂	0.96	0	4.2	0
C ₃	4.0	0	35.5	0
C ₄	48.6	0	31.	0
C ₅	10.5	0	4.9	0
C ₆	23.1	0.03	8.0	0.02
C ₇	2.1	0.8	1.6	1.1
C ₈	1.7	3.2	1.3	4.3
C ₉	0.8	2.1	0.7	3.5
C ₁₀	0.5	0.6	0.5	0.9
C ₁₁₊	0	0.98	0	1.5

Table B-4. Amount of product captured every 20 min during the 3 h of experiment (at total pressure of 100 psi and preheating temperature of 220 °C)

Reactant mixture	20 min	40 min	60 min	80 min	100 min	120 min	140 min	160 min	180 min
C ₃	2.67	10.73	12.02	12.32	12.63	12.35	12.94	12.96	12.07
C ₃ +C ₂	1.41	8.92	9.49	9.43	9.21	8.30	8.19	8.17	8.18
C ₃ +C ₁	0.25	3.41	3.41	3.53	3.46	3.54	3.39	3.14	3.64
C ₂	0.22	2.74	2.01	1.09	0.1	0	0	0	0
C ₁ +C ₂ +C ₃	0.03	2.35	2.54	2.04	1.98	1.57	1.54	1.14	1.08
C ₃ +H ₂	0.4	2.14	2.18	2.17	2.15	2.18	2.16	2.09	2.12
C ₃ +CO ₂	2.11	2.39	2.5	2.43	2.46	2.52	2.52	2.42	2.49
C ₃ +C ₄	0.4	0.42	0.45	0.43	0.45	0.42	0.32	0.44	0.41

C. Appendix III

Activation energy calculation for the reaction of propene over reduced 5Ni/Siral-40:

Assuming T_0 to be 275 °C (547 K), then the Arrhenius equation relative to T_0 would be:

$$\frac{k}{k_0} = e^{-E_a/R(\frac{1}{T} - \frac{1}{T_0})}$$

$$\ln\left(\frac{k}{k_0}\right) = \frac{-E_a}{R} \left(\frac{1}{T} - \frac{1}{T_0}\right)$$

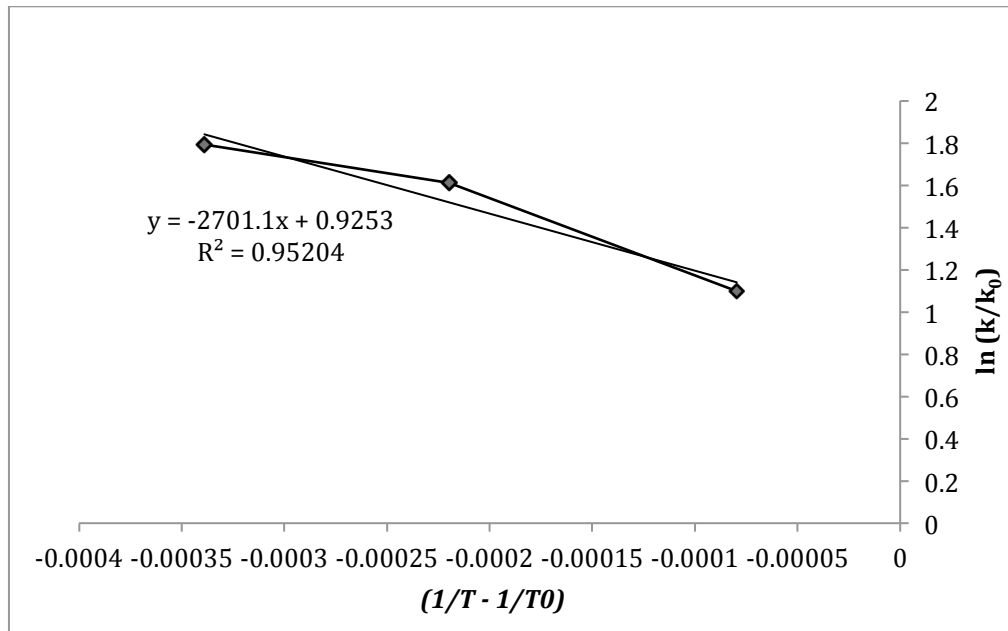


Figure C-1. Arrhenius plot for the reaction of propene over reduced 5Ni/Siral-40

The slope of the line, which equals to $-E_a/R$ is -2701.1. Therefore, the activation energy would be:

$$E_a = 2701.1 \times 8.314 = 22456.9 \text{ J/mol}$$